VOLUME 86 NO. ST11
NOVEMBER 1960

JOURNAL of the

Structural Division

PROCEEDINGS OF THE

AMERICAN SOCIETY
OF CIVIL ENGINEERS

BASIC REQUIREMENTS FOR MANUSCRIPTS

Original papers and discussions of current papers should be submitted to the Manager of Technical Publications, ASCE. Authors should indicate the technical division to which the paper is referred. The final date on which a discussion should reach the Society is given as a footnote with each paper. Those who are planning to submit material will expedite the review and publication procedures by complying with the following basic requirements:

1. Titles must have a length not exceeding 50 characters and spaces.

2. A 50-word summary must accompany the paper, a 300-word synopsis must precede it, and a conclusion must end it.

3. The manuscript (an original and two duplicate copies) should be double-spaced on one side of 8½-inch by 11-inch paper. Three copies of all illustrations, tables, etc., must be included.

4. The author's full name, Society membership grade, and footnote reference stating present employment must appear on the first page of the paper.

5. Mathematics are recomposed from the copy that is submitted. Because of this, it is necessary that letters be drawn carefully, and that special symbols be properly identified.

6. Tables should be typed (an original and two duplicate copies) on one side of 8½-inch by 11-inch paper. Specific illustrations and explanation must be made in the text for each table.

7. Illustrations must be drawn in black ink on one side of 8½-inch by 11-inch paper. Because illustrations will be reproduced with a width of between 3-inches and 4½-inches, the lettering must be large enough to be legible at this width. Photographs should be submitted as glossy prints. Explanations and descriptions must be made within the text for each illustration.

8. Papers should average about 12,000 words in length and must be no longer than 18,000 words. As an approximation, each full page of typed text, table, or illustration is the equivalent of 300 words.

9. Technical papers intended for publication must be written in the third person.

10. If letter symbols are used in the paper they should be defined where they first appear, in the illustrations or in the text, and arranged alphabetically in an Appendix.

This Journal is published monthly by the American Society of Civil Engineers. Publication office is at 2500 South State Street, Ann Arbor, Michigan. Editorial and General Offices are at 33 West 39 Street, New York 18, New York. $4.00 of a member's dues are applied as a subscription to this Journal. Second-class postage paid at Ann Arbor, Michigan.

The index for 1959 was published as ASCE Publication 1960-10 (list price $2.00); indexes for previous years are also available.

Journal of the

STRUCTURAL DIVISION

Proceedings of the American Society of Civil Engineers

CONTENTS

November, 1960

Papers

DISCUSSION

Journal of the
STRUCTURAL DIVISION
Proceedings of the American Society of Civil Engineers

USE OF CONTINUITY-FACTOR AND FINAL POSITION

By Yon-Sun Chou[1]

SYNOPSIS

The purpose of this paper is to introduce the use of the continuity-factor and final position in the analysis of any continuous structures of simultaneous, one-direction, sway movement, especially as applied to a multi-bay multi-story rigid frame. Such a structure or frame will be analyzed by the method of computing unbalanced moments, for which purpose a simple, clear procedure of analysis, is obtained from the previously mentioned factor. A few examples are also presented.

FUNDAMENTAL CONCEPTIONS

Continuity-Factor.—In any continuous structure, suppose one of its joints is under the action of external moments (including fixed end moment caused by external force); this moment will affect other joints through their connecting members. As in Fig. 1, an external moment M_A acts on the joint of A of a continuous girder. This moment causes an angle rotation at A (θ_A). Through the connecting bar AB and BC, joints B and C, have angle changes of θ_B and θ_C respectively.

These angle changes produce the joint moment (unbalanced moments) M_b^u, and M_c^u, respectively. Now let

$$M_b^u = {}_{ab}F_c \; M_a^u, \text{ and } M_c^u = {}_{bc}F_c \; M_b^u \quad \ldots\ldots\ldots\ldots (1)$$

Note.—Discussion open until April 1, 1961. Separate discussions should be submitted for the individual papers in this symposium. To extend the closing date one month, a written request must be filed with the Executive Secretary, ASCE. This paper is part of the copyrighted Journal of the Structural Division, Proceedings of the American Society of Civil Engineers, Vol. 86, No. ST 11, November, 1960.

[1] Asst. Dept. of Civ. Engrg., National Taiwan Univ., Taipei, Taiwan, China.

The value F_c is the continuity-factor. This factor will be evaluated by conventional moment distribution and will be determined as a function of the carry-over ratio.

It becomes necessary now to explain the relationship between M_a and M_a^u. The angle change θ_a is directly proportional to the stiffness of the bars that connect to joint A. But the conventional stiffness used is that which assumes the far end of the bar to be fixed. For a member that has a different far-end condition, such as joint B, the stiffness of AB will be reduced. If, therefore, the moment M_a remains unchanged, the angle rotation must increase for its reduction of stiffness. But, if we unchange the stiffness, it is apparent that the moment must consequently increase.

Because no modification of stiffness is available in this paper, it is necessary to compute the increase of the moment. Or, if we denote M^u as the moment, after considering the increase, M_f denotes the original moment, and it is necessary to establish a relationship between these two moments. Let

$$M^u = J_R M_f \quad \ldots\ldots\ldots\ldots\ldots\ldots \quad (2)$$

Value J_R is called the joint rotation-ratio; it will also be evaluated by conventional moment distribution with some reasonable short-cuts.

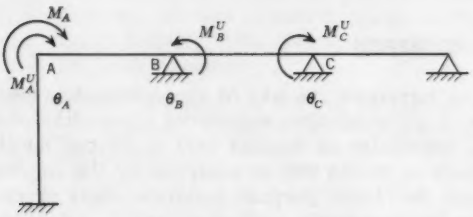

FIG. 1

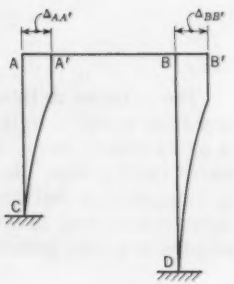

FIG. 2

Final Position.—This concept was first presented by Mr. EA-Lu Tieng.[2] His idea and statement is as follows: Bent ABCD as Fig. 2 has sway movement $\Delta AA'$ and $\Delta BB'$. Suppose A' and B' are the final positions of its movement, and no joint rotation is permitted in this position. Based on integrity, we have

$$\Delta_{AA'} = \Delta_{BB'}, \quad \ldots\ldots\ldots\ldots\ldots\ldots \quad (3)$$

and due to sway movement

$$M_{fac} = -6\,E\,K\,R_{ac} = -6\,E\,K_{ac}\,\frac{\Delta_{AA'}}{L_{ac}} \quad \ldots\ldots\ldots \quad (4)$$

$$M_{fbd} = -6\,E\,K_{bd}\,R_{bc} = -6\,E\,K_{bd}\,\frac{\Delta_{BB'}}{L_{bd}} \quad \ldots\ldots\ldots \quad (5)$$

---

[2] "Taiwan Engineering," by Ea-Lu Tieng, Vol. 10, No. 8.

Therefore,

$$M_{fac} : M_{fbd} = \frac{K_{ac}}{L_{ac}} : \frac{K_{bd}}{L_{bd}} \quad \ldots\ldots\ldots\ldots\ldots (6)$$

If we introduce a variable X, then

$$M_{fac} : \frac{K_{ac}}{L_{ac}} X \quad \ldots\ldots\ldots\ldots\ldots (7a)$$

$$M_{fbd} = \frac{K_{bd}}{L_{bd}} X \quad \ldots\ldots\ldots\ldots\ldots (7b)$$

It means that we can assume a variable X to represent the joint as being fixed and a moment that is due to side-sway. But, for a certain continuous structure the fixed end moment of each column is proportional to its k/L ratio.

In the analysis, this kind of M_f will be included in the value of M_f that is due to external load. After the analysis is completed, the value of X will be solved by means of the bent equation. Therefore, the problem of side sway is

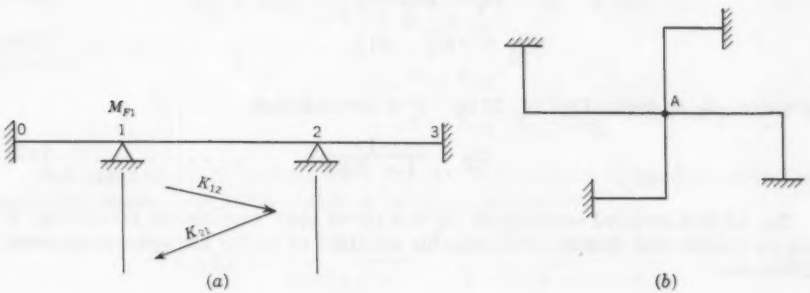

FIG. 3

now free from the additional computation that is needed in the conventional moment distribution, as a result of our introducing the variable X.

DEVIATION OF F_c

Derivation of J_R.—The joint rotation ratio is defined as

$$J_R = \frac{M^u}{M_F} \quad \ldots\ldots\ldots\ldots\ldots (8)$$

Fig. 3(a) is a three span continuous girder; M_{f1} acts on joint 1. According to conventional moment, distribution M_{f1} will carry over to joint 2 and then back to joint 1. The first carry over back moment is equal to $M_{f1}\ K_{12}\ K21$. This moment will distribute and carry over again. Therefore, the total unbalanced moment at joint 1, after summing up the successive carry over back

moments and the original M_f, must satisfy the equation:

$$M_1^u = M_{f1} + M_{f1}\left[K_{12}K_{21} + (K_{12}K_{21})^2 + K_{12}K_{21}^{\,n}\right] \ldots\ldots (9)$$

If $n = \infty$

$$M_1^u = M_{f1} \sum_{n=0}^{\infty} (K_{12}K_{21})^n \quad \ldots\ldots\ldots\ldots\ldots (10)$$

Therefore,

$$1J_R = \frac{M_1^u}{M_{f1}} = \sum_{n=0}^{\infty} (K_{12}K_{21})^n \quad \ldots\ldots\ldots\ldots (11a)$$

$$1J_R = \frac{1}{1-K_{12}K_{21}} \quad \ldots\ldots\ldots\ldots (11b)$$

We have

$$M_1^u = {}_1J_R\, M_{f1} \quad \ldots\ldots\ldots\ldots\ldots (12a)$$

$$M_{21}^u = -M_1^u \cdot K_{12} \quad \ldots\ldots\ldots\ldots\ldots (12b)$$

in which ${}_1J_r$ is defined by Eq. 11(b), it is obvious that

$$J_R = \frac{1}{1 - \Sigma KK} \quad \ldots\ldots\ldots\ldots (13)$$

Eq. 13 is a general equation of J_R in a three span continuous structure. It will be proven that this is an acceptable equation of J_r for any span-continuous structure.

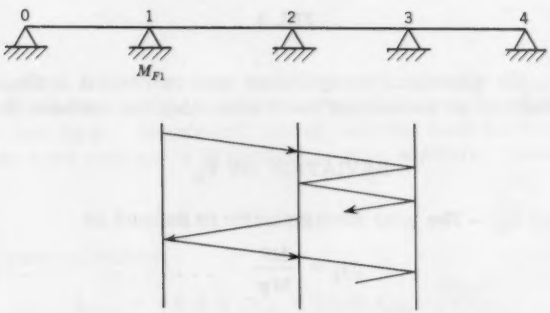

FIG. 4

Fig. 4, is a four span continuous girder. Suppose M_{f1} acts on joint 1; the moment M_{f1} will carry-over to joint 2, this carry-over moment equals $-M_{f1}$ K_{12} and will carry-over in span 2-3. Similar to the derivation of a three span

beam, we have

$$\left(M_2^u\right)_1 = -M_{f1} \quad K_{12} \quad \frac{1}{1-K_{23}K_{32}} \quad \ldots\ldots\ldots\ldots (14)$$

$\left(M_2^u\right)_1$ then will carry-over back to joint 1. The first carry-over back moment of joint 1, therefore is equal to $M_{f1} \quad \frac{K_{12}K_{21}}{1 - K_{23}K_{32}}$.

In a similar way, we can have the second, and third to the nth carry-over back moment at joint 1. Summing up those carry-over back moments, and the original M_f, we have

$$M_1^u = M_{f1} + M_{f1}\left[\frac{K_{12}K_{21}}{1 - K_{23}K_{32}} + \left(\frac{K_{12}K_{21}}{1 - K_{23}K_{32}}\right)^2 + \ldots + \left(\frac{K_{12}K_{21}}{1 - K_{23}K_{32}}\right)^n\right] \ldots (15a)$$

and

$$n = \infty \quad \ldots\ldots\ldots\ldots\ldots\ldots (15b)$$

$$M_1^u = M_{f1} \cdot \sum_{n=o}^{\infty}\left[\frac{K_{12}K_{21}}{1-K_{23}K_{32}}\right]^n = M_f \cdot \phi\ (K) \quad \ldots\ldots (15c)$$

in which

$$\phi\ (K) = \frac{1 - K_{23}K_{32}}{1 - K_{12}K_{21} - K_{23}K_{32}} \quad \ldots\ldots\ldots (16a)$$

This value of $\phi\ (K)$ and J_R from Fig. 11(b) is similar to the corresponding sequence summation factor derived by Mr. Adrian Paun:[3]

$$\phi\ (K) = \frac{1-K_{12}K_{21}}{1-K_{12}K_{21}} \cdot \frac{1 - K_{23}K_{32}}{1 - K_{12}K_{21} - K_{23}K_{32}} \quad \ldots\ldots (16b)$$

$$\phi\ (K) = \frac{1}{1 - K_{12}K_{21}}\left[1 + \frac{K_{12}K_{23}K_{32}K_{21}}{1 - K_{12}K_{21} - K_{23}K_{32}}\right] \quad \ldots\ldots (16c)$$

$$\phi\ (K) = \frac{1}{1-K_{12}K_{21}}\ (1 + \phi'\ (K)) \quad \ldots\ldots\ldots (16d)$$

Because the K value is usually much less than 1/4 in actual structures,

$$\phi'\ (K) \doteqdot K_{12}K_{23}K_{32}K_{21} < (1/4)^4 \quad \ldots\ldots\ (17)$$

In practical use, it is reasonable to neglect this term. If we neglect it

$$M_1^u = M_{F1} \quad \phi\ (K) = M_{F1} \quad \frac{1}{1-K_{12}K_{21}} \quad \ldots\ldots (18)$$

We then have Eq. 11(b) and therefore, Eq. 13 is regarded as a general expression of joint rotation-ratio. We have seen that the small quantities produced by the continuous members beyond the second span are negligible.

---

[3] "Sequence Summation Factor," by Adrian, Paun, Proceedings ASCE, August, 1955.

Derivation of α and F_C.—Eq. 12(a) indicates that the unbalanced moment of any joint is always equal to its fixed end moment times its joint rotation-ratio. In other words, one must compute the fixed end moment first if he wants to compute the unbalanced moment.

Suppose there is M_{F2} on joint 2 (Fig. 4), then we must know M_1^u, due to this M_{F2}; according to the preceeding statement, the fixed end moment of joint 1 must be computed first. Thus, assume joint 3 to be fixed. By Eq. 12(b)

$$M_{F3} = - M_2^{u'} \cdot K_{23} \quad \ldots\ldots\ldots\ldots \quad (19)$$

in which

$$M_2^{u'} = -M_{F2} \cdot {}_2J_R' \quad \ldots\ldots\ldots\ldots \quad (20a)$$

and

$${}_2J_R' = \frac{1}{1-K_{12}K_{21}} \quad \ldots\ldots\ldots\ldots \quad (20b)$$

For convenience, substitute α for J_R' and name it relative joint rotation-ratio. For example, α_{12} means the rotation-ratio of joint 1 relative to joint 2 is regarded as fixed. The general equation of α is

$$\alpha_{12} = \frac{1}{1 - \Sigma KK + K_{12}K_{21}} \quad \ldots\ldots\ldots \quad (21)$$

We then have

$$M_3^u = M_{F3}\ {}_3J_R = - M_2^{u'}\ K_{23}\ {}_3J_R \quad \ldots\ldots\ldots \quad (22a)$$

$$M_3^u = -\alpha_{23} K_{23}\ {}_3J_R\ M_{F2} \quad \ldots\ldots\ldots \quad (22b)$$

$$M_3^u = -\alpha_{23} K_{23}\ {}_3J_R\ \frac{M_2^u}{{}_2J_R} \quad \ldots\ldots\ldots \quad (22c)$$

Let

$$M_3^u = {}_{23}F_c\ M_2^u \quad \ldots\ldots\ldots\ldots \quad (23)$$

in which

$${}_{23}F_c = -\alpha_{23}\ K_{23}\ \frac{{}_3J_R}{{}_2J_R} \quad \ldots\ldots\ldots\ldots \quad (24)$$

Eq. 24 is a general equation of continuity-factor. It is proportional to the relative joint rotation-ratio and carry-over ratio between two joints, proportional to the rotation-ratio of second joint, and inversely proportional to that of the first joint.

METHOD OF COMPUTING UNBALANCED MOMENTS

One Story Continuous Frame.—This method will be explained by the following illustration: Example 1 (Fig. 5).—This example is selected from "Analysis of Statically Indeterminate Structures."[4] The result is also noted in the

[4] "An Analysis of Statically Indeterminate Structures," by John I. Parcel and Robert B. B. Moorman, pp. 370-373.

bracket of the last line of Table 1. The procedure of the method is presented in Table 1. Some necessary explanations are as follows:

Line (5); K value is equal to D times C.O.F., but C.O.F. equals 1/2 in this example for all connecting members, therefore, K equals 1/2 of D.

Line (6)-KK; For example, $(KK)_{AB} = K_{AB}\,K_{BA} = 0.335 \times 0.2 = 0.067$;

Line (7)-J_R; Uses Eq. 13 to compute J_R. For example, ${}_BJ_R = 1/(1-0.067-0.0455) = 1.133$;

Line (9) F_C; Uses Eq. 24 to compute F_C equal to $-(8) \times (5) \times \frac{J_R}{J_R}$. For example, ${}_{AB}F_C = -1.0 \times 0.335 \times \frac{1.133}{1.05} = -0.353$;

Line (10) F.E.M.; in this line $M_{FAE} = 15X$, $M_{FCG} = 4.8X$ $M_{FDM} = 40\,X$. These values of F.E.M. are caused by sway movement, because of $(k/L)_{AE}$: $\left(\frac{K}{L}\right)_{BF} : \left(\frac{K}{L}\right)_{CG} : \left(\frac{K}{L}\right)_{DH} = 15 : 15 : 4.8 : 40$

Line (11); Uses Eq. 12(a) and 23 to compute this line as:

$$85 + 17X = (75+15X) \cdot 1.133\ , \quad -16.9-3.38X = (85+17X)(-0.199)$$
$$-71 + 5.35X = (-63.75+4.8X) - 1.114, \quad -3.46+0.26X = (17.4-1.31X)\cdot 1.05$$

Line (13); Uses Eq. 12(b) to compute this line as $6.8 - 4.17\,X = -(-20.21 + 12.47X) \cdot 0.335$

This line offers a check. The summation of this line of a certain joint must "nearly" equal the difference between the M^u and M_F of that joint. For example, at joint B,

$$6.8 - 4.17\,X + 19.8 + 1.875X \doteq 101.63 + 12.71X - 75 + 15X$$

The reason for using "nearly" is that something was dropped when the joint rotation-ratio J_R was derived.

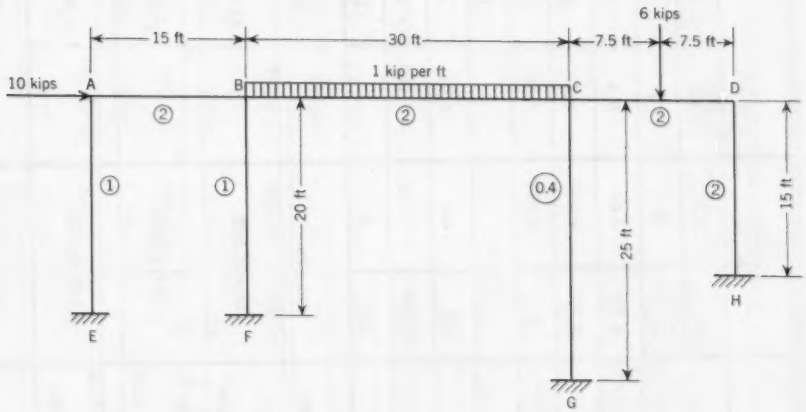

FIG. 5

Line (15); is equal to line (10) + (13) + (14)

After computing the result of each bar, then solve the variable X by the bent equation:

$$\sum \frac{M\ \text{col.}}{L} = H. \quad \ldots\ldots\ldots\ldots\ldots \quad (25)$$

TABLE 1.—EXAMPLE ONE

(1)	Joint	A		B			C			D	
(2)	Bar	AE	AB	BA	BF	BC	CB	CG	CD	DC	DH
(3)	k	1	2	2	1	2	2	0.4	2	2	2
(4)	D	0.33	0.67	0.4	0.2	0.4	0.4546	0.0908	0.4546	0.5	0.5
(5)	K	0.165	0.335	0.2	0.1	0.2	0.2273	0.0454	0.2273	0.25	0.25
(6)	KK	0	0.067	0.067	0	0.0455	0.0455	0	0.0568	0.0568	0
(7)	Jr	1.075		1.133			1.114			1.06	
(8)	α	1.0	1.0	1.05	1.0	1.075	1.08	1.0	1.05	1.0	1.0
(9)	Fc	- 0.165	- 0.353	- 0.199	- 0.1	- 0.211	- 0.245	- 0.0454	- 0.227	- 0.262	- 0.25
(10)	F.E.M.	15x	0	0	15x	75	-75	4.8x	11.25	-11.25	40x
(11) U.M. due to M_F	M_A=15x	16.13x		-5.7x			1.2x			-0.273x	
	$M_B=\overset{75}{\underset{+15x}{}}$	-16.9-3.38x		85+ 17x			-17.9-3.58x			4.07-0.814x	
	$M_C=\overset{-63.75}{\underset{+ 4.8x}{}}$	3.46+ 0.261x		17.4-1.31x			-71+ 5.35x			16.1-1.214x	
	$M_D=\overset{-11.25}{\underset{40x}{}}$	0.152-0.542x		-0.766+ 2.72x			3.12-11.1x			-11.92+ 42.4x	

(12) Total U.M.	-20.21+ 12.47x		101.63+ 12.71x			-85.78-8.13x			8.25+ 41.73x	
(13) U.M. of Bar		-20.33 - 2.54x	6.8 - 4.17x		19.48 + 1.875x	-20.33 - 2.54x		- 2.07 -10.44x	19.48 + 1.85x	
(14) Dist.	6.7 - 4.11x	13.6 - 8.34x	-40.6 - 5.09x	-20.3 - 2.55x	-40.6 - 5.09x	39 3.69x	7.78 0.74x	39 3.69x	- 4.125 -20.87x	- 4.125 -20.87x
(15) Result.	6.7 10.89x	- 6.73 -10.89x	-33.8 - 9.26x	-20.3 12.45x	53.88 - 3.215x	-56.33 1.15x	- 7.78 5.54x	48.18 - 6.71x	4.11 -19.02x	- 4.125 19.13x
	26.03	-26.06	-50.28	1.84	48.17	-54.27	17.56	36.31	-29.7	29.87
	[26.03]	[-26.04]	[-50.19]	[1.88]	[48.32]	[-54.08]	[17.68]	[36.33]	[29.73]	[29.737]
	EA			FB			GC			HD
F.E.M.	15x			15x			4.8x			40x
C.O.M.	3.35 - 2.06x			-10.15 - 1.28x			3.94 0.356x			- 2.063 -10.44x
Result	3.35 12.94x			-10.15 13.72x			3.94 5.16x			- 2.063 29.56x
	26.35			14.25			13.11			50.23
	[26.35]			[14.27]			[13.11]			[50.42]

$$\frac{10.05 + 23.83x - 30.45 + 26.17x}{20} + \frac{11.82 + 10.68x}{25} + \frac{-6.2 + 48.68}{15} = 10 \qquad x = 1.778$$

Multi-Story Frame.—To analyze this kind of Frame (Fig. 6), we must first compute the story ABCD on the assumption of joint EFGH being fixed, then release joint EFGH but regard IJKL as fixed. When we released the joint EFGH, must modify the stiffness of bars EA, FB, GF, and HD and compute the carry-over factor from each joint to the other joints. The purpose of these modifications is to separate the story ABCD from EFGH when the story EFGH is computed. The method of these modifications is to compute the end rotation constant of each column.[5] But it will soon be found that a great part of the work of computation has been included in the computation of the story ABCD.

When the computation from upper story down to bottom is finished, then the carry-over moments from bottom story to the uppermost are computed. The result is the computed moment plus the carry-over moment.

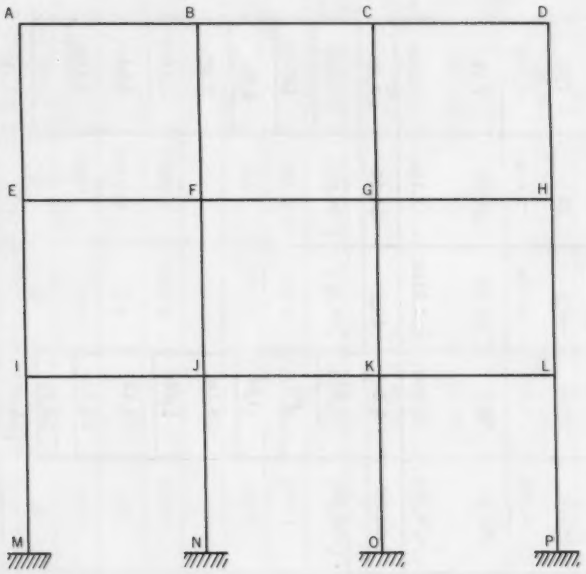

FIG. 6

Example 2.—This example (Fig. 7) is selected from the same source as that of example 1.[4] The computation of X is as follows:

$$-30.55 - 15.28 + 27.88 + 13.94 + 8.42 + 4.21 + (0.802 + 1.001 + 1.372 + 1.856 + 0.518 + 0.759)\,X = (4)(12)$$

$$X = \frac{39.38}{6.308} = 6.23$$

The procedure of this method coincides with the order of the following tables. Computation work of story ABC (Table 2) is exactly similar in every step, to example 1.

5 "Continuous Frame of Reinforced Concrete," by Hardy Cross, p. 117.

Computation of the modified stiffness of columns DA, EB, FC, and the carry over factor is shown in Table 3. When computing k'_{DA}, we applied unit moment at DA. The carry-over moment at joint A thus is equal to 0.5. This moment will be used with Table 2 to compute the unbalanced moment of other joints. The $(M^u)_\theta$ value in the tables denotes the unbalanced moment due to rotation only (excluding the moment due to side sway). This unbalanced moment can be computed from Table 2. For example, when we compute k'_{DA}

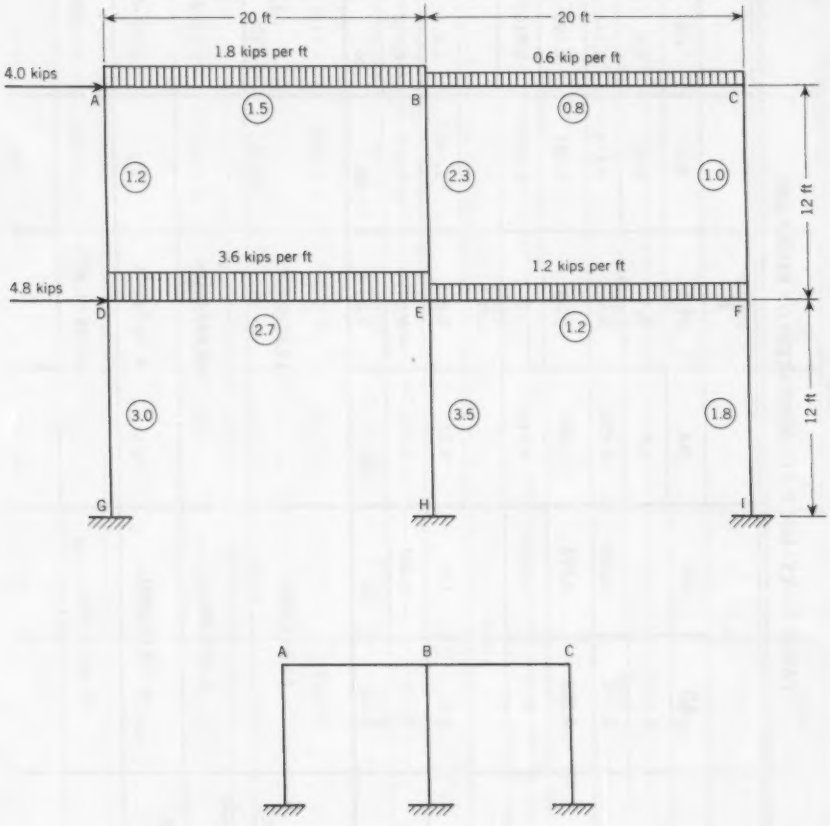

FIG. 7

the $(M^u)_\theta$ is equal to $0.5/M_{FA}$ times the first line of line (11) in Table 2, as $(M^u_A)_\theta = \frac{62.5}{2 \times 60} = 0.523$. The $(M^u)_\theta$ of joint DEF equals the $(M^u)_\theta$ of ABC times the carry over ratio as $(M^u_D) = 0.523\ (-0.222) = -0.116$.

The unbalanced moment due to the sway movement is independent of any external load; therefore, this part of M^u in Table 3 is taken from Table 2. The

TABLE 2.—EXAMPLE 2 COMPUTATION OF STORY ABC

①	Joint	A		B			C	
②	Bar	AD	AB	BA	BE	BC	CB	CF
③	k	1.2	1.5	1.5	2.3	0.8	0.8	1.0
④	D	0.444	0.556	0.326	0.5	0.174	0.444	0.556
⑤	K	0.222	0.278	0.163	0.25	0.087	0.222	0.278
⑥	KK	0	0.0453	0.0453	0	0.0193	0.0193	0
⑦	Jr	1.048		1.067			1.02	
⑧	α	1.0	1.0	1.02	1.0	1.048	1.0	1.0
⑨	Fc	- 0.222	- 0.283	- 0.163	- 0.25	- 0.087	- 0.232	- 0.278
⑩	F.E.M.	1.2x	60	-60	2.3x	20	-20	X
⑪ U.M. due to M_F	$M_A = {}^{60}_{+1.2x}$	62.8+1.258x		-17.81-0.357x			1.55+0.031x	
	$M_B = {}^{-40\ 2.3x}$	6.96-0.399x		-42.68+2.45x			3.71-0.213x	
	$M_C = {}^{-20\ x}$	-0.772+0.039x		4.73-0.236x			-20.4+1.02x	
⑫	Total U.M.	68.99+0.898x		-55.76+1.857x			-15.14+0.837x	

(13) U.M. of Bar		9.07 - 0.302x	-19.15 - 0.266x		3.36 - 0.186x	4.85 - 0.162x	
(14) Dist.	-30.55 - 0.398x	-38.4 - 0.499x	18.2 - 0.605x	27.88 - 0.928x	9.7 - 0.328x	6.72 - 0.355x	8.42 - 0.482x
(15) F. M.	-30.65 0.802x	30.67 - 0.811x	-61.03 - 0.871x	27.88 1.372x	33.06 - 0.509x	- 8.43 - 0.517x	8.42 0.518x
	-25.56	25.62	-66.46	36.45	29.89	-11.66	11.66
	DA			EB			FC
F. E. M.	1.2x			2.3x			x
C. O. M.	-15.28 - 0.199x			13.94 - 0.464x			4.21 - 0.241x
F. M.	-15.28 1.001x			13.94 1.856x			4.21 0.759x
	9.05			25.52			8.93

final M^u of joint D is equal to $1-(M^u)_\theta$ whereas the other joints are equal to $(M^u)_\theta$.

Using the bent equation to solve X yields

$$X + 1.0 + 0.5 + 3\left[(M^u_D)_\theta + (M^u_E)_\theta + (M^u_F)_\theta\right] = 0$$

$$X = \frac{-1.5 - 3\left[(M^u_D)_\theta + (M^u_E)_\theta + (M^u_F)_\theta\right]}{\Sigma}$$

whereas Σ equals the Σ in Table 2 $\Sigma = 6.308$ in the example.

The function k'_{DA} equals the final moment of D times the original stiffness of the bar DA, the carry-over factor (C.O.F.) from joint D to other joints is

TABLE 3.—MODIFIED STIFFNESS AND CARRY-OVER FACTOR

M = 1 at Bar DA $x = -\frac{1.252}{6.308} = -0.198$

	D (DA)	A	B	E (EB)	C	F (FC)
F. E. M.	1.0	0.5	0	0	0	0
$(M^u)_\theta$	-0.116	0.523	-0.1485	0.0371	0.0129	-0.0036
F. M.	0.884 1.001x	0.523 0.898x	-0.1485 1.857x	0.0371 1.856x	0.0129 0.837x	-0.0036 0.759x
	0.686	0.345	-0.5165	-0.331	-0.143	-0.1536
k'	0.825					
C. O. F.		0.502	-0.753	-0.482	-0.208	-0.224

M = 1 at Bar EB $x = -\frac{1.198}{6.308} = -0.19$

F. E. M.			0.5	1.0		
$(M^u)_\theta$	0.0194	-0.0871	0.532	-0.133	-0.0463	0.0129
F. M.	0.0194 1.001x	-0.0871 0.898x	0.532 1.857x	0.867 1.856x	-0.0463 0.837x	0.0129 0.759x
	-0.171	-0.257	0.18	0.515	-0.205	-0.131
k'				1.183		
C. O. F.	-0.332	-0.5	0.35		-0.398	-0.254

M = 1 at Bar Fc $x = -\frac{1.15}{6.308} = -0.182$

k'						0.715
C. O. F.	-0.26	-0.202	-0.644	0.434	0.5	

equal to the final moment of other joints in this table divided by the final moment of joint D, as

$$k'_{DA} = (0.686)\ (1.2),\ 0.52 = 0.345/0.686$$

In Table 4, the story DEF is computed. Lines (4) to (9) needs some explanation. From joint D to E, or from E to F there are two paths of carry over, DE and DAE. In this case, the total carry-over ratio between joint D and E

equals $K_{DE} + K_{DAE}$, $(KK)_{DE} = \left(K_{DE} + K_{DAE}\right)\left(K_{ED} + K_{EBD}\right)$ for example;

$$(KK)_{DE} = 0.146 \cdot 0.1103 = 0.0161.\ D^{J}R = 1.018 = 1/(1 - 0.00141 - 0.0161).$$

$$\alpha DAF = \frac{1}{(1-0.016)},\ \alpha DAE = \frac{1}{(1-0.00141-0.0325)}$$

and

$$\alpha DE = \frac{1}{(1-0.00141-0.00285)}$$

Because there are two paths of carry-over between joints D and E, there are, therefore, two continuity-factors ${}_{DE}F_{C}$ between those two joints. Thus,

$$M_{G}^{u} = \left({}_{DE}F_{C} + {}_{DAE}F_{C}\right) M_{D}^{u}$$

Similarly,

$$M_{E}^{u} = \left({}_{FE}F_{C} + {}_{FCE}F_{C}\right) M^{u}$$

The M^{u} of joint D and F in the second line of line (12) of Table 4 has two values. Behind each value there is a small letter that denotes the place from which the value comes. For example, 0.1 - 0.0064 X is the M_{D}^{u} that comes from joint F, $M_{D}^{u} = {}_{FAD}F_{C}\, M_{F}^{u}$. Thus, 0.1 - 0.0064X = (1.95 - 0.125 X) 0.051.

In Table 5 carry-over moments are computed, and the result of joint ABC is presented at the last line.

Line (3) of Table 5 is taken from Table 3. The distributed moment comes from Table 4. For example, the distributed moment of joint D, -18.66, equals line (15) of Table 4, (-14.7 - 0.34X), in which X = 1.088.

Line (4) denotes the M^{u} of each joint, and is equal to the distributed moment times the C.O.F. as: -9.37 = -18.66 0.502, 1.79 = 5.13; 0.35. and so forth.

Line (6) is the M^{u} of each bar. For example, -2.47 = -15.13 0.163, 3.38 = - (-12.15) 0.278. The M^{u} of AD equals -12.15 - (-2.47) = -9.68. M_{GB}^{u} = 15.18 -(3.38 - 0.53) = 12.88.

Care must be taken that there is no carry-over moment to joint DEF, after the distribution of the M^{u} at joints A,B, and C respectively; those carry-over moments were considered when the modified stiffness K' was computed.

Line (8) is equal to lines (6) + (7). Line (10) as a result is equal to line (8) plus line (9).

Example 3.—The main purpose of this example (Fig. 8) is to illustrate the computation of carry-over moment between two separate stories, GHI and ABC.

The upper two stories, ABC and DEF, are the same as example 2 it is not necessary to repeat the computation work here. Only the lower half of Table 8 must be explained. This part is to carry over the distributed moment of the upper half to joints ABC. Actually, these computations can combine with Table 5, and in practical analysis, Table 5 will be put in the last position.

The result of joints ABC is the carry-over moment in Table 8 plus the result of Table 5.

CONCLUSIONS

1. The great advantage of using continuity-factor, final position and the method of computing unbalanced moments to analyze a continuous frame is to eliminate the process of successive distributions and carry-over that which is

TABLE 4.—COMPUTATION OF STORY DEF

(1)	Joint	D				E					F			
(2)	Bar	DG	DA		DE	EH	ED	EB		EF	FE	FC		FI
			DAF	DAE				EBD	EBF			FCE	FCD	
(3)	k	3.0	0.825		2.7	3.5	2.7	1.183		1.2	1.2	0.715		1.8
(4)	D	0.46	0.1265		0.414	0.408	0.315	0.138		0.14	0.323	0.192		0.485
(5)	C.O.F.	0.5	-0.224	-0.482	0.5	0.5	0.5	-0.332	-0.254	0.5	0.5	-0.434	-0.26	0.5
(6)	K	0.23	-0.0283	-0.061	0.207	0.204	0.157	-0.0468	-0.035	0.07	0.1675	-0.083	-0.05	0.2435
				0.146			0.1102		0.035		0.0785			
(7)	KK	0	0.00141	0.0161		0	0.0197		0.00274		0.00274		0.00141	0
				0.00285	0.0325		0.0325	0.00285	0.0029	0.0113	0.0113	0.0029		
(8)	J_R	1.018				1.022					1.005			
(9)	α		1.015	1.025	1.005		1.008	1.035	1.03	1.022	1.004	1.012	1.002	
(10)	F_C		0.0284	0.0628	-0.209		-0.157	0.0481	0.0354	-0.0703	-0.165	0.0856	0.051	
(11)	F.E.M.	3x	-9.05		120	3.5x	-120	25.52		40	-40	8.93		1.8X
	U.M. due D=110.95/3x	112.9+3.054x				-16.5-0.446x					3.18+0.086x, 0.534+0.0144x } 3.714, +0.1004x			D, E
(12)	E=-54.48/3.5x	6.13-0.394x, 0.1-0.0064x } 6.23, -0.4x			E, F	-55.7+3.58x					1.95-0.125x, 0.16-0.01x } 2.11, -0.135x			E, D
	to M_F F=-31.07/1.8x	-1.59+0.0922x, -0.271+0.016x } -1.86, +0.108x				2.47-0.1435x					-31.2+1.81x			
(13)	Total U.M.	117.27+2.762x				-69.83+2.99x					-25.38+1.775x			
(14)	U.M. of Bar		-1.263	-3.26	10.93		-24.3	7.15	-2.1	4.09	4.88	-2.44	3.32	
			0.099x	0.14x	- 0.47x		- 0.573x	0.168x	+0.147x	--0.286x	- 0.209x	0.105x	0.08x	

⑮ Dist.	-54 - 1,27x	-14.8 - 0,35x	-48.47 - 1,142x	28,42 - 1,22x	22 - 0,942x	9,63 - 0,413x	9,76 - 0,418x	8,17 - 0,574x	4,86 - 0,341x	12,25 - 0,86x
⑯ Result	-54 1,73x	-28,37 - 0,111x	82,46 - 1,612x	28,42 2,28x	-122,3 - 1,523x	40,2 - 0,095x	53,85 - 0,704x	-26,95 - 0,783x	14,67 - 0,156x	2,25 0,94x
	-35,2	-29,58	64,94	53,22	-138,9	39,17	46,2	-35,45	12,97	22,45
	[-35,27]	[-29,6]	[64,94]	[53,31]	[-138,66]	[39,08]	[46,24]	[-35,44]	[13,06]	[22,38]
	GD			HE						IF
F.E.M.	3x			3,5x						1,8x
C.O.M.	-27 -0,635x			14,21 - 0,61x						6,125 - 0,43x
F. M.	-27 2,365x			14,21 2,89x						6,125 1,37x
	- 1,3			45,63						21,03
	[- 1,387]			[45,62]						[20,94]

$$-54-27+28,42+14,21+12,25+6,125$$
$$+(1,73+2,365+2,28+2,89+0,94+1,37)X$$
$$=(4+4,8)x12$$

$$X = \frac{125,6}{11,57} = 10,88$$

TABLE 5.—CARRY-OVER MOMENTS AND RESULTS

		A		B			C	
		AD	AB	BA	BE	BC	CB	CF
(1)	D	0.444	0.556	0.326	0.5	0.174	0.444	0.556
(2)	K	0.222	0.278	0.163	0.25	0.087	0.222	0.278
(3) C.O.F. from joint	D	0.502		-0.753			-0.208	
	E	-0.5		0.35			-0.398	
	F	-0.202		-0.644			0.5	
(4) U.M. due to Dist. Mom.	M_D=-18.66	-9.37		14.05			3.88	
	M_E=5.13	-2.56		1.79			-2.04	
	M_F=1.1	-0.222		-0.71			0.55	
(5)	Total U.M.	-12.15		15.13			2.39	
(6)	U.M. of Bar	- 9.68	- 2.47	3.38	12.88	- 0.53	- 1.32	3.71
(7)	Dist.	5.4	6.76	- 4.93	- 7.57	- 2.64	- 1.06	- 1.33
(8)	C.O.M.	- 4.28	4.29	- 1.55	4.71	- 3.17	- 2.38	2.38
(9)	Mom. from table 1	25.55	25.67	-66.46	36.45	29.89	-11.66	11.66
(10)	Result	-29.83	29.96	-68.01	41.16	26.72	-14.04	14.04
		[-30]	[30]	[-67.91]	[41.27]	[26.65]	[-14.26]	

TABLE 6.—MODIFIED STIFFNESS AND CARRY-OVER FACTOR

$M = 1$ at Bar GD $\quad x = -\frac{1.182}{11.57} = -0.102$

	GD	D	E	HE	F	IF
F. E. M.	1.0	0.5				
$(M^u)_\theta$	-0.117	0.509	-0.0745	0.0152	0.017	-0.0041
F. M.	0.983 2.354x	0.509 2.762x	-0.0745 2.99x	0.0152 2.89x	0.017 1.775x	-0.0041 1.37x
	0.743	0.227	-0.3785	-0.2788	-0.164	-0.144
k'	2.23					
C. O. F.		0.306	-0.51	-0.376	-0.221	-0.194

$M = 1$ at Bar HE $\quad X = -\frac{1.247}{11.57} = -0.108$

k'				2.39		
C. O. F.	-0.242	-0.514	0.277		-0.309	-0.21

$M = 1$ at Bar IF $\quad x = -\frac{1.138}{11.57} = -0.0985$

k'						1.52
C. O. F.	-0.282	-0.288	-0.396	-0.327	0.389	

needed in the method of conventional moment distribution and self-checking. For a complicated problem such as multi-bay, multi-story frames, one can stop the process of analysis anywhere without ending in confusion. Line (13) in Table 2, line (14) in Table 4 and Table 7 are all checking lines. If there is any mistake in the foregoing computation, these lines will indicate a need to check and prevent any further computation.

2. A multi-story frame that is analyzed by this method is reduced into several single bents; it becomes, therefore, possible to solve those problems without solving any simultanuous equations.

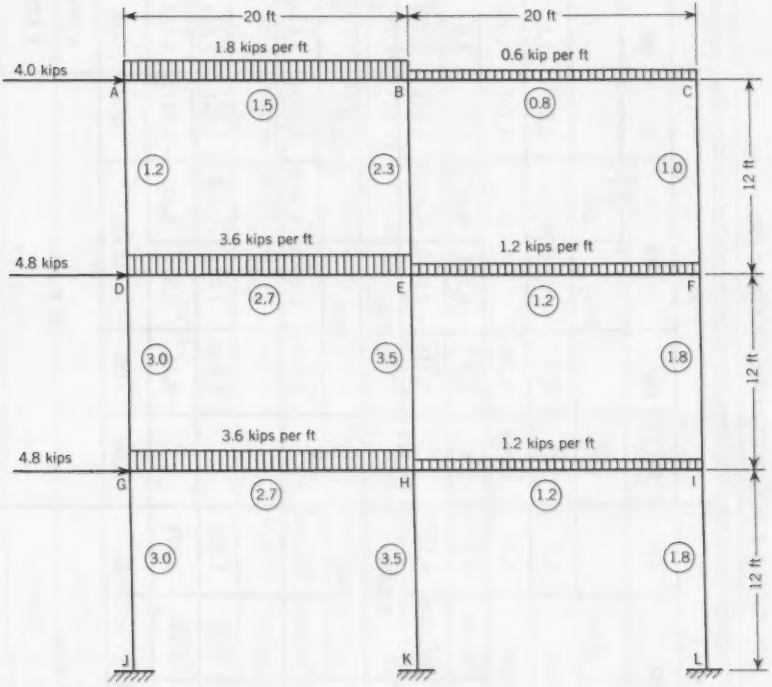

FIG. 8

3. In order to use the equations of J_R, α and F_C one must bear them in mind when the computation work is done. Those necessary memories will be helped by the table. One will find out that the table presents a clear working procedure.

4. Because small quantities have been dropped, as the rotation-ratio J_R was derived; the solution is therefore, only an approximate value.

APPENDIX . NOTATIONS

k : relative stiffness against rotation;

M_F : Fixed end moment;

TABLE 7.—COMPUTATION OF STORY GHI

① Joint	G				H					I				
② Bar	Gj	GD		GH	Hk	HG	HE		HI	IH	IF		II	
		GDI	GDH				HEG	HEI			IFH	IFG		
③ k	3.0	2.23		2.7	3.5	2.7	2.39		1.2	1.2	1.52		1.8	
④ D	0.379	0.281		0.34	0.358	0.276	0.244		0.122	0.266	0.336		0.398	
⑤ C.O.F.	0.5	-0.194	-0.376	0.5	0.5	0.5	- 0.242	-0.21	0.5	0.5	- 0.327	-0.282	0.5	
⑥ K	0.1895	-0.0545	-0.1055	0.17	0.179	0.138	- 0.0591	-0.0513	0.061	0.133	- 0.11	-0.095	0.199	
			0.0645			0.0789		0.01		0.023				
⑦ KK	0	0.0052	0.0051		0	0.0051		0.00023		0.00023		0.0052	0	
			0.0063	0.0234		0.0234	0.0063	0.0056	0.0081	0.0081	0.0056			
⑧ J_R	1.011					1.005				1.005				
⑨ α		1.005	1.03	1.015		1.009	1.023	1.013	1.011	1.011	1.034	1.001		
⑩ F_C		0.0544	0.108	- 0.171		- 0.14	0.061	0.052	- 0.0617	- 0.135	0.114	0.0957		
⑪ F.E.M.	3x	- 1.3		120	3.5x	-120	45.63		40	-40	21.03		1.8x	
U.M. G= 118.7/3x	120+3.033x				-7.55-0.191x					6.52+0.1645x / 0.073+0.0019x		6.593 +0.1664x		

(12) due to M_F	34.37 H= 3.5x	2.721-0.278x 0.032-0.003x	2.753 -0.28x			-34.5+3.52x				0.334-0.034x 0.148-0.015x	0.482 -0.049x		
	-18.97 I= 1.8x	-1.82+0.173x -0.032+0.002x	-1.852 +0.176x			0.4-0.038x				-19.05+1.81x			
(13) Total U.M.		120.9+2.928x				-41.65+3.291x				-11.975+1.927x			
(14) U.M. of Bar			-1.134 0.184x	-2.46 0.195x	5.75 -0.454x		-20.5 - 0.498x	12.72 0.309x	-1.312 0.212x	1.59 -0.256x	2.54 - 0.2x	- 2.135 0.169x	6.57 0.16x	
(15) Dist.	-45.7 - 1.11x	-33.9 - 0.822x		-41.2 - 0.995x	14.9 - 1.175x	11.5 - 0.908x	10.15 - 0.802x		5.06 -0.401x	3.18 - 0.513x	4.01 - 0.647x		4.75 - 0.765x	
(16) Result	-45.7 1.89x	-38.79 - 0.443x		84.55 - 1.449x	14.9 2.325x	-129 - 1.406x	67.19 - 0.281x		46.65 - 0.657x	-34.28 - 0.713x	29.48 - 0.318x		4.75 1.035x	
	-14	-46.23		60.25	54	-152.6	62.47		35.65	-46.23	24.14		22.1	
	jG				kH								lI	
F.E.M.	3x				3.5x								1.8x	
C.O.M.	-22.85 - 0.555x				7.45 0.588x	$X = \frac{202.1}{12.024} = 16.8$							2.38 0.383x	
F. M.	-22.85 2.445x				7.45 2.912x								2.38 1.417x	
	18.25				56.25								26.13	

TABLE 8.—CARRY-OVER

		D				E				
		DG	DA		DE	EH	ED	EB		EF
			DAF	DAE				EBD	EBF	
(1)	D	0.46	0.1265		0.414	0.408	0.315	0.138		0.14
(2)	K	0.23	-0.0283	-0.061	0.207	0.204	0.157	-0.0468	-0.035	0.07
(3) C.O.F. from joint	G	0.306				- 0.51				
	H	- 0.514				0.277				
	I	- 0.288				- 0.396				
(4) U.M. due to Dist. Mom.	M_{ED} =-47.7	-14.6				24.3				
	M_{HE} =-3.3	1.69				- 0.914				
	M_{IF} =-6.84	1.965				2.7				
(5)	Total U.M.	-10.95				26.09				
(6)	U.M. of Bar	- 8.513	0.443	1.22	- 4.1	2.396	2.265	-0.668	0.735	- 1.43
(7)	Dist.	5.03	1.384		4.53	-10.65	- 8.21	- 3.6		- 3.65
(8)	C.O.M.	- 3.48	3.047		0.43	13.31	- 5.945	- 3.533		- 5.08
(9)	Mom. from table 3	-35.2	-29.58		64.94	53.22	-138.9	39.17		46.2
(10)	Result	-38.68	-26.5		65.37	66.53	-144.85	35.64		41.12

C.O.M. : Carry-over moment;

M^u : Unbalanced Moment; for example, M^u_{ab}; unbalanced moment of joint A due to carry-over from joint B.

C.O.F. : Carry-over factor;

F. M. : Final moment;

D : Distribution factor;

K : Carry-over ratio, equal to D times C.O.F.;

J_R : Joint rotation-ratio;

α : Relative joint rotation ratio; for example, $_{AB}$ means the rotation ratio of a joint relative to joint B that is considered as fixed;

F_C : Continuity-Factor $_{AB}F_C$: The continuity-factor of bar AB in direction from A to B; and

Sign convention : Counterclockwise moment as positive, (member as free body).

MOMENT AND RESULT

	F			A		B			C	
	FE	FC	FI	AD	AB	BA	BE	BC	CB	CF
		FCE FCD								
	0,323	0,192	0,485	0,444	0,556	0,326	0,5	0,174	0,444	0,556
	0,1615	-0,083 -0,05		0,222	0,278	0,163	0,25	0,087	0,222	0,278
		- 0.221			0,502		-0,753			-0,208
		- 0.309			-0,5		0,35			-0,398
		0,389			-0,202		-0,644			0,5
		10,52			0,696		-1,041			-0,288
		1,02			1,8		-1,26			1,43
		- 2,68			0,343		1,09			-0,85
		8,86			2,839		-1,21			0,292
	- 1,825	0,913 -0,31	10,08	2,66	0,197	- 0,788	0,228	- 0,65	0,105	0,187
	- 2,86	- 1,7	- 4,3	- 1,26	- 1,57	0,394	0,605	0,21	- 0,128	- 0,164
	- 4,685	- 1,097	5,78	1,4	- 1,37	- 0,394	0,832	- 0,44	- 0,023	0,023
	-35,45	12,97	22,95	-29,83	29,96	-68,01	41,16	26,72	-14,04	14,04
	-40,14	11,87	28,23	-28,43	28,59	-68,4	41,99	25,28	-14,06	14,06

Journal of the
STRUCTURAL DIVISION
Proceedings of the American Society of Civil Engineers

CORRECTED DEFLECTION THEORY OF SUSPENSION BRIDGES

By John Szidarovszky[1]

SYNOPSIS

This paper presents a deflection theory of stiffened suspension bridges that considers several effects neglected in previous theories such as those due to shear force and due to elongation of the cable. Only the theory, and not a practical method of solution, is dealt with.

INTRODUCTION

This introduction refers to the theory only and not to the method of solution.

Notation.—The letter symbols adopted for use in this paper are defined and arranged alphabetically, for convenience of reference, in the Appendix.

Definitions.—Truss type stiffening truss and plate girder type stiffening girder are termed stiffening truss unless otherwise referred to; cable and chain will be termed cable unless otherwise referred to; dead load refers to loads causing no stress in the stiffening truss; live load refers to loads and effects producing stresses in the stiffening truss, such as moving load, temperature change and that part of dead load that causes stress in the stiffening truss; the horizontal component of the tensile force in the cable will be termed cable stress; the term cable stress increment refers to increase in cable stress due to live load; shear refers to vertical component of the resultant force acting on the left-hand side; unloaded position refers to the shape of the bridge when only dead load acts on it; loaded position refers to the shape of the bridge

Note.—Discussion open until April 1, 1961. To extend the closing date one month, a written request must be filed with the Executive Secretary, ASCE. This paper is part of the copyrighted Journal of the Structural Division, Proceedings of the American Society of Civil Engineers, Vol. 86, No. ST 11, November, 1960.

[1] Engr., Designing Office UVATERV, Budapest, Hungary.

under live load; and panel point refers to the vertical live of a hanger. In the coordinate system, the positive "x" and "ξ" point to the right, the positive y, η, and $\overline{\eta}$ point downwards. Loads are positive when acting downwards, moment is positive if its rotation is clockwise, and shear force is positive when pointing upwards.

Theory.—The first theory of the stiffened suspension bridge developed by Rankine[2] was developed on the assumption that the stiffening truss distributes the loads on the cable uniformly. Another method of analysis, the so-called Elastic Theory, assumes the shape of bridge under dead load and asserts that no stress develops in the stiffening truss due to dead load.

The main equation[3,4] of this theory (Fig. 1) for a two-hinged stiffening truss is

$$M = M_g - Hy \quad \ldots\ldots\ldots\ldots\ldots\ldots (1)$$

The cable stress increment is to be determined as redundant force, as in Eq. 3.

Based on the preceding assumption, the principle of superposition is valid.

Müller-Breslau[5] presented a differential equation taking into account the effect of vertical displacement of the cable. The basic differential equation of this so-called "Deflection Theory" is.[6]

$$M'' - \frac{H_w + H}{E\,J}\,M = M_g'' - H\,y'' \quad \ldots\ldots\ldots\ldots (2)$$

The cable stress increment is to be determined by equation

$$-\int y''\,\eta\,dx = \frac{H\,L_s}{E_c\,A_{cm}} + \omega\,t\,L_t \quad \ldots\ldots\ldots\ldots (3)$$

When developing Eqs. 2 and 3, assumptions were made as follows:

1. The distance between hangers is so small compared with the span that the hangers may be replaced by a screen.
2. The deformation of towers and hangers, as well as the displacement of anchorages due to live load and temperature change, may be neglected.
3. The deformation of stiffening truss due to shear and axial forces may be neglected.
4. The horizontal displacement of cable is to be neglected.
5. Extension of cable due to live load and temperature change may be neglected when analyzing bending moment.
6. Deflection of stiffening truss compared with cable ordinates may be neglected when analyzing cable stress increment.

H. Rode[7] took into consideration the effect of the horizontal displacement of cable on the bending moment, and presented a new differential equation as follows

$$M'' - \left[\left(1 + y'^2\right)\int \frac{H_w + H}{E\,J}\,M\,dx\right]' = M_g'' - H\,y'' \quad \ldots\ldots (4)$$

---

2 "The Stiffness of Suspension Bridges," by S. Timoshenko, Transactions, ASCE, Vol. 94, 1930, p. 377.

3 "The Theory and Practice of Modern Framed Structures," by Johnson, Bryan, and Turneaure, 10th ed., 1928.

4 "Theorie und Berechnung der Eisernen Brücken," by F. Bleich, 1924.

5 "Theorie der durch einen Balken versteiften Kette," by Müller-Breslau, 1881, Zeitschrift der Arch und Ing, Vereins zu Hannover.

6 "Theorie der eisernen Bogenbrücken und der Hängebrücken," by J. Melan, 1888.

7 "New Deflection Theory," by H. H. Rode, Kgl. Norske Videnskabers Selskabs Skrifter, 1930, Nr. 3.

Atkinson, Southwell[8] and Crosthwaite[9] simplified certain assumptions, but the accuracy of the result is in doubt.

The Deflection Theory was extended by Moisseiff and Turneaure[3] to cover the side spans, and generalized by D. B. Steinman[10] for continuous stiffening trusses.

Grüning[11] took into consideration the fact that individual hangers, and not a screen, are applied; he also considered the continuity of stiffening truss.

The main equations are:

for analyzing bending moment

$$M_k + (H_w + H)\eta_k = M_{gk} - H y_k \quad \ldots\ldots\ldots\ldots (5)$$

and

$$-\eta_{k-1} + 2\eta_k - \eta_{k+1} = \frac{a^2}{6E}\left[\frac{M_{k-1}}{J_k} + 2M_k\left(\frac{1}{J_k} + \frac{1}{J_{k+1}}\right) + \frac{M_{k+1}}{J_{k+1}}\right] \quad \ldots\ldots (6)$$

For determining cable stress increment

$$-\left(1 - \frac{H}{E_c A_{cm}}\right)y'' \sum_0^n \eta_k = \frac{H L_s}{E_c A_{cm}} \quad \ldots\ldots\ldots (7)$$

RELATIONS BETWEEN DEFLECTION AND FORCES

Relations between deflection and forces are to be investigated by consideration of the geometry of the loaded bridge.

For determining deflections due to external forces, cable stress increment, and temperature change these relations may be written:

1. Relation between the deflection of the stiffening truss and the forces acting on it;
2. Relation between cable deflection, on one hand, and external forces, cable stress increment and temperature change, on the other; and
3. relation between deflection of the cable and the stiffening truss.

The relations to be developed are equations referring to one panel, namely to a length between two hangers, or verticals. Therefore, the number of equations for each of the relations mentioned is equal to that of the panels. These three systems of equations, however, may be reduced to one system.

In general, the number of hangers is very great, and the lengths of individual members of the stiffening truss are very small compared to the span. Thus the effect of individual hangers may be substituted by that of distributed load, and the deflection and slope of the stiffening truss may be dealt with in much the same manner as those of the stiffening girder.

By this substitution, the systems of equations will turn into one differential equation.

Finally, after the relations between deflection, external forces, and cable stress increment have been developed, relations can be found between the cable

---

8 "On the Problem of Stiffened Suspension Bridges, and its Treatment by Relaxation Methods," by R. J. Atkinson and R. V. Southwell, J. Inst. Civ. Engrs., 1939.

9 "The Corrected Theory of the Stiffened Suspension Bridge," by Ch. D. Crosthwaite, J. I. Inst. Civ. Engrs., 1947.

10 "A Generalized Deflection Theory for Suspension Bridges," by D. B. Steinman, Proceedings, ASCE, 1934.

11 "Eisenbau," by Grüning, 1929.

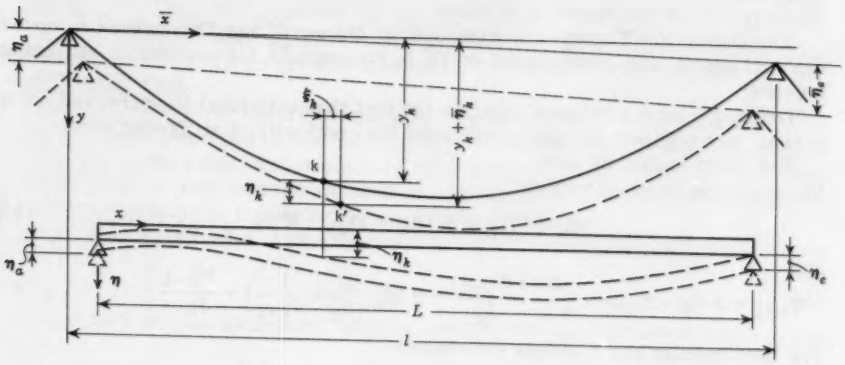

FIG. 1

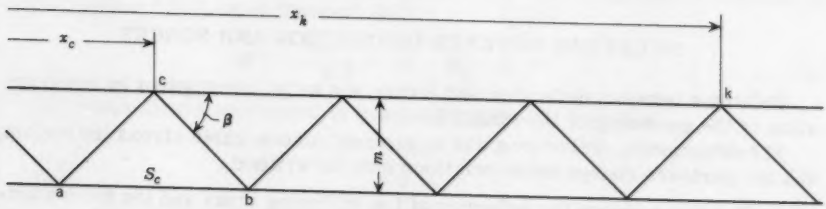

FIG. 2

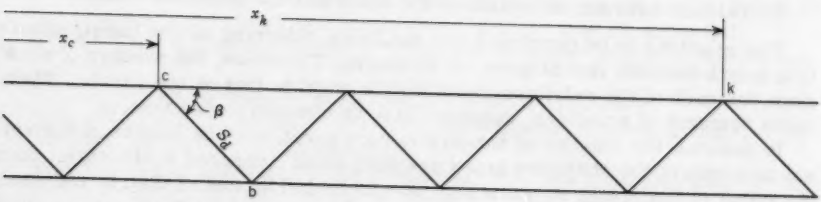

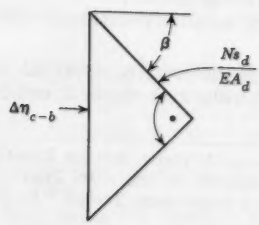

FIG. 3

stress increment, on the one hand, and the deflection of stiffening truss under live load and temperature change, on the other hand.

RELATION BETWEEN THE DEFLECTION OF STIFFENING TRUSS AND THE FORCES

The slope of a plate-girder type stiffening truss is

$$\kappa = -\int_0^x \frac{M}{E\,J}\,dx + \frac{M'}{E\,A_e} + \kappa_0 \qquad \ldots\ldots\ldots (8)$$

if the centroidal axis of the girder is horizontal and the flanges are parallel.

The vertical deflection is

$$\eta = -\iint_0^x \frac{M}{E\,J}\,dx\,dx + \int_0^x \frac{M'}{E\,A_e}\,dx + \kappa_0\,x + \eta_0 \qquad \ldots\ldots\ldots (9)$$

in which the value of A_e is to be determined by

$$\frac{1}{A_e} \sim \frac{E}{G\,A_{web}} \qquad \ldots\ldots\ldots\ldots\ldots (10)$$

In the following, the validity of a similar equation is proved and the value of A_e is determined for the truss type stiffening truss. The vertical deflection

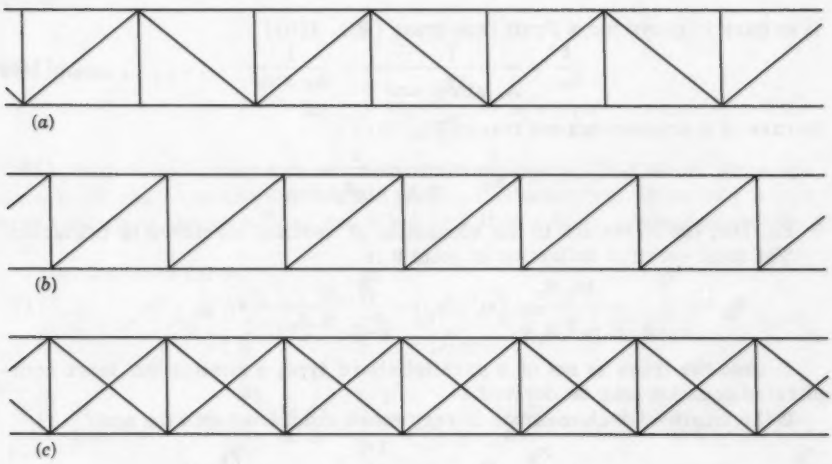

FIG. 4

of a truss-girder consists of two parts. One is the effect due to the change in length of chord members, the other one is to that of web members.

The chord member, marked a -b, elongates owing to the member force. This causes a deviation in angle at the "principal point" C, with the ordinate x_c, (Fig. 2). With parallel chord system, this elongation produces

$$\eta_{a\text{-}b} = \frac{N\,S_c}{E\,A_{ch}\,m}\,(x_k - x_c) = -\frac{-M_c\,S_c}{E\,A_{ch}\,m^2}\,(x_k - x_c) \qquad \ldots\ldots\ldots\ldots (11)$$

vertical deflection for point k with ordinate x_k.

Vertical deflection of point k, due to the elongation of all the upper and the lower chord members on the left, is

$$\eta_{ch} = -\sum_{x_c=0}^{x_k} \frac{M_c S_c}{E A_{ch} m^2} (x_k - x_c) \quad \ldots\ldots\ldots\ldots\ldots (12)$$

The vertical deflection of point k, due to the elongation of diagonal marked c-b (Fig. 3), is

$$\eta_{c\text{-}b} = \frac{N S_d}{E A_d \sin\beta} = \frac{M' r}{E A_d \sin^2\beta \cos\beta} \quad \ldots\ldots\ldots\ldots (13)$$

since

$$M' = V \quad \ldots\ldots\ldots\ldots\ldots\ldots\ldots (14)$$

The vertical deflection of point k, due to the elongation of all verticals and diagonals on the left, is

$$\eta_{web} = \sum_{0}^{x_k} \frac{M' r}{E A_e} \quad \ldots\ldots\ldots\ldots\ldots\ldots\ldots (15)$$

in which, in case of a Warren type truss (Fig. 4(a)).

$$\frac{1}{A_e} = \frac{1}{A_d \sin^2\beta \cos\beta} \quad \ldots\ldots\ldots\ldots (16a)$$

It is easy to prove for a Pratt type truss (Fig. 4(b)).

$$\frac{1}{A_e} = \frac{1}{A_d \sin^2\beta \cos\beta} + \frac{1}{A_v \sin\beta} \quad \ldots\ldots\ldots\ldots (16b)$$

In case of a counter-braced truss (Fig. 4(c)).

$$\frac{1}{A_e} = \frac{1}{2 A_d \sin^2\beta \cos\beta} \quad \ldots\ldots\ldots\ldots (16c)$$

In Eq. 16c, the effect due to the elongation of vertical members is neglected.

The total vertical deflection of point k is

$$\eta_k = -\sum_{x_c=0}^{x_k} \frac{M_c S_c}{E m^2 A_{ch}} (x_k - x_c) + \sum_{x=0}^{x_k} \frac{M' r}{E A_e} + \kappa_0 x_k + \eta_0 \quad \ldots\ldots (17)$$

In case the truss is not of a parallel chord type, a similar but more complicated equation may be derived.

If the length of each member is very small compared with the span

$$\sum_{x_c=0}^{x_k} \frac{M}{E m^2 A_{ch}} (x_k - x_c) = \iint_0^{x_k} \frac{M}{E m^2} \left[\frac{1}{A_{ct}} + \frac{1}{A_{cb}}\right] dx\, dx = \iint_0^{x_k} \frac{M}{EJ} dx\, dx \quad \ldots (18)$$

and

$$\sum_{0}^{x_k} \frac{M' r}{E A_e} = \int_0^{x} \frac{M' dx}{E A_e} \quad \ldots\ldots\ldots\ldots\ldots (19)$$

in which

$$\frac{1}{J} = \frac{1}{m^2} \left[\frac{1}{A_{ct}} + \frac{1}{A_{cb}}\right] \quad \ldots\ldots\ldots\ldots (20a)$$

J is termed moment of inertia of the stiffening truss.

In case $A_{cb} = A_{ct} = A_{ch}$

$$J = \frac{m^2 A_{ch}}{2} \quad \ldots\ldots\ldots\ldots\ldots\ldots (20b)$$

After Eqs. 18 and 19 have been substituted in Eq. 17, the result will be Eq. 9.

The difference between deflections of two succeeding panel points from Eqs. 9 and 17 is

$$\Delta\eta_k = \eta_k - \eta_{k-1} = -\, a_k \int_0^{x_{k-1}} \frac{M\,dx}{E\,J} - \iint_0^{a_k} \frac{M\,dz\,dz}{E\,J} + \int_0^{a_k} \frac{M'\,dz}{E\,A_e} + 0\,a_k \quad \ldots (21a)$$

or

$$\Delta\eta_k = -\, a_k \sum_1^{k-1} \frac{M_c\,S_c}{E\,m^2\,A_{ch}} - \sum_{z=0}^{a_k} \frac{M_c\,S_c\,(a_k - z)}{E\,m^2\,A_{ch}} + \sum_{z=0}^{a_k} \frac{M'\,r}{E\,A_e} + \kappa 0\,a_k \quad \ldots . (21b)$$

in which z is the distance from the left-hand panel point.

In the following, the bending moment will be expressed in terms of the shear force.

Live loads are supposed to be acting on panel points only. The bending moment in the stiffening truss between points i-1 and i (see Fig. 8) is

$$M_{(z)} = M_{i-1} + V_i\,z \quad \ldots\ldots\ldots\ldots\ldots (22)$$

Similarly

$$M_i = M_{i-1} + V_i\,a_i \quad \ldots\ldots\ldots\ldots\ldots\ldots (23)$$

From these

$$M_{(z)} = M_0 + \sum_{j=1}^{i-1} V_j\,a_j + V_i\,z \quad \ldots\ldots\ldots (24)$$

The shear force marked V_j is constant along panel k. This shear force appears in all the formulas for bending moment as indicated. When $i \geqslant j$ it is a term containing produce $V_j\,a_j$ and when $i = j$ it is a term containing product $V_i\,z$.

Thus, for plate girders

$$\int_0^{x_k} \frac{M}{E\,J}\,dx = M_0 \sum_{i=1}^{k-1} \int_0^{a_i} \frac{dz}{E\,J} + \sum_{j=1}^{k-1} V_j \quad a_j \sum_{i=j+1}^{k-1} \int_0^{a_i} \frac{dz}{E\,J} + \int_0^{a_i} \frac{z\,dz}{E\,J} \quad \ldots . (25a)$$

and

$$\iint_0^{a_k} \frac{M}{E\,J}\,dz\,dz = M_0 \iint_0^{a_k} \frac{dz\,dz}{E\,J} + \sum_{j=1}^{k-1} V_j\,a_j \iint_0^{a_k} \frac{dz\,dz}{E\,J} + V_k \iint_0^{a_k} \frac{z\,dz\,dz}{E\,J} \ldots (25b)$$

and for open web girder

$$\sum_1^{k-1} \frac{M_c\,S_c}{E\,m^2\,A_{ch}} = M_0 \sum_{i=1}^{k-1} \sum(i)\,\frac{S_c}{E\,m^2\,A_{ch}}$$

$$+ \sum_{j=1}^{k-1} V_j \left[a_j \sum_{i=j+1}^{k-1} \sum(i)\,\frac{S_c}{E\,m^2\,A_{ch}} + \sum(j)\,\frac{S_c\,z}{E\,m^2\,A_{ch}} \right] \ldots\ldots (26a)$$

and

$$\sum_{z=0}^{a_k} \frac{M_c\, S_c\,(a_k - z)}{E\, m^2\, A_{ch}} = M_0 \sum(k) \frac{S_c\,(a_k - z)}{E\, m^2\, A_{ch}}$$

$$+ \sum_{j=1}^{k=1} V_j\, a_j \sum(k) \frac{S_c\,(a_k - z)}{E\, m^2\, A_{ch}} + V_k \sum(k) \frac{S_c\,(a_k - z)\, z}{E\, m^2\, A_{ch}} \quad \ldots\ldots \quad (26b)$$

Substituting these into Eqs. 21a or 21b, the result will be

$$E\, J_0 \Delta\ \eta_k = - M_0 \left[b_k^2 + a_k \sum_{i=1}^{k-1} c_i \right] - \sum_{j=1}^{k-1} V_j \left[a_k \left(b_j^{*2} - a_j \sum_{i=j+1}^{k-1} c_i \right) + \right.$$

$$\left. + a_j\, b_k^2 \right] + V_k \left[r_k^3 - c_k^{*3} \right] + \kappa_0\, a_k\, E\, J_0 \quad \ldots\ldots\ldots\ldots \quad (27)$$

In case of an open-web-girder-type stiffening truss

$$b_k^2 = \sum(k) \frac{A_0\, S_c\,(a_k - z)}{A_{ch}} \quad \ldots\ldots\ldots\ldots\ldots \quad (28a)$$

$$c_i = \sum(i) \frac{A_0\, S_c}{A_{ch}} \quad \ldots\ldots\ldots\ldots\ldots\ldots \quad (28b)$$

$$b_j^{*2} = \sum(j) \frac{A_0\, S_c\, z}{A_{ch}} \quad \ldots\ldots\ldots\ldots\ldots\ldots \quad (28c)$$

$$c_k^{*3} = \sum(k) \frac{A_0\, S_c\,(a_k - z)\, z}{A_{ch}} \quad \ldots\ldots\ldots\ldots\ldots \quad (28d)$$

$$r_k^3 = \sum(k) \frac{A_0\, m^2\, r}{A_e} \quad \ldots\ldots\ldots\ldots\ldots\ldots \quad (28e)$$

and

$$J_0 = A_0\, m^2 \quad \ldots\ldots\ldots\ldots\ldots\ldots \quad (28f)$$

and A_0 is an average area of chord members chosen at random.

In case of a plate-girder-type stiffening truss

$$b_k^2 = \int_0^{a_k} \int \frac{J_0\, dz\, dz}{J} \quad \ldots\ldots\ldots\ldots\ldots \quad (29a)$$

$$c_i = \int_0^{a_i} \int \frac{J_0\, dz}{J} \quad \ldots\ldots\ldots\ldots\ldots\ldots \quad (29b)$$

$$b_j^{*2} = \int_0^{a_j} \frac{J_0\, z\, dz}{J} \quad \ldots\ldots\ldots\ldots\ldots \quad (29c)$$

$$c_k^{*3} = \int_0^{a_k} \int \frac{J_0\, z\, dz\, dz}{J} \quad \ldots\ldots\ldots\ldots \quad (29d)$$

and

$$r_k^3 = \int_0^{a_k} \frac{J_0\, dz}{A_e} \quad \ldots\ldots\ldots\ldots\ldots\ldots \quad (29e)$$

and J_0 is an average moment of inertia chosen at will.

If the moment of inertia of a plate-girder-type stiffening truss is constant along each panel

$$E\, J_0\, \Delta\eta_k = -\, M_0\, a_k \left(\frac{\bar{a}_k}{2} + \sum_{i=1}^{k-1} \bar{a}_i \right) - \sum_{j=1}^{k-1} V_j\, A_k \left(\frac{a_j\, \bar{a}_j}{2} + a_j \sum_{i=j+1}^{k-1} \bar{a}_i + \frac{a_k\, \bar{a}_k}{2} \right) +$$

$$+ V_k\, a_k \left[\frac{J_0}{A_e} - \frac{a_k\, \bar{a}_k}{6} \right] + \kappa_0\, a_k\, E\, J_0 \ldots\ldots\ldots \quad (30)$$

in which

$$\bar{a}_i = \frac{J_0\, a_i}{J_i} \quad \ldots\ldots\ldots\ldots\ldots\ldots\ldots\ldots \quad (31)$$

and when the inertia moment of a stiffening truss is constant all along the span, and the distribution of hangers is uniform $(a = a_i,\ J = J_0 = J_i)$

$$E\, J\, \Delta\eta_k = -\, M_0\, a^2 \left(k - \frac{1}{2} \right) - \sum_{j=1}^{k-1} V_j\, a^3\, (k - j)$$

$$+ V_k\, a^3 \left(\frac{J_0}{A_e\, a^2} - \frac{1}{6} \right) + \kappa_a\, \bar{a}\, E\, J \quad \ldots\ldots\ldots \quad (32)$$

RELATION BETWEEN CABLE DEFLECTION AND FORCES

The main part of dead load is suspended on the cable, and the stiffening truss is unstressed except by its own weight between two hangers. This latter effect is the same as that of a simple beam. It will be neglected in the following procedure, but it can be taken into account by a simple addition. This position will be called the unloaded position.

The vertical component of all internal forces in the section crossing panel k, is equal to the external forces on the left. So in unloaded position

$$V_{wk} = H_w\, t\, g\, \phi_k \quad \ldots\ldots\ldots\ldots\ldots\ldots \quad (33a)$$

and in loaded position

$$V_{wk} + V_{gk} = V_k + \left(H_w + H_k \right) t\, g\, \left(\phi_k + \alpha_k \right) \ldots\ldots \quad (33b)$$

The tangential angles are (Fig. 5 and 6)

$$t\, g\, \phi_k = \frac{\Delta\, y_k}{a_k} + \frac{q\, a_k}{2\, H_w} \quad \ldots\ldots\ldots\ldots\ldots\ldots \quad (34a)$$

$$t\, g\, \left(\phi_k + \alpha_k \right) = \frac{\Delta\, y_k + \Delta\, \bar{\eta}_k}{a_k^x} + \frac{q\, a_k}{2\, (H_w + H)} \quad \ldots\ldots\ldots\ldots \quad (34b)$$

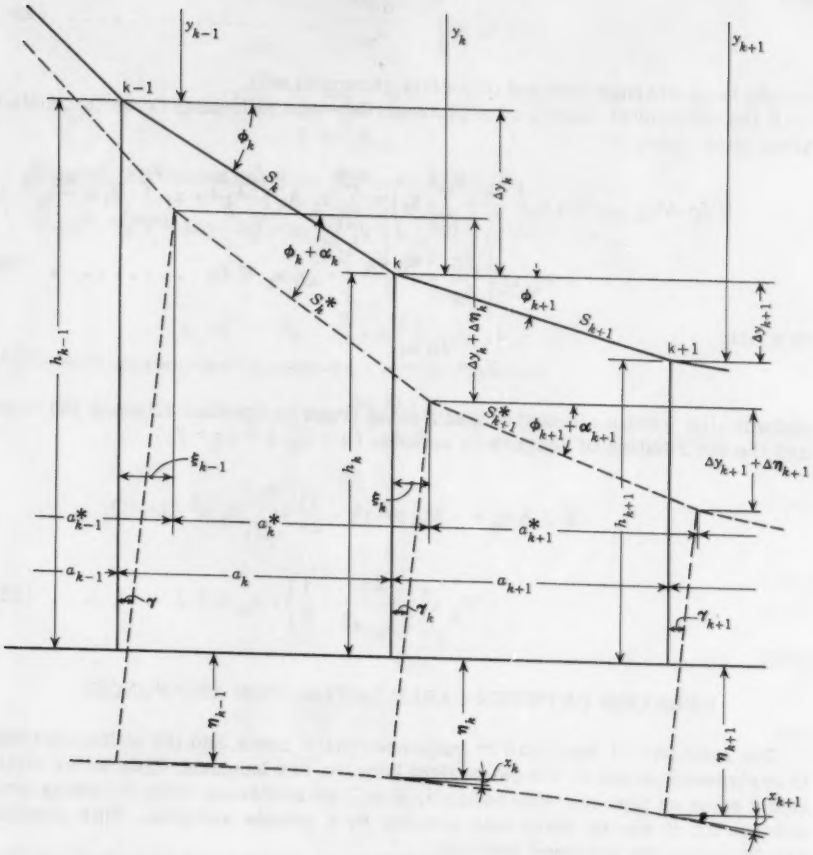
y_{k-1}
y_k
y_{k+1}
k−1
k
k+1
ϕ_k
S_k
Δy_k
$\phi_k + \alpha_k$
S_k^*
ϕ_{k+1}
S_{k+1}
Δy_{k+1}
h_{k-1}
$\Delta y_k + \Delta \eta_k$
S_{k+1}^*
$\phi_{k+1} + \alpha_{k+1}$
$\Delta y_{k+1} + \Delta \eta_{k+1}$
ξ_{k-1}
h_k
ξ_k
h_{k+1}
a_{k-1}^*
a_k^*
a_{k+1}^*
a_{k-1}
a_k
a_{k+1}
γ
γ_k
γ_{k+1}
η_{k-1}
η_k
η_{k+1}
ε_k
ε_{k+1}

FIG. 5

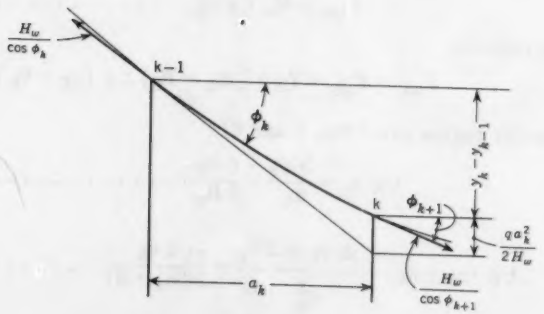
$\frac{H_\omega}{\cos \phi_k}$
k−1
ϕ_k
$y_k - y_{k-1}$
k
ϕ_{k+1}
$\frac{q a_k^2}{2 H_\omega}$
a_k
$\frac{H_\omega}{\cos \phi_{k+1}}$

FIG. 6

In the case of a chain, the last term vanishes. In these equations,

$$\Delta y_k = y_k - y_{k-1} \quad \ldots\ldots\ldots\ldots\ldots \quad (35a)$$

and

$$\Delta \bar{\eta}_k = \bar{\eta}_k - \bar{\eta}_{k-1} \quad \ldots\ldots\ldots\ldots\ldots \quad (35b)$$

From Eqs. 33 and 34, since $V = M'$:

$$M'_k + (H_w + H_k)\frac{\Delta y_k + \Delta \bar{\eta}_k}{a^x_k} = M'_{gk} + H_w \frac{\Delta y_k}{a_k} \quad \ldots\ldots\ldots \quad (36)$$

The horizontal distances a_k and a^*_k (Fig. 5) are

$$a_k = \left[S_k^2 - \Delta y_k^2\right]^{\frac{1}{2}} \quad \ldots\ldots\ldots\ldots\ldots \quad (37a)$$

and

$$a^x_k = \left[S^{x2}_k - (\Delta y_k + \Delta \bar{\eta}_k)^2\right]^{\frac{1}{2}} \quad \ldots\ldots\ldots \quad (37b)$$

S_k and S^*_k are distances between two adjacent joints in unloaded and loaded position, respectively.

Extension of cable due to H_k cable stress increment and to temperature change is

$$\Delta S_k = S^x_k - S_k = \left[\frac{1}{E_c A_{ck}}\left(\frac{H_w + H_k}{\cos(\phi_k + \alpha_k)} - \frac{H_w}{\cos \phi_k}\right) + \omega t\right] S_k \quad \ldots\ldots \quad (38)$$

Using Eq. 42 shown subsequently and neglecting smaller quantities

$$\frac{1}{\cos(\phi_k + \alpha_k)} = \frac{S^x_k}{a^x_k} \sim \frac{S_k}{a^x_k} \sim \frac{S_k}{a_k}\left(1 + \frac{\Delta y_k \Delta \bar{\eta}_k}{a_k^2} + \frac{\Delta \bar{\eta}_k^2}{2 a_k^2}\right) \quad \ldots\ldots\ldots\ldots \quad (39)$$

and

$$\Delta S_k = \left\{\frac{1}{E_c A_{ck} \cos \phi_k}\left[H_k + (H_w + H_k)\left(\frac{\Delta y_k \Delta \bar{\eta}_k}{a_k^2} + \frac{\Delta \bar{\eta}_k^2}{2 a_k^2}\right)\right] + \omega t\right\} S_k \quad \ldots (40)$$

Smaller quantities, such as the powers of $\Delta \bar{\eta}_k$ higher than $\Delta \bar{\eta}_k^2$ and those of ΔS_k, as well as the product $\Delta S_k \Delta \bar{\eta}_k$ are negligible and $\cos \phi_k$ is substituted for $\frac{a_k}{S_k}$. Thus

$$a^x_k = a_k \left\{1 - \frac{\Delta y_k \Delta \bar{\eta}_k}{a_k^2} - \frac{\Delta \bar{\eta}_k^2}{2 a_k^2}\left(1 + \frac{\Delta y_k^2}{a_k^2}\right) + \right.$$

$$\left. \frac{H_k + (H_w + H_k)\left(\frac{\Delta y_k \Delta \bar{\eta}_k}{a_k^2} + \frac{\Delta \bar{\eta}_k^2}{2 a_k^2}\right)}{E_c A_{ck} \cos^3 \phi_k} + \frac{\omega t}{\cos^2 \phi_k}\right. \quad \ldots\ldots\ldots \quad (41)$$

and

$$\frac{1}{a_k^x} = \frac{1}{a_k}\left\{1 + \frac{\Delta y_k \, \Delta \overline{\eta}_k}{a_k^2} + \frac{\Delta \overline{\eta}_k^2}{2\, a_k^2}\left(1 + \frac{3\, \Delta y_k^2}{a_k^2}\right) - \right.$$

$$\left. - \frac{H_k + (H_w + H_k)\left(\dfrac{\Delta y_k \, \Delta \overline{\eta}_k}{a_k^2} + \dfrac{\Delta \overline{\eta}_k}{2\, a_k^2}\right)}{E_c \, A_{ck} \cos^3 \phi_k} - \frac{\omega\, t}{\cos^2 \phi_k}\right\} \quad \ldots\ldots (42)$$

In deriving the Deflection Theory according to Müller-Breslau, a_k and a_k^* are taken as equal. Rode, developing his equation, neglected the effect of cable extension and the value of $\Delta \overline{\eta}_k^2$.

From Eqs. 36 and 42, having neglected the smaller quantities,

$$M_k' + (H_w + H_k)\frac{\Delta \overline{\eta}_k}{a_k}\left[1 + \frac{\Delta y_k^2}{a_k^2} + \frac{3}{2}\frac{\Delta y_k \, \Delta \overline{\eta}_k}{a_k^2}\left(1 + \frac{\Delta y_k^2}{a_k^2}\right)\right] =$$

$$= M_g' - H_k\left[1 - \frac{H_w + H_k}{E_c \, A_{cm}}\left(1 + p\,\frac{\Delta y_k^2}{a_k^2}\right)\right]\frac{\Delta y_k}{a_k} +$$

$$+ (H_w + H_k)\frac{\Delta y_k}{a_k}\omega\, t\left(1 + \frac{\Delta y_k^2}{a_k^2}\right) \quad \ldots\ldots\ldots\ldots (43)$$

as

$$\frac{1}{\cos^2 \phi_k} = 1 + t\, g^2 \phi_k = 1 + \frac{\Delta y_k^2}{a_k^2} \quad \ldots\ldots\ldots (44)$$

In case of chain

$$A_{ck} \sim \frac{A_{cm}}{\cos \phi_k} \quad \ldots\ldots\ldots\ldots\ldots (45)$$

and

$$\frac{1}{E_c \, A_{ck} \cos^3 \phi_k} \sim \frac{1 + \dfrac{\Delta y_k^2}{a_k^2}}{E_c \, A_{cm}} = \frac{1 + p\,\dfrac{\Delta y_k^2}{a_k^2}}{E_c \, A_{cm}} \quad \ldots\ldots\ldots (46)$$

and in case of cable

$$A_{ck} = A_{cm} \quad \ldots\ldots\ldots\ldots\ldots (47)$$

and

$$\frac{1}{E_c \, A_{ck} \cos^3 \phi_k} \sim \frac{1 + \dfrac{3}{2}\dfrac{\Delta y_k^2}{a_k^2}}{E_c \, A_{cm}} = \frac{1 + p\,\dfrac{\Delta y_k^2}{a_k^2}}{E_c \, A_{cm}} \quad \ldots\ldots\ldots (48)$$

In the case of a chain p = 1, in the case of a cable p = 3/2 = 1.5.

If a suspending screen is substituted for individual hangers, Eq. 42 will turn into

$$M' + (H_w + H)\bar{\eta}'\left[1 + y'^2 + 1.5\, y'\bar{\eta}'\left(1+y'^2\right)\right] = M'_g - H y'\left[1 - \right.$$

$$\left. - \frac{H_w + H}{E_c A_{cm}}\left(1 + p\, y'^2\right)\right] + (H_w + H) y' \omega t\left(1 + y'^2\right) \quad \ldots\ldots\ldots \quad (49)$$

For most of the suspension bridges, parts of the stiffening truss next to the supports are not suspended, for constructional and mechanical reasons. At these parts no hanger force arises, so $H = H_w = 0$, and the differential equation under Eq. 64 will be simplified along these parts into

$$M' = M'_g \quad \ldots\ldots\ldots\ldots\ldots\ldots \quad (50)$$

RELATION BETWEEN DEFLECTION OF THE CABLE AND THAT OF THE STIFFENING TRUSS

The hanger tension due to dead-load as per Fig. 7 is

$$S_{wk} = H_w\left(t\,g\,\phi_k - t\,g\,\phi_{k+1}\right) = H_w\left(\frac{\Delta y_k}{a_k} - \frac{\Delta y_{k+1}}{a_{k+1}}\right) \quad \ldots\ldots \quad (51)$$

That under live load is

$$S_{wk} + S_k \approx \left(H_w + H_k\right)\left[t\,g\left(\phi_k + \alpha_k\right) - t\,g\left(\phi_{k+1} + \alpha_{k+1}\right)\right] \quad \ldots\ldots \quad (52)$$

Its increment, owing to live load, based on Fig. 9, is

$$S_k = V_{k+1} - V_k + P_k \quad \ldots\ldots\ldots\ldots\ldots \quad (53)$$

Using Eq. 43, neglecting smaller quantities, and substituting η for $\bar{\eta}$, the hanger-force increment will be

$$S_k = \left(H_w + H_k\right)\left[\frac{\Delta \eta_k}{a_k}\left(1 + \frac{\Delta y_k^2}{a_k^2}\right)\right.$$

$$\left. - \frac{\Delta \eta_{k+1}^2}{a_{k+1}}\left(1 + \frac{\Delta y_{k+1}^2}{a_{k+1}^2}\right)\right] + H_k\left(\frac{\Delta y_k}{a_k}\,\frac{\Delta y_{k+1}}{a_{k+1}}\right) \quad \ldots\ldots\ldots \quad (54)$$

Namely,

$$V_{g(k+1)} = V_{gk} - P_k \quad \ldots\ldots\ldots\ldots\ldots \quad (55)$$

If the distance between two hangers is very small compared with the span

$$S = -\left(H_w + H\right) a\,\eta''\left(1 + y'^2\right) - H a\, y'' \quad \ldots\ldots\ldots \quad (56)$$

The vertical deflection of suspended points of the stiffening truss, when taking into account the elongation of hanger, is

$$\eta_k = \bar{\eta}_k + \left(\frac{S_k}{E\, A_{hk}} + \omega t\right) h_k \quad \ldots\ldots\ldots\ldots\ldots \quad (57)$$

And the difference

$$\Delta \bar{\eta}_k = \Delta \eta_k - \Delta \bar{\epsilon}_k \quad \ldots\ldots\ldots\ldots\ldots\ldots (58)$$

in which, based on Eq. 53,

$$\Delta \bar{\epsilon}'_k = h_k\left(\frac{V_{k+1} - V_k + P_k}{E\,A_{hk}} + \omega t\right) - h_{k-1}\left(\frac{V_k - V_{k-1} + P_{k-1}}{E\,A_{hk-1}} + \omega t\right) \ldots (59)$$

when $1 < k < n$, and

$$\Delta \bar{\epsilon}_1 = \bar{\eta}_0 - \eta_0 + h_1\left(\frac{V_2 - V_1 + P_1}{E\,A_{h1}} + \omega t\right) \quad \ldots\ldots\ldots (60)$$

$$\Delta \bar{\epsilon}_n = \eta_n - \bar{\eta}_n - h_{n-1}\left(\frac{V_n - V_{n-1} + P_{n-1}}{E\,A_{h(n-1)}} + \omega t\right) \quad \ldots\ldots\ldots (61)$$

From Eqs. 54 and 57

$$\eta_k = \bar{\eta}_k + \frac{h_k}{E\,A_{hk}}\left\{(H_w + H_k)\left[\frac{\Delta \eta_k}{a_k}\left(1 + \frac{\Delta y_k^2}{a_k^2}\right)\right.\right.$$

$$\left.\left. - \frac{\Delta_{k+1}}{a_{k-1}}\left(1 + \frac{\Delta y_{k+1}^2}{a_{k-1}^2}\right)\right] + H_k\left(\frac{\Delta y_k}{a_k} - \frac{\Delta y_{k+1}}{a_{k+1}}\right)\right\} + \omega t\, h_k \quad \ldots\ldots\ldots (62)$$

When a screen is substituted for individual hangers, Eq. 54 will turn into

$$\eta = \bar{\eta} - h\left[a\,\frac{(H_w + H)(1 + y'^2)\,\eta'' + H y''}{E\,A_h} - \omega t\right] \ldots (63)$$

SYSTEM OF EQUATIONS FOR DETERMINING SHEAR FORCES

Relation between the deflection of stiffening truss and the forces, as well as that between cable deflection and forces, and finally that between the deflection of cable and stiffening truss has been deduced.

Eqs. 27 and 58, being substituted into Eq. 43, the principal system of equations of stiffened suspension bridges for determining shear forces is as follows:

$$V_k\left[1 + \mu_k\left(r_k^3 - c_k^{*3}\right)\right] - \sum_{j=1}^{k-1} V_j\left[a_k\left(b_j^{*2} - a_j \sum_{i=j+1}^{k-1} c_i\right) + a_j\, b_k^2\right]\mu_k -$$

$$- M_0\left(b_k^2 + a_k \sum_{i=1}^{k-1} c_i\right)\mu_k + a_k\, E\, J_0\, \mu_k\, \kappa_0 - E\, J_0\, \mu_k\, \Delta\epsilon_k = V_{gk} - H_k\,\frac{\Delta y_k}{a_k}\left[1 -\right.$$

$$\left. - \frac{H_w + H_k}{E_c\, A_{cm}}\left(1 + p\,\frac{\Delta y_k^2}{a_k^2}\right) + (H_w + H)\frac{\Delta y_k}{a_k}\omega t\left(1 + \frac{\Delta y_k^2}{a_k^2}\right)\right. \quad \ldots\ldots\ldots (64)$$

in which

$$\mu_k = \left[1 + \frac{\Delta y_k^2}{a_k^2} + \frac{3}{2}\frac{\Delta y_k \Delta \bar{\eta}_k}{a_k^2}\left(1 + \frac{\Delta y_k}{a_k^2}\right)\right]\frac{H_w + H_k}{a_k E J_0} \quad \ldots (65)$$

If the moment of inertia of a plate-girder-type stiffening truss is constant along each panel,

$$V_k\left[1 + \rho_k\left(\frac{J_0}{A_e} - \frac{a\,\bar{a}_k}{6}\right)\right] - \sum_{j=1}^{k-1} V_j\left(\frac{a_j \bar{a}_j}{2} + a_j \sum_{i=j+1}^{k-1} \bar{a}_i + \frac{a_k \bar{a}_k}{2}\right)\rho_k -$$

$$- M_a\left(\frac{a_k}{2} + \sum_{i=1}^{k-1} \bar{a}_i\right)\rho_k + E J_0 \rho_k \kappa_0 - E J_0 \rho_k \frac{\Delta \bar{\epsilon}_k}{a_k} = V_{gk} -$$

$$-H_k \frac{\Delta y_k}{a_k}\left[1 - \frac{H_w + H_k}{E_c A_{cm}}\left(1 + P\frac{\Delta y_k^2}{a_k^2}\right) + \left(H_w + H_k\right)\frac{\Delta y_k}{a_k}\omega t\left(1 + \frac{\Delta y_k^2}{a_k^2}\right)\right. \quad (66)$$

in which

$$\rho_k = \left[1 + \frac{\Delta y_k^2}{a_k^2} + \frac{3}{2}\frac{\Delta y_k \Delta \bar{\eta}_k}{a_k^2}\left(1 + \frac{\Delta y_k^2}{a_k^2}\right)\right]\frac{H_w + H_k}{E J_0} \quad \ldots\ldots (67)$$

And finally, when the moment of inertia of a stiffening truss is constant all along the span and the distribution of hangers is uniform

$$V_k\left[1 + \rho_k a^2\left(\frac{J}{A_c a^2} - \frac{1}{6}\right)\right] - \sum_{j=1}^{k-1}{}' V_j a^2(k-j)\rho_k - M a\left(k - \frac{1}{2}\right)\rho_k +$$

$$+ E J_0 \rho_k \kappa_0 - E J_0 \frac{\rho_k}{a}\Delta \bar{\epsilon}_k = V_{gk} -$$

$$-H_k \frac{\Delta y_k}{a}\left[1 - \frac{H_w + H_k}{E_c A_{cm}}\left(1 + \rho\frac{\Delta y_k^2}{a^2}\right)\right] + \left(H_w + H_k\right)\frac{\Delta y_k}{a}\omega t\left(1 + \frac{\Delta y_k^2}{a^2}\right) \ldots (68)$$

DIFFERENTIAL EQUATION FOR DETERMINING THE INTERNAL FORCES ON THE SUSPENDED SECTION

A differential equation of deflection of the stiffening truss, another differential equation of cable deflection, and a third giving relation between deflection of cable and that of stiffening truss are given in Eqs. 9, 49, and 63.

From Eq. 9

$$\eta'' = -\frac{M}{E J} \quad \ldots\ldots\ldots\ldots\ldots\ldots (69)$$

This value substituted into Eq. 63 and the result into Eq. 9 gives

$$\bar{\eta}' = -\int \frac{M}{E\,J}\,dx + \frac{M'}{E\,A_e} - \left\{\left[-a\,\frac{(H_w+H)(1+y'^2)}{E\,A_h}\,\frac{M}{E\,J} + a\,\frac{H\,y''}{E\,A_h} - \omega\,t\right]H\right\}' + \kappa_0 \quad . . (70)$$

But

$$y = h_m - h \quad \ldots\ldots\ldots\ldots\ldots\ldots\ldots\ldots \quad (71)$$

$$y' = -\,h' \quad \ldots\ldots\ldots\ldots\ldots\ldots\ldots\ldots \quad (72)$$

$$\left(\frac{H\,h\,a\,y''}{E\,A_h}\right)' \sim -\,\frac{H\,a\,y'\,y''}{E\,A_h} \quad \ldots\ldots\ldots\ldots\ldots \quad (73)$$

and

$$\left(\frac{h\,a}{A_h\,J}\right)' \sim -\,\frac{a\,y'}{A_h\,J} \quad \ldots\ldots\ldots\ldots\ldots\ldots\ldots \quad (74)$$

After substituting Eqs. 72, 73, and 74 into Eq. 64 and the result into Eq. 49, neglecting smaller quantities, and substituting η for $\bar{\eta}$ there is obtained the basic differential equation of suspension bridges:

$$M'\left[1 + \frac{(H_w+H)(1+y'^2)}{E\,J}\left(\frac{J}{A_e} + \frac{(H_w+H)(1+y'^2)}{E\,J}\,\frac{h\,a\,J}{A_h}\right) -\right.$$

$$\left. - M(H_w+H)(1+y'^2)\left[\frac{(H_w+H)(1+y'^2)}{E\,J}\,\frac{a\,h}{E\,A_h}\right]'\right. -$$

$$-\int \frac{M}{E\,J}\,dx\left\{(H_w+H)\left[1+y'^2+1.5\,y'\,\eta'\,(1+y'^2)\right]\right\} = M_g' - H\,y'\left[1 -\right.$$

$$\left. - \frac{H_w+H}{E_c\,A_{cm}}\,(1+p\,y'^2) + \frac{(H_w+H)y''\,a}{E\,A_h}\right] - (H_w+H)\left[1+y'^2+1.5\,y'\,\eta'\,(1+y'^2)\right]\kappa_0 \quad . . \quad (75)$$

The terms of Eq. 75 will be examined separately. First consider the left-hand side. In the coefficient of M', after having multiplied, M' is the shear to be determined,

$$M'\,\frac{(H_w+H)(1+y'^2)}{E\,A_e}$$

expresses the effect of shear force, and

$$M'\,\frac{(H_w+H)^2(1+y'^2)^2\,h\,a}{E\,J\,E\,A_h}$$

is the first part of the effect due to the elastic elongation of hangers. The moment M multiplied by its coefficient is the second part due to the elastic elongation of hangers. As the effect of the elastic elongation of hangers is very small, except for very long bridges, it is negligible.

$$\int \frac{M}{E\,J}\,dx\,\left[H_w+H\right]$$

is the effect of the vertical deflection of the stiffening truss. This term occurs in the well-known Deflection Theory, given in Eq. 2,

$$\int \frac{M}{E\,J}\,dx\,\left[H_w+H\right]y'^2$$

is used in Rode's theory, it is due to the horizontal deflection of the cable.

$$\int \frac{M}{E\,J}\,dx\,\left[H_w+H\right]\;1.5\;y'\,\bar{\eta}'\,\left(1+y'^2\right)$$

is very small, and it also derives from the horizontal deflection of the cable. In this term,

$$\bar{\eta}' \sim -\int \frac{M}{E\,J}\,dx+\kappa_0$$

may be substituted. On the right-hand side M_g' is the shear on a simple beam. The term H_y' occurs in the Elastic Theory indicated in Eq. 1 and

$$H\,y'\,\frac{H_w+H}{E_c\,A_{cm}}\left(1+p\,y'^2\right)$$

expresses the effect of the elastic elongation of cable under cable stress increment.

$$\frac{H\left(H_w+H\right)y'y''a}{E\,A_h}$$

is the third part due to elongation of hangers under cable stress increment. The third term of the right-hand side, that contains κ_0, is nearly constant.

The effect of temperature change does not appear in Eq. 75. The reason for it is that all along the bridge the amount of vertical elongation of the cable and the hangers due to temperature change is constant. The temperature change causes, however, a relative settlement of supports affecting the intermediate joints of the stiffening truss, and the relative temperature of cable and hangers cause stresses in the stiffening truss, so careful consideration of this effect is to be taken in the numerical calculation.

RELATION BETWEEN THE CABLE STRESS INCREMENT AND THE DEFLECTION OF THE STIFFENING TRUSS AND THE TEMPERATURE CHANGE

Distance between anchorages in unloaded position is

$$D=\sum_{1}^{i}\sum_{k+1}^{n}a_k \qquad \ldots\ldots\ldots\ldots\ldots\ldots\ldots\ldots \quad (76)$$

The first Σ refers to every span and the second to every panel.

A change in distance between anchorages will take place owing to change in the cable stress and the temperature. This new distance is

$$D + d + \delta\, H_c + \epsilon t = \sum_{1}^{i} \sum_{k=1}^{n} a_k{}^x \quad \ldots\ldots\ldots\ldots (77)$$

Eqs. 41 and 76 substituted into Eq. 77 give

$$d + \delta\, H_0 + \epsilon t = \sum_{1}^{i} \left[-\sum_{k=1}^{n} \frac{\Delta y_k\, \Delta \bar{\eta} k}{a_k} - \sum_{k=1}^{n} \frac{\Delta \bar{\eta}_k{}^2}{2\, a_k} \left(1 + \frac{\Delta y_k{}'^2}{a_k{}^2} \right) \right. +$$

$$\left. + \sum_{k=1}^{n} \frac{H_k + (H_w + H_k) \left(\frac{\Delta y_k + \Delta \bar{\eta}_k}{a_k{}^2} + \frac{\Delta \bar{\eta}_k{}^2}{2\, a_k{}^2} \right)}{E_c\, A_{ck} \cos^3 \phi_k} a_k + \omega\, t \sum_{k=1}^{n} \frac{a_k}{\cos^2 \phi_k} \right] \quad \ldots\ldots (78)$$

Considering that

$$\sum_{k=1}^{n} \frac{\Delta y_k\, \Delta \bar{\eta}_k}{a_k} = -\sum_{k=1}^{n-1} \left(\frac{y_{k+1} - y_k}{a_{k+1}} - \frac{y_k - y_{k-1}}{a_k} \right) \bar{\eta}_k + \frac{\Delta y_n}{a_n} \bar{\eta}_n -$$

$$- \frac{\Delta y_1}{a_1} \bar{\eta}_0 = -\sum_{k=1}^{n-1} \left(\frac{\Delta y_{k+1}}{a_{k+1}} - \frac{\Delta y_k}{a_k} \right) \bar{\eta}_k + \frac{\Delta y_n}{a_n} \bar{\eta}_n - \frac{\Delta y_1}{a_1} \bar{\eta}_0 \quad \ldots\ldots\ldots (79)$$

Similarly,

$$\sum_{k=1}^{n} \frac{\Delta \bar{\eta}_k{}^2}{a_k} = -\sum_{k=1}^{n-1} \left(\frac{\Delta \bar{\eta}_{k+1}}{a_{k+1}} - \frac{\Delta \bar{\eta}_k}{a_k} \right) \bar{\eta}_k + \frac{\Delta \bar{\eta}_n}{a_n} \bar{\eta}_n - \frac{\Delta \bar{\eta}_1}{a_1} \bar{\eta}_0 \quad \ldots\ldots (80)$$

and

$$W_1 = \sum_{1}^{i} \sum_{k=1}^{n} \left(\frac{\Delta y_k\, \Delta \bar{\eta}_k}{a_k} + \frac{\Delta \bar{\eta}_k{}^2}{2\, a_k} \right) = -\sum_{1}^{i} \left(\sum_{k=1}^{n-1} \left[\frac{\Delta y_{k+1}}{a_{k+1}} - \frac{\Delta y_k}{a_k} + \right. \right.$$

$$\left. \left. + \frac{\Delta \bar{\eta}_{k+1}}{2\, a_{k+1}} - \frac{\Delta \bar{\eta}_k}{2\, a_k} \right] \bar{\eta}_k + \left(\frac{\Delta y_n}{a_n} + \frac{\Delta \bar{\eta}_n}{2\, a_n} \right) \bar{\eta}_n - \left(\frac{\Delta y_1}{a_1} + \frac{\Delta \bar{\eta}_1}{2\, a_1} \right) \bar{\eta}_0 \right) \quad \ldots (81)$$

But mostly, except a few special cases,

$$\bar{\eta}_0 = \bar{\eta}_n = 0 \quad \ldots\ldots\ldots\ldots\ldots (82)$$

therefore, the value of the last two terms of the preceding equations are zero.

Based on Eqs. 46 and 48

$$\sum_{k=1}^{n} \frac{H_k\, a_k}{E_c\, A_{ck} \cos^3 \phi_k} \sim H_a \sum_{k=1}^{n} \frac{a_k}{E_c\, A_{ck} \cos^3 \phi_k} + \sum_{k=1}^{n} \frac{\Delta H_k \left(1+p \frac{\Delta y_k^2}{a_k^2}\right)}{E_c\, A_{cm}}\, a_k \quad \ldots (83)$$

and

$$\sum_{k=1}^{n} \frac{H_w + H_k}{E_c\, A_{ck} \cos^3 \phi_k} \left(\frac{\Delta y_k\, \Delta \bar{\eta}_k}{a_k} + \frac{\Delta \bar{\eta}_k^2}{2\, a_k}\right) \sim \sum_{k=1}^{n} \frac{H_w + H_a}{E_c\, A_{cm}} \left(\frac{\Delta y_k\, \Delta \bar{\eta}_k}{a_k} + \frac{\Delta \eta_k^2}{2\, a_k}\right)$$

$$\left(1 + p \frac{\Delta y_k^2}{a_k^2}\right) + \sum_{k=1}^{n} \frac{\Delta H_k}{E_c\, A_{cm}} \left(1 + p \frac{\Delta y_k^2}{a_k^2}\right) \left(\frac{\Delta y_k\, \Delta \bar{\eta}_k}{a_k} + \frac{\Delta \bar{\eta}_k^2}{2\, a_k}\right) \ldots . (84)$$

Applying the symbols

$$L_s = \sum_{1}^{i} \sum_{k=1}^{n} \frac{A_{cm}\, a_k}{A_{ck} \cos^3 \phi_k} - \delta\, E_c\, A_{cm} \quad \ldots \ldots \ldots \ldots (85)$$

and

$$L_t = \sum_{1}^{i} \sum_{k=1}^{n} \frac{a_k}{\cos^2 \phi_k} - \frac{\epsilon}{\omega} \quad \ldots \ldots \ldots \ldots \ldots \ldots (86)$$

From Eqs. 78, 83, 84, 85 and 86, after having neglected smaller quantities, Eq. 87 results.

$$d + \delta\, \Delta H_0 = \frac{H_a}{E_c\, A_{cm}} \left\{ L_s + \sum_{1}^{i} \sum_{k=1}^{n} \left[\left(\frac{\Delta y_k\, \Delta \bar{\eta}_k}{a_k} + \frac{\Delta \bar{\eta}_k^2}{2\, a_k} \right) \left(1+p \frac{\Delta y_k^2}{a_k^2} \right) \right] \right\} +$$

$$+ \frac{1}{E_c\, A_{cm}} \sum_{1}^{i} \sum_{k=1}^{n} \Delta H_k \left(1+p \frac{\Delta y_k^2}{a_k^2}\right) a_k + \frac{H_w}{E_c\, A_{cm}} \sum_{1}^{i} \sum_{k=1}^{n} \left(1+p \frac{\Delta y_k}{a_k^2}\right)$$

$$\left(\frac{\Delta y_k\, \Delta \bar{\eta}_k}{a_k} + \frac{\Delta \bar{\eta}_k^2}{2\, a_k} \right) + L_t\, \omega\, t - \sum_{1}^{i} \sum_{k=1}^{n} \left(\frac{\Delta y_k\, \Delta \bar{\eta}_k}{a_k} + \frac{\Delta \bar{\eta}_k^2}{2\, a_k} \right) \ldots . (87)$$

Based on Eq. 76 and using

$$W_2 = \sum_{1}^{i} \sum_{k=1}^{n} \left(\frac{\Delta y_k\, \Delta \bar{\eta}_k}{a_k} + \frac{\Delta \bar{\eta}_k^2}{2\, a_k} \right) \left(1+p \frac{\Delta y_k^2}{a_k^2}\right) \quad \ldots \ldots \ldots (88)$$

and

$$W_3 = \sum_{1}^{i} \left[\sum_{k=1}^{n} \Delta H_k \left(1+p \frac{\Delta y_k^2}{a_k^2}\right) a_k \right] - \delta\, \Delta H_a\, E_c\, A_{cm} \quad \ldots \ldots (89)$$

the H_a average cable stress increment is defined as

$$W_3 = 0 \quad \ldots \ldots \ldots \ldots \ldots \ldots \ldots (90)$$

so that

$$H_a = \frac{W_1 - L_t\,\omega\,t + a - \dfrac{H_w}{E_c\,A_{cm}}\,W_2}{L_s + W_2}\,E_c\,A_{cm} \quad \ldots\ldots\ldots\ldots (91)$$

If a suspending screen is assumed:
in case of chain

$$L_s = \sum_1^i \int_0^{\bar{l}} \frac{d\bar{x}}{\cos^2\phi} - \delta\,E_c\,A_{cm} \quad \ldots\ldots\ldots\ldots\ldots (92)$$

in case of cable

$$L_s = \sum_1^i \int_0^{\bar{l}} \frac{d\bar{x}}{\cos^3\phi} - \delta\,E_c\,A_{cm} \quad \ldots\ldots\ldots\ldots\ldots (93)$$

And both in the case of cable and chain

$$L_t = \sum_1^i \int_0^{\bar{l}} \frac{d\bar{x}}{\cos^2\phi} - \frac{\epsilon}{\omega} \quad \ldots\ldots\ldots\ldots\ldots\ldots (94)$$

$$W_1 = -\sum_1^i \int_0^{\bar{l}} y''\bar{\eta}\,d\bar{x} + \frac{1}{2}\int_0^{\bar{l}} \bar{\eta}''\,\bar{\eta}\,d\bar{x} + \left(y_n' + \frac{\eta_n'}{2}\right)\bar{\eta}_n - \left(y_1' + \frac{\bar{\eta}_1'}{2}\right)\bar{\eta}_0 \quad \ldots (95)$$

$$W_2 = \sum_1^i \left[\int_0^{\bar{l}} \left(y' + \frac{\bar{\eta}'}{2}\right)\bar{\eta}'\,\left(1+p\,y'^2\right)d\bar{x}\right] \quad \ldots\ldots\ldots\ldots (96)$$

and

$$W_3 = \sum_1^i \left[\int_0^{\bar{l}} \Delta H\left(1+p\,y'^2\right)d\bar{x}\right] - \delta\,\Delta H_0\,E_c\,A_{cm} \quad \ldots\ldots\ldots (97)$$

DETERMINATION OF THE LOCAL DEVIATION IN CABLE STRESS INCREMENT

The relative horizontal deflection on the length of a_j according to Eq. 41 is

$$\Delta\xi_j = \xi_j - \xi_{j-1} = a_j^x - a_j = a_j\left[-\frac{\Delta y_j\,\Delta\bar{\eta}_j}{a_j^2} - \frac{\Delta\bar{\eta}_j^2}{2\,a_j^2}\left(1+\frac{\Delta y_j^2}{a_j^2}\right) + \frac{H_j + \left(H_w + H_j\right)\left(\dfrac{\Delta y_j\,\Delta\bar{\eta}_j}{a_j^2} + \dfrac{\Delta\bar{\eta}_j^2}{2\,a_j^2}\right)}{E_c\,A_{cj}\cos^3\phi_j} + \frac{\omega\,t}{\cos^2\phi_j}\right] \quad \ldots\ldots\ldots (98)$$

The relative horizontal deflection of joint k is

$$\xi_k = \sum_{j=g}^{k} \Delta\xi_j \qquad \ldots\ldots\ldots\ldots\ldots\ldots \quad (99)$$

The connection at joint g transmits horizontal forces from the stiffening truss to the cable, therefore, no relative horizontal displacement between cable joint and stiffening truss arises here. In general, it is in the middle of the main span.

The angular rotation of hanger k (Fig. 5) is

$$\tan\gamma_k = \frac{\xi_k}{h_k} \qquad \ldots\ldots\ldots\ldots\ldots\ldots\ldots \quad (100)$$

In the following, t_1 is supposed to be a temperature difference between the cable and the stiffening truss.

The horizontal component of hanger force (Fig. 7)

$$\Delta Q_k = \left(S_{wk} + S_k\right) t\, g\, y_k \qquad \ldots\ldots\ldots\ldots\ldots\ldots \quad (101)$$

From Eqs. 34b and 52, after simplification,

$$\Delta Q_k = \left(H_w + H_k\right)\left[\frac{\Delta y_k + \Delta\bar{\eta}_k}{a_k} - \frac{\Delta y_{k+1} + \Delta\bar{\eta}_{k+1}}{a_{k+1}}\right]\frac{\xi_k}{h_k} \qquad \ldots\ldots\ldots \quad (102)$$

And the cable stress increment in joint f

$$H_f = H_g + \sum_{k=g}^{f} \Delta Q_k \qquad \ldots\ldots\ldots\ldots\ldots\ldots \quad (103)$$

From Eqs. 98, 99, 102, and 103

$$H_f = H_g + \sum_{k=g}^{f} \frac{H_w + H_k}{h_k}\left(\frac{\Delta y_k + \Delta\bar{\eta}_k}{a_k} - \frac{\Delta y_{k+1} + \Delta\bar{\eta}_{k+1}}{a_{k+1}}\right)\sum_{j=g}^{k}\left\{ a_j\left[-\frac{\Delta y_j\,\Delta\bar{\eta}_j}{a_j^2} - \right.\right.$$

$$\left.\left. - \frac{\Delta\bar{\eta}_j^2}{2\,a_j^2}\left(1 + \frac{\Delta y_j^2}{a_j^2}\right) + \frac{H_j + \left(H_w + H_j\right)\left(\frac{\Delta y_j\,\Delta\bar{\eta}_j}{a_j^2} + \frac{\Delta\bar{\eta}_j^2}{2\,a_j^2}\right)}{E_c\,A_{cj}\cos^3\phi_j} + \frac{\omega\, t}{\cos^2\phi_j}\right]\right\} \quad \ldots \quad (104)$$

As in this equation, the second term on the right-hand side is very small compared with H_g; further simplifications are possible.

Thus, H_a may be substituted for H_j, unity may be taken for $1 + \Delta y^2/a^2$ furthermore, $\bar{\eta}^2/2\,a^2$ is negligible beside $\Delta y\,\Delta\bar{\eta}/a^2$ and so is $\Delta\bar{\eta}$ beside Δy.

The simplified form, therefore, is

$$H_f = H_g + \sum_{k=g}^{f} \frac{\left(H_w + H_a\right)}{h_k}\left(\frac{\Delta y_k}{a_k} - \frac{\Delta y_{k+1}}{a_{k+1}}\right)\sum_{j=g}^{k}\left[a_j\left(-\frac{\Delta y_j\,\Delta\eta_j}{a_j^2} + \frac{H_a}{E_c\,A_{cm}}\right)\right] \quad \ldots (105)$$

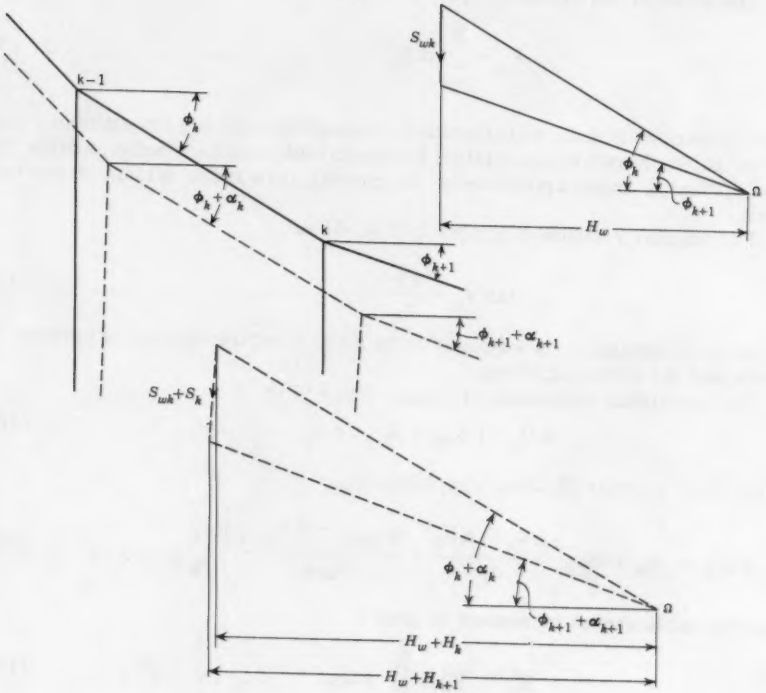

FIG. 7

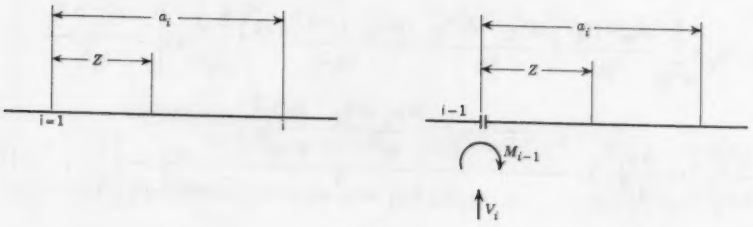

FIG. 8

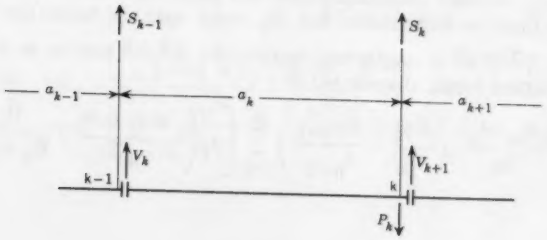

FIG. 9

If a suspending screen is assumed,

$$H_f = H_g + \int_{\bar{x}=x_g}^{\bar{x}f} \frac{1}{h}\left(H_w + H_A\right) y'' \left[\int_{z=\bar{x}_g}^{\bar{x}} y' \,\bar{\eta}'\, dz = \int_{z=\bar{x}_g}^{\bar{x}} \frac{H_a}{E_c\, A_{cm}}\, dz\right] d\bar{x} \;\; . \; . \; (106)$$

For determination of the value of H_f, in Eqs. 105 and 106, H_a is taken for H_g. So

$$H_f{}^x = H_f - \Delta H_g = H_a + \sum_{k=g}^{f} \frac{H_w + H_a}{h} \left(\frac{\Delta y_k}{a_k} - \frac{\Delta y_{k+1}}{a_{k+1}}\right) \sum_{\gamma=g}^{k} \left[a_j \left(-\frac{\Delta y_j{}^2\, \Delta \eta_j}{a_j{}^2} + \frac{H_a}{E_c\, A_{cm}}\right)\right] \;\; . \; . \; . \; . \; . \; . \; . \; . \; . \; . \; . \; . \; . \; (107)$$

or

$$H_f{}^x = H_f - \Delta H_g = H_a + \int_{\bar{x}=\bar{x}_g}^{\bar{x}f} \frac{H_w + H_a}{h}\, y'' \left\{\int_{z=\bar{x}_g}^{\bar{x}} y' \eta'\, dz - \int_{z=\bar{x}_g}^{\bar{x}} \frac{H_a}{E_c\, A_{cm}}\, dz\right\} d\bar{x} \; . \; . \; (108)$$

From Eqs. 89 or 86 and from Eq. 90

$$W_3 = 0 = \sum_1^i \left[\sum_{k=1}^{n} \left(H_k{}^x - H_a\right)\left(1 + p\, \frac{\Delta y_k{}^2}{a_k{}^2}\right) a_k\right] - \delta \left(H_0{}^x - H_a\right) E_c\, A_{cm} + \left[\sum_1^i \left(\sum_{k=1}^{n} \left(1 + p\, \frac{\Delta y_k{}^2}{a_k{}^2}\right) a_k\right) - \delta\, E_c\, A_{cm}\right] \Delta H_g \;\; . \; . \; . \; . \; . \; . \; . \; (109)$$

or

$$W_3 = 0 = \sum_1^i \left[\int_0^1 \left(H^x - H_a\right)\left(1 + p\, y'\right) d\bar{x}\right] - \delta \left(H_0{}^x - H_a\right) E_c\, A_{cm} + \left\{\sum_1^i \left[\int_0^1 \left(1 + p\, y'\right) d\bar{x}\right] - \delta\, E_c\, A_{cm}\right\} \Delta H_g \;\; . \; . \; . \; . \; . \; . \; . \; . \; . \; (110)$$

The value of $\Delta H_g = H_g - H_a$ is to be determined from Eq. 107 or 108.

CONCLUSION

In the present mathematical and statical treatise, a deflection theory of stiffened suspension bridges is developed. Eq. 64 supplies enough equations for determining the internal forces developed by vertical loading. In case of a continuous screen being substituted for individual hangers, this equation system turns into a differential equation, Eq. 75.

This theory is more precise than the ones published so far; it covers the effects of vertical and horizontal cable deflection as well as the effects of shear force due to the cable and hanger elongation under the change in cable stress and temperature.

The horizontal deflection of cable causes a deviation of hangers from the vertical that results in a non-uniformity in cable stress increment to be computed by Eq. 105 or 106 when assuming a suspending screen.

Solution of the system of equations of Eq. 64 is very cumbersome, and that of the differential equation under Eq. 75 is not to be found as a tabulated function except in isolated cases.

ACKNOWLEDGMENTS

The paper is dedicated to the memory of my father, John Szidarovszky (1888-1947), Professor of Classic Philology at the Hungarian Teachers' Training Institute and Corresponding Member of the Hungarian Academy of Sciences, who taught me to like culture and sciences.

The author is also indebted to Kurt H. Gerstle, M. ASCE, for editing this paper to correct my errors in language and style.

APPENDIX.—NOTATION

The following symbols are adopted for use in the paper.

Referring to stresses:

q = unit weight of cable;

H_w = cable stress due to dead load;

H = cable stress increment, namely cable stress increases due to live load;

H_a = average value of H;

S_w = hanger force due to dead load;

S = hanger force increment (due to live load);

P = external live load acting on the line of a hanger;

Q = horizontal component of hanger force;

$\Delta H = H - H_a$ = local deviation in cable stress increment;

M = bending moment in the stiffening truss;

M_g = bending moment due to live load on a beam;

M_o = bending moment at $x = 0$;

V = shear on the stiffening truss;

V_g = shear due to live load on a beam;

V_w = shear due to dead load on a beam; and

N = normal force (member force).

Referring to measurements in length dimension:

L = span of stiffening truss (Fig. 1);

l = horizontal distance between cable shoes (Fig. 1);

a = horizontal distance between two adjacent cable joints or hangers in unloaded position (Fig. 5);

a^* = same as a, but in loaded position (Fig. 5);

S = distance between two adjacent cable joints in unloaded position (Fig. 5);

S^* = same as S, but in loaded position (Fig. 5);

h = length of a hanger (Fig. 5);

y = ordinate of cable in unloaded position (Fig. 1 and 5);

$\Delta y_k = y_k - y_{k-1}$;

$\bar{\eta}$ = vertical deflection of cable due to live load (Fig. 1 and 5);

$\Delta\bar{\eta}_k = \eta_k - \bar{\eta}_k$

η = vertical deflection of the stiffening truss due to live load (Fig. 1 and 5);

$\eta_k = \eta_k - \eta_{k-1}$;

x = abscissa measured from the left-side support (Fig. 1);

$\bar{x}$ = abscissa measured from the left-side cable shoe;

z = abscissa measured from the left-side panel point;

$\bar{z}$ = abscissa as $\bar{x}$;

ξ = horizontal deflection of cable joint;

$\Delta\xi_k = \xi_k - \xi_{k-1}$;

d = inelastic decrease in the horizontal distance between cable anchorages;

δ = elastic decrease in the horizontal distance between cable anchorages due to cable stress increment of value unity;

ϵ = decrease in the horizontal distance between cable anchorages due to unit temperature change;

$\Delta\bar{\epsilon}$ = relative deflection defined by Eqs. 59, 50 and 61;

S_c = length of a chord member;

S_d = length of a diagonal;

m = perpendicular distance between centroidal axes of the upper and the lower chord. It is the vertical projection of diagonals;

r = horizontal projection of diagonals;

D = horizontal distance between cable anchorages (or shoes);

L_s, L_t = cable constants, Eqs. 85 and 86;

W_1, W_2, W_3 = cable functions, Eqs. 86, 88 or 89;

b_k = parameter defined by either of Eqs. 28 and 29;

c_i = parameter defined by either of Eqs. 28 and 29;

b_j^* = parameter defined by either of Eqs. 28 and 29;

c_k^* = parameter defined by either of Eqs. 28 and 29;

r_k = parameter defined by either of Eqs. 28 and 29; and

$\bar{a}_i$ = parameter defined by Eq. 31.

Referring to measurements not dimensions of length:

A_c = gross area of cable;

A_{cm} = gross area of cable in the middle of span;

A_h = gross area of hanger;

A_{web} = gross area of web plate;

A_e = equivalent area of web plate and web members respectively, Eqs. 10 and 16;

A_{ch} = gross area of chord member;

A_{ct} = gross area of top chord member;

A_{cb} = gross area of bottom chord member;

A_o = average area of chord members chosen at will;

A_d = gross area of diagonal member;

A_v = gross area of vertical member;

J = moment of inertia of stiffening truss Eq. 20;

J_o = average moment of inertia of the stiffening truss chosen at will;

β = tangential angle of diagonal member (Fig. 3);

ϕ = tangential angle of cable in unloaded position (Fig. 5);

α = change in tangential angle of cable due to live load (Fig. 5);

κ = slope of stiffening truss due to live load (Fig. 5); and

γ = angular rotation of hanger.

Referring to coefficients:

E = modulus of elasticity relating to the stiffening truss;

E_c = modulus of elasticity relating to the cable;

G = torsional modulus;

ω = coefficient of temperature expansion;

t = temperature change;

μ_k = defined by Eq. 65;

ρ_k = defined by Eq. 67;

Referring to footnotes:

0 = refers to point $x = 0$ or $\bar{x} = 0$;

x = refers to point x;

$\bar{x}$ = refers to point $\bar{x}$;

k = refers to section and point k respectively;

f = refers to point f;

i = refers to section and point i;

J = refers to point J;

g = refers to point g or to the abscissa of point g;

l = refers to point $x = l$ or $\bar{x} = l$; and

w = refers to dead load.

Other notation:

i = number of spans;

n = number of bays (hanger distances) along one span;

g = number of joint g where not horizontal displacement arises; and

p = constant. In case of chain $p = 1$, in case of cable $p = 1.5$.

Journal of the
STRUCTURAL DIVISION
Proceedings of the American Society of Civil Engineers

RESEARCH ON FIRE RESISTANCE OF PRESTRESSED CONCRETE

By Hubert Woods[1]

SNYOPSIS

Most of the engineering information available on the fire endurance of concrete is of an empirical nature. A science of design for fire endurance, comparable to the existing science of design for mechanical loads, has not yet been developed.

With the strikingly rapid increase in use of prestressed concrete, the need for research facilities devoted specifically to concrete became pressing. Such facilities have been provided, as described, in the new Fire Research Center of Portland Cement Association (PCA).

The research program there comprises two separate but intimately related parts; there are tests with large furnaces and small-scale basic research on properties of concrete and steel at high temperatures. A long range objective is to assist in the development of reliable predictive methods.

In the lighter prestressed flexural elements, the concrete cover over the steel, and the mass or cross-sectional area are both important to fire endurance. Research in the Netherlands has resulted in recommendations that take both factors into account.

Note.—Discussion open until April 1, 1961. To extend the closing date one month, a written request must be filed with the Executive Secretary, ASCE. This paper is part of the copyrighted Journal of the Structural Division, Proceedings of the American Society of Civil Engineers, Vol. 86, No. ST 11, November, 1960.

[1] Dir. of Research, Portland Cement Assoc. Research and Development Lab., Skokie, Ill.

At present, prestressed members can be designed to have any reasonable fire endurance period. More work needs to be done to achieve the ultimate in lightness and economy.

INTRODUCTION

Prestressed concrete was well known and widely used in Europe long before it had any considerable use in the United States. It is therefore natural that European research and development work on prestressed concrete should have been, until recently, considerably advanced over that in the United States. This is particularly true with respect to investigations on fire resistance of prestressed concrete. Much of the significant work on this subject has been done in Europe, particularly in England and in the Netherlands. Unfortunately, some code authorities in the United States and either unaware of that work, or seem unwilling to accept it. A good deal of it is applicable to types of elements of construction used in this country, although some of it is not.

Most of the engineering information now available on the fire endurance of concrete, or to speak more accurately, on the fire endurance of building elements made of concrete (prestressed or conventionally reinforced), is of a purely empirical nature. This information has been developed over the years by relatively few agencies who have commonly found themselves so pressed for commercial fire "ratings" and other "ad hoc" information, that little time and money have been available for research. In consequence, there has not been a science of design developed for fire endurance comparable to the existing science of design for mechanical loads.

NEW RESEARCH FACILITIES PROVIDED

In view of these circumstances, and with the strikingly rapid increase in the use of prestressed concrete structural members in this country, the need for adequate fire research facilities in the United States, specifically devoted to concrete, became very pressing. Aware of this need, the Portland Cement Association, in 1957, started construction of a unique fire research laboratory to house the necessary personnel and equipment. This laboratory, known as the Fire Research Center, is shown in Fig. 1. The interior arrangement is shown in Fig. 2. The frontal two-story wing contains a fundamental research laboratory, furnace control and recording equipment, a shop, and offices.

The first full-scale furnace installed was a beam furnace shown in Fig. 3. This has a firebox 40 ft long and 6 ft 4 in. wide. The furnace is provided with outboard hydraulic hold-down systems at the ends, for use in studies of the effects of continuity, and when so used can accommodate beams 60 ft long. Live load is applied by other hydraulic cylinders at the top. The furnace is gas fired, and can be programmed to follow various time-temperature curves. At present, the standard ASTM curve is being used.

All control functions and all recording of temperatures of furnace and of steel or concrete in specimens, and of all strains, deflections, and loads, are centralized in the control room shown in Fig. 4. The recording and control equipment in this room can also be used with any of several other furnaces to be

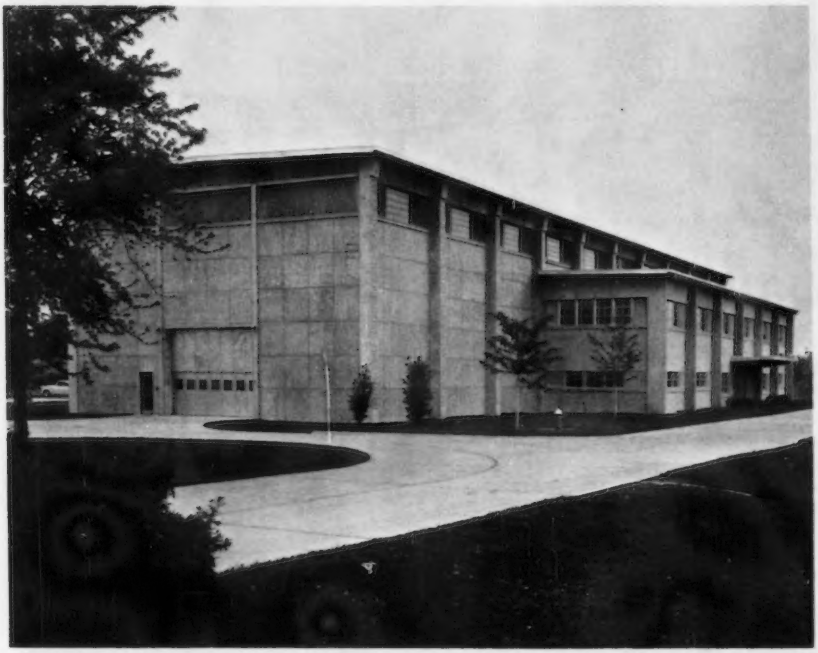

FIG. 1.—FIRE RESEARCH CENTER

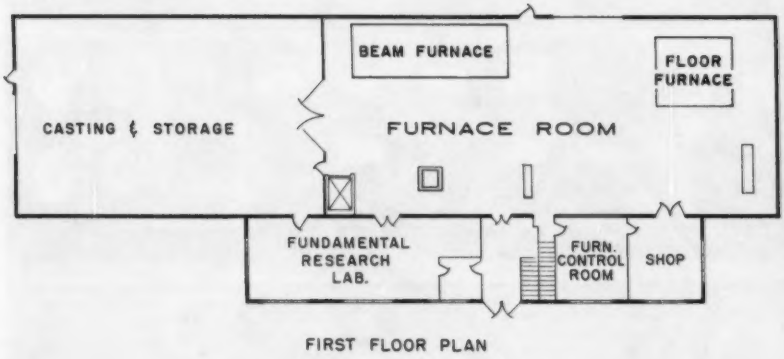

FIG. 2.—INTERIOR ARRANGEMENT OF THE FIRE RESEARCH CENTER

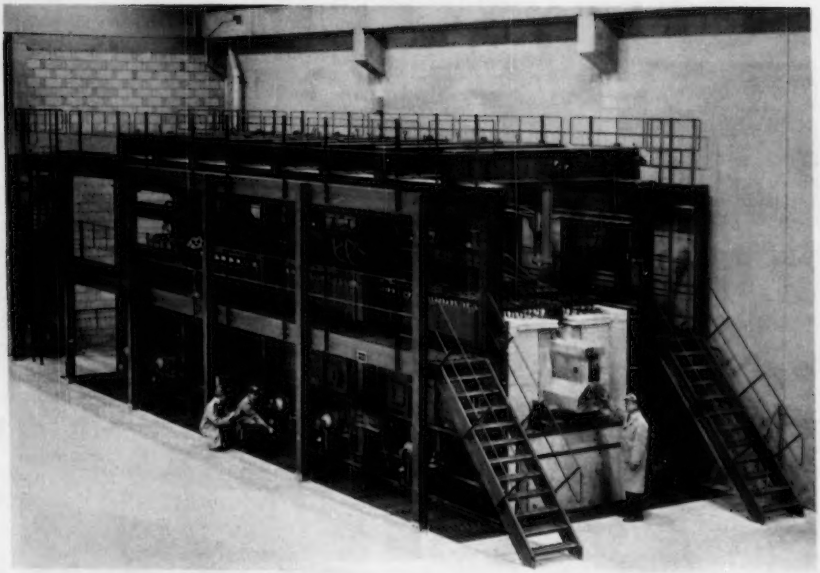

FIG. 3.—BEAM FURNACE

FIG. 4.—CONTROL ROOM

provided. One of these additional furnaces, now under construction, is a floor furnace for specimens 14 ft by 18 ft. A unique feature of this floor furnace is the provision of means for applying known amounts of edge restraint and edge moment to elements under test.

EDGE RESTRAINT

The present standard fire testing procedure is not specific regarding the amount of edge restraint, if any, to be applied to floor or roof sections under test. It merely says, in effect, that if the assembly to be tested represents a form of construction that restrains structural elements, then that assembly will be surrounded by a restraining frame that simulates such restraint. However, there seems to be no information as to how much edge restraint is actually imposed on a floor section in a building during a fire. It seems evident that the edge restraint would depend greatly upon the nature and size of the building in which it is located, and on its specific position in the building.

Nevertheless, it has long been common practice, in fire testing floor sections, to surround them with a very heavy steel restraining frame, resulting in a large but unknown restraint. The specific effect of this restraint upon the observed fire endurance of elements under test is not known, but could be highly significant. It was this consideration that led to the provision of hydraulic edge restraint means, in the floor furnace described, so that the matter can be investigated.

FIRE TEST OF A PRESTRESSED BEAM

The beam furnace (Fig. 3) has been in use for some months. The first beam to be tested was a heavy duty prestressed bridge beam 43 ft 6 in. long. This beam is not an exceptionally large one as prestressed beams go, but it probably is the largest so far to be tested for fire endurance. A cross-section of this beam is shown in Fig. 5. There are twenty one 7/16 in. diam strands; the seven 7/16 in. diam harped strands are indicated in the shaded zone. In the furnace, it was loaded with a 92,000 lb design load distributed equally over eight equally-spaced points, and subjected to the standard ASTM firing schedule shown in Fig. 6. After firing for 4 hr 31 min at which time the furnace temperature was 2050° F, the fire was shut off, principally because there was no reason for continuing it further. The beam was still intact and carrying full load. Initial deflection due to dead and live loads before firing was 0.3 in. When the firing was stopped, the deflection was 6.35 in. Twenty-four hours later it was 5.25 in. A close-up view of the beam after test, but still in the furnace, is shown in Fig. 7. This shows that a small amount of concrete had spalled off the lower corners, exposing one of the strands. The vertical pipe near the center is one of a number of thermocouple tubes used in furnace control.

In view of the excellent fire endurance of this beam, it was subsequently subjected to an ultimate structural load test to determine the beam's residual strength. The beam failed at a total live load of 117,700 lb distributed over 12 equally-spaced load points, by the crushing of concrete in the upper flange.

Center deflection at failure, due to fire test and application of ultimate load, was 10 in.

IMPORTANCE OF MASS AND COVER

The remarkable performance of this beam no doubt depended largely on its great mass, and hence its capacity for absorbing heat. Research in this country and abroad has shown that the mass or cross-sectional area of beams, and the amount of cover over steel strands, are both of great importance to their fire endurance. The reason why both cross section and cover are important is

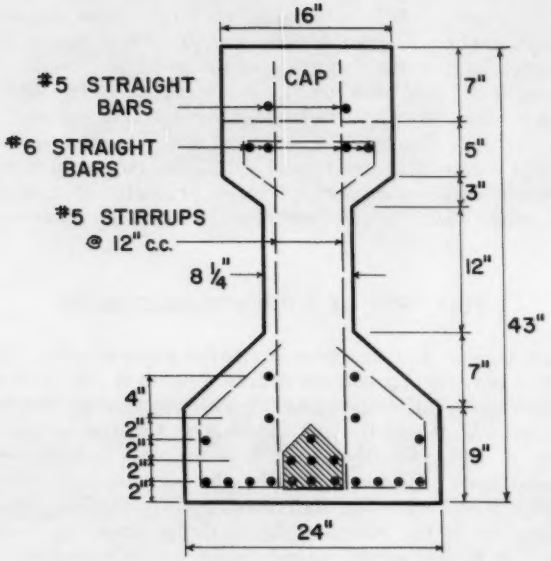

FIG. 5.—CROSS-SECTION AT THE CENTER LINE

simple; both affect the rate of heating of the prestressed strands, and it is commonly the loss of prestress in these strands at elevated temperature that is directly responsible for failure of the element. In the Netherlands, recommendations which take both factors into account are emphasized and are shown[2] in Table 1.

PROPERTIES OF PRESTRESSING STEEL AT ELEVATED TEMPERATURE

The high tensile strength wire, ordinarily used for prestressing, is relatively more sensitive to high temperature than is ordinary steel. Fig. 8 shows[3] some

[2] Adapted from "Fire Tests of Prestressed Concrete Beams," Commissie Voor Uitvoering van Research . . . C.U.R., Rapport 13, Netherlands, January, 1958. In Dutch.

[3] "Steel Wire for Prestressed Concrete," by W. O. Everling, presented at First National Prestressed Concrete Short Course, St. Petersburg, Fla., October, 1955.

of the significant properties of currently used prestressing steel as influenced by elevated temperature. Fig. 9 (a) shows the lowered strength as temperature is raised, the strength being reduced by 50% at about 705° F. Fig. 9 (b) shows the elongation, or creep, of the wire during one hour at the indicated temperatures when the stress is maintained at 50% of original ultimate strength. In addition to the effects of temperature on strength and creep of high tensile strength wires, it has been observed that the modulus of elasticity decreases with temperature, so that at about 575° F the modulus may be 80% of its value at room

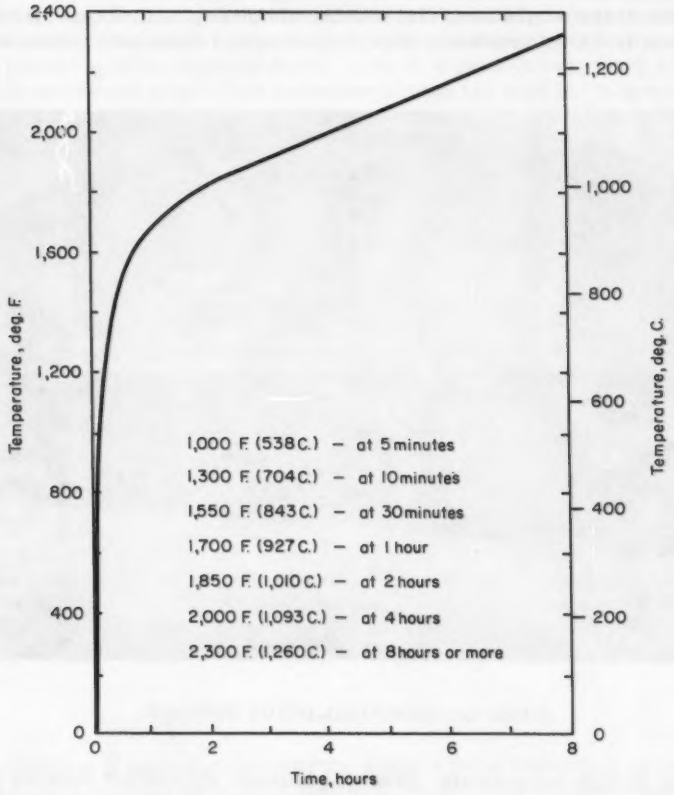

FIG. 6.—STANDARD TIME-TEMPERATURE CURVE

temperature. The combined result of these several effects is to induce virtually complete loss of prestress at a wire temperature of about 800° F, though the wire strength is still about half that at room temperature.

PREDICTION OF FIRE ENDURANCE

From an analytical point of view, the problem of predicting the fire endurance of a prestressed concrete element resolves itself, in the first place, into

that of predicting the time required for the prestressing wires or cables to reach the critical temperature of 800° F. If the temperature of the gases to which the element is exposed were known, as well as the surface coefficient of heat transfer, the conductivity and specific heat of the concrete, and of any insulating coating that might be used, and if the element were a simple geometric shape such as a semi-infinite flat slab in which the heat flow was uni-directional, then it might appear that a solution could be had using mathematical methods already worked out for heat flow. However, the surface coefficients are not known, and the conductivity and specific heat or concrete are not constants, but change with temperature and are inadequately known.

It can, therefore, be seen that even the simplest practical case is not simple analytically. Other practical cases, for example, a beam with bottom and sides

FIG. 7.—BEAM STILL INSIDE FURNACE

exposed to high temperature, present additional difficulties because the heat flow is bi-directional rather than uni-directional; and if the beam does not have a regular cross section, further difficulties of a geometric nature will be met. These considerations are presented to suggest some of the reasons why complete analytical solutions have not been reached.

NEED FOR BASIC RESEARCH

With building construction and new building methods and materials playing such an important role in our economy, the volume of required fire test work has grown tremendously. With present standard methods, such work is very slow and costly. More rapid and less expensive methods and approaches must

be developed. This need is providing an impetus for fundamental research in this field, looking toward a much improved science of design. Specifically, the needs are (1) acceptably reliable analytical solutions for predicting fire endurance and (2) reliable small-scale methods for fire testing to confirm predictions and substitute, at least in part, for the costly full-scale testing now required. It is not to be expected that such developments will completely eliminate the need for full-scale tests, but they will minimize the need for them.

Some progress has been made; Clarke[4,5] has applied heat-flow principles to slabs and other geometric shapes with some degree of success. Robertson and Gross[6] and Lawson and McGuire[7] have used electric network analogs in which voltage represents temperature, electrical resistance represents thermal resistivity, electrical capacitance represents heat capacity, and so on. The use of physical models suggests itself. This is a powerful approach that will eventually contribute greatly to a reduction of time and cost in research and in the engineering estimation of fire endurance. However, "scaling" laws have not been developed to the point of confidence in their application, and, indeed, are

TABLE 1.—RECOMMENDED COVER AND CROSS-SECTIONAL AREA FOR PRESTRESSED CONCRETE BEAMS FOR VARIOUS FIRE ENDURANCE PERIODS.

Required endurance time, in hours	Depth of cover required, in inches				
	Cross sectional area, in square feet				
	16-32	32-78	78-160	160-320	Over 320
1/2	1.2	0.8	0.8	0.8	0.8
1	-	2.0	1.6	1.2	1.2
1 1/2	-	-	2.4	1.6	1.2
2	-	-	-	2.4	2.0
3	-	-	-	-	3.2
4	-	-	-	-	4.0?

not likely to be so developed, or accepted, until a much better basic understanding of the full-size case is in hand. Nevertheless, models are now being used to save time and cost in studying the effect of certain variables and in gaining a better understanding of the heating process, even though the results cannot always be applied quantitatively and directly to the full-size case.

PRESENT STANDARD TEST METHODS

The attention of investigators over the world is being focused on the adequacy and realism of current methods of testing and specifying the fire endurance of building elements. Several specific points are at issue.

4 "The Estimation of the Fire Endurance of Floors, Columns, and Beams," by J. H. Clarke, Technical Record No. B.S. 44/153/1/226, unpublished report, Experimental Bldg. Sta., Commonwealth of Australia, June, 1958.

5 "Method of Assessing Probable Fire Endurance of Load-Bearing Columns," by J. H. Clarke, Journal ACI, Vol. 31, No. 12, June, 1960, p. 1223.

6 "An Electrical Analog Method for Transcient Heat-Flow Analysis," by A. F. Robertson and Daniel Gross, Journal of Research, N.B.S., Vol. 61, No. 2, August, 1958, pp. 105-115.

7 "The Solution of Transcient Heat Flow Problems by Analogous Electric Networks, by D. I. Lawson and J. H. McGuire, Proceedings, Inst. Mech. Engr., A, 167, 1952, p. 275.

Fire Severity.—The standard ASTM time-temperature curve (Fig. 6), that is in use in many countries, requires a continuously rising temperature up to eight hours. This is not at all characteristic of the great majority of fires in buildings in which the temperature starts to decline well before eight hours. This discrepancy between the present standard time-temperature curve and most real fires is particularly marked in buildings constructed of noncombustible materials. In such cases, the only fuel available to sustain a fire is the combustible material stored in the building, and the quantity of such material ranges from very little, in some occupancies, up to a maximum in others. The present testing procedure takes no account of the nature of the occupancy of the building,

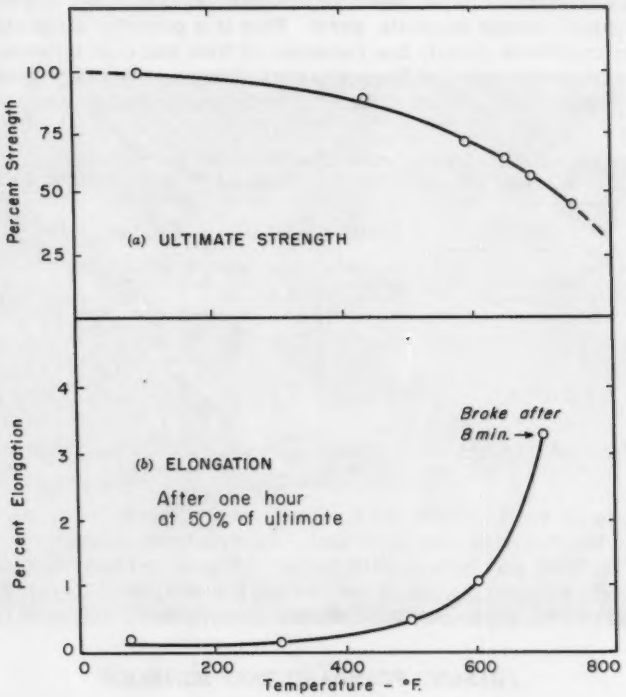

FIG. 8.—PROPERTIES OF PRESTRESSING STEEL AT ELEVATED TEMPERATURES.

that is, the amount of combustible material, or fuel, that is, or may be, present.

Early consideration should be given to a change in the testing procedure by adopting a "fire-load exposure" or limited heat input, in place of the present arbitrary time-temperature curve.

Criteria of Failure.—(1) At present, a floor construction undergoing a standard fire test is deemed to have failed if it collapses, if holes or cracks develop in it of a size to pass sufficient flame or hot gas to ignite cotton waste, or if the unexposed face (that is, the face away from the fire) increases in temperature by 250° F. Generally, the beginning temperature in a building would be about

70° F, so when the temperature of the unexposed face reaches 320° F, for example, the fire endurance period is deemed to have ended. This limitation is imposed with the thought of preventing spread of fire by ignition of combustibles stored on a floor under which there is a fire. However, the requirement is unrealistic and unnecessarily severe, and thus arbitrarily penalizes certain constructions. A British fire authority has stated privately that, in investigations of thousands of fires in London, no case of ignition and fire spread from temperature rise of the unexposed surface was uncovered.

(2) There is at present no generally accepted criterion of failure of a beam in a fire test other than failure to sustain the design load. Does this mean actual collapse? It would seem better to define the end point in some other and more definite way, perhaps by a limiting deflection stated in terms of the span.

An ASTM Committee (E-5) is currently studying these and other problems connected with fire testing of elements of construction. A number of agencies, including several in the United States and Canada, in England, the Netherlands, Russia, Japan, and Australia are active in fire research and fire testing. Some of these agencies are vitally interested in the basic problems previously discussed and are doing significant work on them.

PRESENT PROGRAM AT PCA

The current program of research at the new laboratory of the PCA has two primary aspects that are intimately related.

1. Fundamental research is being conducted on the properties of concrete and concrete materials at elevated temperatures; of importance in this connection are thermal properties and elastic properties. Knowledge of such properties will be essential in model studies and in contributing to the improvement of analytical approaches for predicting performance of structural concrete elements. It is also required in arriving at a better understanding of some aspects of the observed behavior of concrete elements subjected to fire, such as the spalling that sometimes occurs.

2. At present, work in large scale fire research is concerned with flexural elements of prestressed concrete. The following matters are being or will be investigated:

A. Effect of concrete thickness over prestressing steel;

B. Influence of aggregate type and moisture condition of concrete at time of testing;

C. Method of prestressing - pretensioning and post-tensioning;

D. Effect of cross-sectional shape and size (mass);

E. Effect of partial prestressing and supplementary mild steel reinforcing;

F. Exploratory study of influence of continuous design on fire resistance of prestressed concrete beams; and

G. Supplementary investigations.

Part A is now in progress using I-beams. Concrete cover is 1 in., 2 in., and 3 in. Aggregates are sand and gravel for half the beams and expanded shale for the others. Part B will use I-beams with 2 in. minimum cover over the

steel. Aggregates will include sand and gravel, crushed limestone and natural sand, expanded shale, clay, or slate, and slag. Two moisture contents will be employed: that corresponding to the present 70% relative humidity recommended by ASTM Committee E-5, and that corresponding to 50% relative humidity. The results of these researches will be reported from time to time in the technical press.

CONCLUSIONS

It may be observed that prestressed concrete structural elements can be produced to have any reasonably required fire endurance period. This is clearly shown by work already carried out by other investigators and exemplified in Table 1. It is, however, evident that to approach the ultimate in lightness and economy consistent with fire safety will require much more study.

2643 November, 1960 ST 11

Journal of the
STRUCTURAL DIVISION
Proceedings of the American Society of Civil Engineers

PRINCIPLE OF VIRTUAL WORK IN STRUCTURAL ANALYSIS

By Frank L. DiMaggio,[1] M. ASCE

SYNOPSIS

The principle of virtual work is derived for plane structures composed of straight members to permit a general interpretation of the function usually called "virtual displacement" and is applied to the determination of deflections in elastic, viscoelastic, and elastic-plastic structures, and to the problem of deriving equilibrium equations.

INTRODUCTION

Although it is true that the principle of virtual work is discussed and applied in almost any modern textbook on structural analysis, even the best derivations are, probably for reasons of expediency, too restrictive to bring out the generality of this powerful idea. The principal aim of this paper is to present a fairly rigorous and general derivation applicable to plane structures composed of straight members and one that includes, as special cases, the various known applications as well as a few that are believed to be new.

It is to be emphasized that many of the points that are brought out in this paper (more clearly and consistently, it is hoped, than would be possible with a more restrictive interpretation of the "virtual displacement") are well known. The determination of elastic displacements is treated in any elementary text. The fact that redundants may be neglected in part of the calculations for de-

Note.—Discussion open until April 1, 1961. To extend the closing date one month, a written request must be filed with the Executive Secretary, ASCE. This paper is part of the copyrighted Journal of the Structural Division, Proceedings of the American Society of Civil Engineers, Vol. 86, No. ST 11, November, 1960.

[1] Assoc. Prof., Dept. of Civ. Engrg. and Engrg. Mech., Columbia Univ., New York, N. Y.

flections in indeterminate structures is pointed out and illustrated[2,3,4,5] in many places. Structures composed of material with non-linear stress strain laws have been treated,[6,7,8] and the use of virtual displacements that violate constraints in order to determine equilibrium equations have also been considered.[9,10]

RESTRICTED DERIVATION FOR A BEAM

Consider a straight beam with arbitrarily varying section containing a plane of symmetry and loaded by transverse forces acting in this plane (see Fig. 1). The equilibrium equation relating bending moment and load for any element is

$$M''' = - W \quad \ldots\ldots\ldots\ldots\ldots\ldots \quad (1)$$

in which primes denote differentiation with respect to x, and the usual strength of materials sign convention is used. If both sides of Eq. 1 are multiplied by an arbitrary function $\eta(x)$ and integrated over the length of the beam, one obtains

$$\int_A^B M'' \, \eta \, dx = - \int_A^B W \, \eta \, dx \quad \ldots\ldots\ldots\ldots\ldots \quad (2)$$

When no concentrated force acts between A and B, the shear diagram V(x) is a continuous function and, since

$$M' = V \quad \ldots\ldots\ldots\ldots\ldots\ldots \quad (3)$$

the function M' is continuous. Assuming $\eta(x)$ to be continuous also, the left hand side of Eq. 2 may be integrated by parts to give

$$\int_A^B \eta \, dM' = \eta(B) \, V_B - \eta(A) \, V_A - \int_A^B \eta' \, dM \ldots\ldots \quad (4)$$

If no concentrated couples act between A and B, M(x) is continuous. If $\eta'(x)$ were also continuous, the integral on the right hand side of Eq. 4 could be integrated by parts directly from A to B. Allowing, however, for the possibility of a discontinuity in $\eta'(x)$ at $x = x_S$ such that

$$\eta' \left(x_S^+\right) - \eta' \left(x_S^-\right) = \theta_S \quad \ldots\ldots\ldots\ldots\ldots \quad (5)$$

---

2 "Elementary Structural Analysis," by J. B. Wilbur and C. H. Norris, McGraw-Hill Book Co., Inc., New York, 1948, p. 433.

3 "Note on the Calculation of Deflections of Indeterminate Structures," by B. A. Boley and R. H. Moore, Journal of Aeronautical Science, August, 1950, pp. 526-527.

4 "The Analysis of Structures," by N. J. Hoff, John Wiley & Sons, New York, 1956, p. 84.

5 "Elastic Energy Theory," by Van den Broek, John Wiley & Sons, New York, 1942, p. 67.

6 "Aircraft Structures," by D. J. Perry, McGraw-Hill Book Co., Inc., New York, 1950, p. 428.

7 "The Analysis of Structures," by N. J. Hoff, John Wiley & Sons, New York, 1950, p. 394.

8 "The Theory of a Statically Indeterminate Pinjointed Framework and Material of Which Does Not Follow Hooke's Law," by A. Ylinen and A. Eskola, Preliminary Publication, Internatl. Assoc. of Bridge and Struct. Engrg., Stockholm, 1960, pp. 167-176.

9 "The Plastic Methods of Structural Analysis," by B. G. Neal, John Wiley & Sons, New York, 1956, p. 83.

10 "Plastic Analysis of Structures," by P. G. Hode, Jr., McGraw-Hill Book Co., Inc., New York, 1959, p. 28.

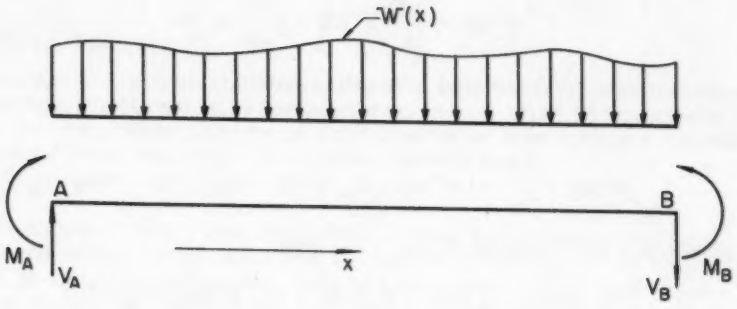

FIG. 1

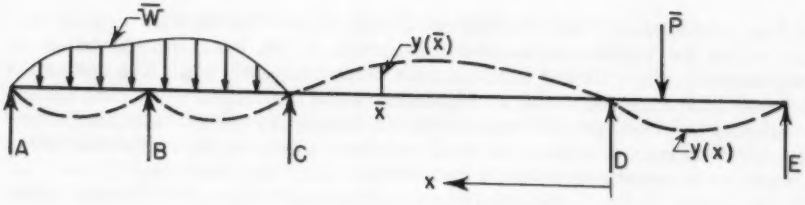

(*a*) STRUCTURE $\bar{S}$

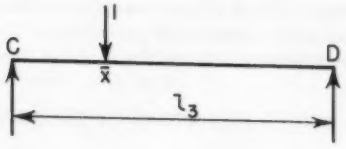

(*b*) STRUCTURE S

FIG. 2

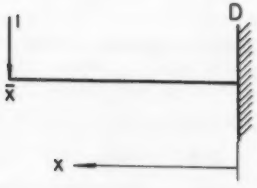

FIG. 3

the integration by parts must be split up at x_S;

$$\int_A^B \eta' \, dM = \int_A^{x_S^-} \eta' \, dM + \int_{x_S^+}^B \eta' \, dM \quad \ldots\ldots\ldots \quad (6)$$

Since the functions $\eta'(x)$ and $M(x)$ are continuous within the limits of each integral, integration by parts may be performed and using the definition of Eq. 5 results in

$$- \int_A^B \eta' \, dM = \int_A^B M \, \eta'' \, dx + M_A \, \eta'(A) - M_B \, \eta'(B) + M(x_S) \, \theta_S \quad \ldots(7)$$

and substituting Eq. 7 into Eq. 4, Eq. 2 becomes

$$\int_A^B W \, \eta \, dx + V_B \, \eta(B) - V_A \, \eta(A) + M_A \, \eta'(A) - M_B \, \eta'(B)$$

$$= - \int_A^B M \, \eta'' \, dx - M(x_S) \, \theta_S \quad \ldots\ldots\ldots\ldots \quad (8)$$

Eq. 8 is a statement of the principle of virtual work. The function $\eta(x)$ is usually called the virtual displacement (although it has been introduced as an arbitrary function of x and need not be a displacement at all). The quantities on the left and right hand side of Eq. 8 are called the virtual work done by external and internal forces, respectively (although in general, they have absolutely nothing to do with the concept of real mechanical work). Note that $M(x_S)$ is positive in a sense opposite to the virtual relative rotation, θ_S.

With regard to Eq. 8, it is important to note the following: (1) The so called virtual "displacement" $\eta(x)$ is not necessarily related to the equilibrium system W, M, V, or the structure they act on in any way. Therefore, Eq. 8 could not possibly be derived from any energy principle. Note the natural absence of any 1/2 multipliers. (2) The function $\eta(x)$ does not necessarily satisfy any of the constraints on deflection of the structure acted on by W. Both the support constraint or continuity constraints may be violated.

GENERALIZATION OF DERIVATION

For clarity of presentation, a number of unnecessary restrictions were imposed in the derivation of the previous section that may now be relaxed.

Concentrated Downward Load P Acting at $x = x_p$.—In integrating the left hand side of Eq. 2 by parts, the integration must be split at $x = x_p$ because $M' = V$ is discontinuous there;

$$V(x_p^-) - V(x_p^+) = P \quad \ldots\ldots\ldots\ldots\ldots\ldots \quad (10)$$

If this is done, an additional term appears on the left hand side of Eq. 8

$$+ P \, \eta(x_p)$$

Concentrated External Clockwise Couple C at $x = x_c$.—Because

$$M(x_c^+) - M(x_c^-) = C \quad \ldots\ldots\ldots\ldots\ldots\ldots \quad (11)$$

the left hand side of Eq. 6 cannot be integrated by parts across $x = x_c$. Split-

ting the integration there, another term will be added to the left hand side of Eq. 8;

$$+ C\ \eta'(x_c)$$

Discontinuity In η At $x = x_d$.—If

$$\eta(x_d^+) - \eta(x_d^-) = \delta_d \quad \ldots\ldots\ldots\ldots\ldots\ldots (12)$$

then the integration by parts of Eq. 4 would have to be split at $x = x_d$ and an additional term appears on the right hand side of Eq. 8;

$$+ V(x_d)\ \delta_d$$

Presence of Thrust (see Appendix I).—Thus, the principle of virtual work says that the total virtual work done by external forces equals the total virtual work done by internal forces. This is a conclusion, not an assumption. It is to be emphasized that the theorem, as here derived, deals with all external forces including reactions, and that the virtual "displacements" are to be interpreted as in the section dealing with restricted derivation for a beam.

APPLICATION TO DETERMINING DEFLECTIONS

General.—If it is desired to find the value of a function $\eta(x)$, (that may be a deflection, a velocity, the Laplace transform of a deflection, and so on) at $x = \bar{x}$ of a structure $\bar{S}$ loaded with external loads $\bar{W}$ producing a bending moment $\bar{M}$ and shear $\bar{V}$, then $\eta(x)$ is considered the virtual displacement in conjunction with the external force system that results from the application of a unit concentrated load at the section $x = \bar{x}$ of a structure S, that is usually chosen the same as $\bar{S}$, if $\bar{S}$ is statically determinate. If $\bar{S}$ is indeterminate, however, S is usually chosen as a statically determinate structure obtained from $\bar{S}$ by relaxing constraints, so that the reactions due to the unit load do no virtual work with respect to the virtual displacement $\eta(x)$, unless there is a known support settlement in $\bar{S}$. Letting M(x) be the bending moment diagram for S acted upon by the unit load, Eq. 8, with the additions previously noted, yields (if no discontinuities exist in η' or η)

$$1\ \eta(\bar{x}) = -\int_S M\ \eta''\ dx \quad \ldots\ldots\ldots\ldots\ldots\ldots (13)$$

in which the integration is to be performed over the structure S. By substituting the appropriate relation between η'' and $\bar{M}$, corresponding to the stress strain relation of the material of structure $\bar{S}$, and then expressing M and $\bar{M}$ as functions of x, the right hand side of Eq. 13 may be integrated, either in closed form for simple materials and loading, or by numerical methods for more complicated cases. If it is desired to find $\eta'(\bar{x})$ instead of $\eta(\bar{x})$, a unit concentrated couple is applied at $\bar{x}$ in S, and Eq. 13 with η' replacing η holds.

Linearly Elastic Structures.—If it is desired to find the displacement $y(\bar{x})$ of the continuous beam with rigidity E I, shown in Fig. 2(a), then the structure S may be taken as in Fig. 2(b). If deflections due to shear are neglected, and no temperature gradients exist (see Appendix II for the consideration of these),

$$y'' = -\frac{\bar{M}}{E\,I} \quad \ldots\ldots\ldots\ldots\ldots\ldots (14)$$

and, if no support settlement takes place in $\bar{S}$, Eq. 14 may be substituted into Eq. 13 to yield

$$y(\bar{x}) = \int_0^{l_3} \frac{M \bar{M}}{E I} dx \quad \ldots\ldots\ldots\ldots\ldots\ldots (15)$$

It is to be noted that M is the statically determinate bending moment of structure S. If S had been chosen identical with $\bar{S}$, then two statically indeterminate stress analyses would have been necessary and the integration would have to be performed from A to E.

If, in addition, it is desired to find the rotation at D, then either structure S of Fig. 2 could be used again with a unit couple at D instead of a unit load at $\bar{x}$, or a new structure S, shown in Fig. 3 could be used. Noting that $M_1(0) = -\bar{x}$ does virtual work with respect to the rotation in $\bar{S}$ at D, Eq. 8 gives, upon substitution of Eq. 14,

$$-\bar{x}\, y'(0) + 1\, y(\bar{x}) = \int_0^{\bar{x}} \frac{\bar{M}}{E I} (x - \bar{x})\, dx \quad \ldots\ldots\ldots\ldots (16)$$

from which $y'(0)$ is obtained, if $y(\bar{x})$ has been previously computed using Eq. 15.

In some cases, it may be desirable to compute deflections or rotations with respect to some line other than the original line of the member. This is done by choosing virtual displacements with respect to the desired line. If the equation of the line, with respect to which deformations are desired, is

$$y_0 = a + b\, x \quad \ldots\ldots\ldots\ldots\ldots\ldots (17)$$

then the virtual displacements are chosen as

$$\eta(x) = y(x) - y_0(x) = y(x) - (a + b\, x) \quad \ldots\ldots\ldots\ldots (18)$$

and Eq. 13 is applied. Since, as may be easily seen from Eq. 18,

$$\eta'' = y'' \quad \ldots\ldots\ldots\ldots\ldots\ldots (19)$$

the moment curvature relationship is not affected by this change, but the structure S must be chosen such that its reactions do no virtual work with respect to η.

Suppose, for instance, it is desired to find the deflection with respect to the deflected chord line AC' of the section $\bar{x}$ of span AB of structure $\bar{S}$ shown in Fig. 4(a) and acted upon by a concentrated load $\bar{P}$ at C producing a moment M(x). Then $\eta(x)$ is the deflection with respect to AC', and if S is chosen, as in Fig. 4(b), so that its reactions do no virtual work with respect to η, Eq. 13 still holds, and, remembering Eq. 19, becomes

$$\eta(\bar{x}) = -\int_A^C M\, y''\, dx \quad \ldots\ldots\ldots\ldots\ldots\ldots (20)$$

that, if $\bar{S}$ is elastic, becomes, using Eq. 14,

$$\eta(\bar{x}) = \int_A^C \frac{M \bar{M}}{E I} dx \quad \ldots\ldots\ldots\ldots\ldots\ldots (21)$$

It may be readily seen that Eq. 21 gives the same result as direct application of the conjugate beam method to this problem. The integral in Eq. 21 equals the bending moment at $\bar{x}$ in "conjugate beam" S loaded by a distributed load $\bar{M}/E I$. Similarly, the rotation with respect to the chord line AC', as obtained from virtual work as

$$\eta'(\bar{x}) = \int_A^C \frac{M \bar{M}}{E I} dx \quad \ldots\ldots\ldots\ldots\ldots\ldots (22)$$

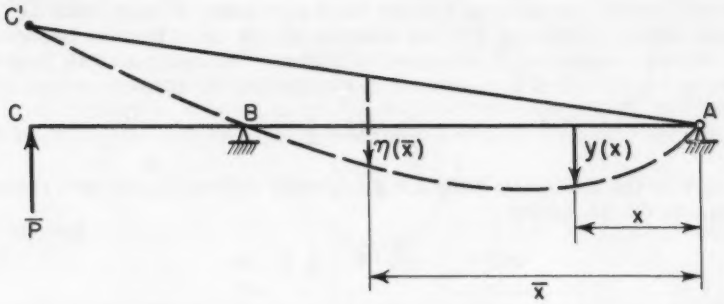

(*a*) STRUCTURE $\bar{S}$

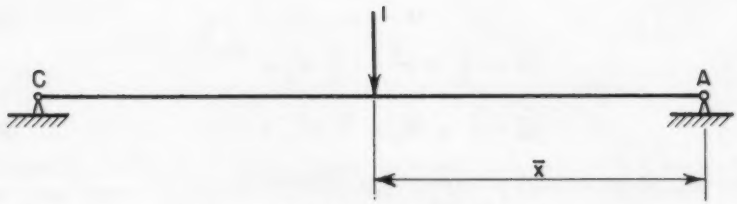

(*b*) STRUCTURE S

FIG. 4

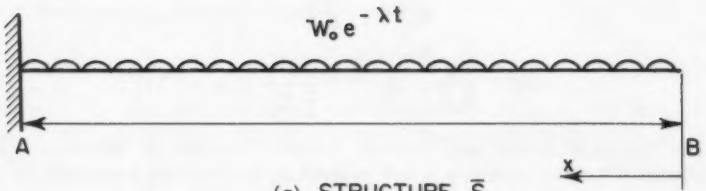

(*a*) STRUCTURE $\bar{S}$

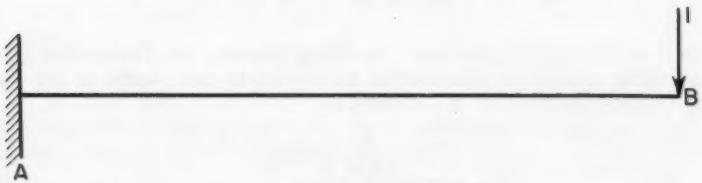

(*b*) STRUCTURE S

FIG. 5

in which M is now the moment diagram for S loaded with a unit concentrated couple at C, is just the shear at $\bar{x}$ in the "conjugate beam" S loaded with $\overline{M}/E\,I$.

Linear Maxwell Material.—If the function $\eta(x)$ is considered to be the velocity $v(x)$ of a structure $\overline{S}$ composed of a linear Maxwell material, then the velocity at a section $\bar{x}$ of $\overline{S}$ is obtained by substituting the Maxwell relationship

$$v'' = -\frac{1}{E\,I}\left(\dot{\overline{M}} + \frac{1}{\tau}\overline{M}\right) \quad \ldots\ldots\ldots\ldots\ldots\ldots (23)$$

in which τ is the relaxation time and dots denote differentiation with respect to time, into Eq. 13, giving

$$v(\bar{x}) = \int_S \frac{M}{E\,I}\left(\dot{\overline{M}} + \frac{1}{\tau}\,M\right) dx \quad \ldots\ldots\ldots\ldots\ldots\ldots (24)$$

Consider, for example, a cantilevered beam of uniform section acted on by a uniform load decaying exponentially with time. If it is desired to find the velocity at the free end as a function of time, the structures $\overline{S}$ and S and their respective loadings are chosen as shown in Figs. 5(a) and 5(b). Then substituting

$$M = -x \quad \ldots\ldots\ldots\ldots\ldots\ldots\ldots\ldots (25)$$

$$\overline{M} = -\frac{1}{2}\,W\,x^2 = -\frac{1}{2}\,W_0\,e^{-\lambda t}\,x^2 \quad \ldots\ldots\ldots\ldots (26)$$

and

$$\dot{\overline{M}} = \frac{1}{2}\,\lambda\,W_0\,e^{-\lambda t}\,x^2\,,\ t > 0 \quad \ldots\ldots\ldots\ldots (27)$$

into Eq. 24, the velocity at the free end is obtained as

$$v(0) = \frac{W_0\,l^4}{8\,E\,I}\left(\frac{1-\lambda\tau}{\tau}\right) e^{-\lambda t}\,,\ t > 0 \quad \ldots\ldots\ldots\ldots (28)$$

This can be integrated to give the displacement $y(0)$, remembering that the initial value of $y(0)$ is the elastic deflection due to W_0

$$y_0(0) = \frac{W_0\,l^4}{8\,E\,I} \quad \ldots\ldots\ldots\ldots\ldots\ldots\ldots (29)$$

so that

$$y(0) = \frac{W_0\,l^4}{8\,E\,I}\left[e^{-\lambda t} + \frac{1}{\lambda\,\tau}\left(1 - e^{-\lambda t}\right)\right] \quad \ldots\ldots\ldots\ldots (30)$$

Linear Kelvin Material and General Linear Viscoelastic Material.—For a Kelvin beam the displacements y are related to the bending moments by

$$y'' + \tau\,\dot{y}'' = -\frac{\overline{M}}{E\,I} \quad \ldots\ldots\ldots\ldots\ldots\ldots\ldots (31)$$

in which τ is the retardation time. Applying Laplace transformation with respect to time, assuming zero initial deflection to both sides of Eq. 31, the Laplace transform of y'', $\tilde{y}''$ is obtained as

$$\tilde{y}'' = -\frac{\tilde{\overline{M}}}{E\,I}\,\frac{1}{1+\tau s} \quad \ldots\ldots\ldots\ldots\ldots\ldots (32)$$

in which $\tilde{\overline{M}}$ is the Laplace transform of the bending moment in $\overline{S}$. Letting $\eta(x)$ in Eq. 13 represent $\tilde{y}(x)$, the transform of displacement at $x = \bar{x}$ of a Kelvin

structure is given by

$$\tilde{y}(\bar{x}) = \frac{1}{1+\tau s} \int_S \frac{M \tilde{\bar{M}}}{E I} dx \quad \ldots\ldots\ldots\ldots\ldots (33)$$

As an example, consider again the structure and loading of the preceding section (Figs. 5(a) and 5(b)). The Laplace transform of $\bar{M}$, given by Eq. 26 is

$$\tilde{\bar{M}} = -\frac{1}{2} W_0 x^2 \frac{1}{s+\lambda} \quad \ldots\ldots\ldots\ldots\ldots (34)$$

Substituting Eqs. 34 and 25 into Eq. 33 for $\bar{x} = 0$ and integrating results in

$$\tilde{y}(0) = \frac{W_0 l^4}{8 E I \tau} \left[\frac{1}{\left(s + \frac{1}{\tau}\right)(s+\lambda)} \right] \quad \ldots\ldots\ldots\ldots (35)$$

that may be inverted to give the desired deflection;

$$y(0) = \frac{W_0 l^4}{8 E I} \frac{1}{1 - \lambda \tau} \left(e^{-\lambda t} - e^{-t/\tau} \right) \quad \ldots\ldots\ldots\ldots (36)$$

For a general linear viscoelastic body, defined by the relation

$$P(y'') = Q(\bar{M}) \quad \ldots\ldots\ldots\ldots\ldots\ldots (37)$$

in which P and Q are arbitrary linear differential operators in time, an identical application of Laplace transformation will yield an expression for the transform $\tilde{y}$. Eq. 23 governing the Maxwell body of the preceding section is another special case of Eq. 37.

Elastic-Plastic Material.—If the structure $\bar{S}$ is not linearly elastic but has a single-valued moment "curvature" relationship

$$\eta'' = -f(\bar{M}) \quad \ldots\ldots\ldots\ldots\ldots\ldots (38)$$

then Eq. 38 is substituted into Eq. 13, yielding, instead of Eq. 15

$$\eta(\bar{x}) = \int_S M f(\bar{M}) dx \quad \ldots\ldots\ldots\ldots\ldots (39)$$

Consider, for example, an ideal elastic plastic member with rectangular section of width b and depth 2h. The moment curvature relation for loading is (see Fig. 6)

$$\frac{\bar{M}}{\bar{M}_y} = \frac{K}{K_y} \qquad 0 \le \bar{M} \le \bar{M}_y \quad \ldots\ldots\ldots (40a)$$

$$\frac{\bar{M}}{\bar{M}_y} = \frac{3}{2} - \frac{1}{2}\left(\frac{K_y}{K}\right)^2 \qquad \bar{M}_y \le \bar{M} \le \bar{M}_p \quad \ldots\ldots (40b)$$

in which M_y is the yield moment, K_y is the curvature at yield, and M_p is the fully plastic moment.

$$|\bar{M}_y| = \sigma_y I/h \quad \ldots\ldots\ldots\ldots\ldots (41)$$

$$K_y = -\bar{M}_y/E I \quad \ldots\ldots\ldots\ldots\ldots (42)$$

and

$$|\bar{M}_p| = \sigma_y b h^2 \quad \ldots\ldots\ldots\ldots\ldots (43)$$

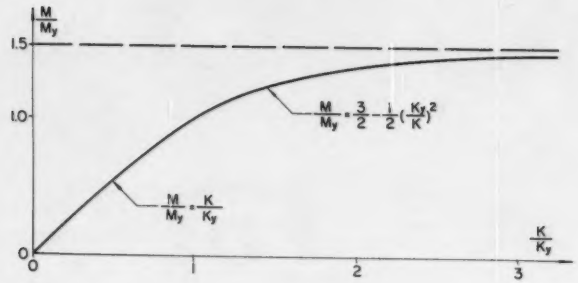

FIG. 6

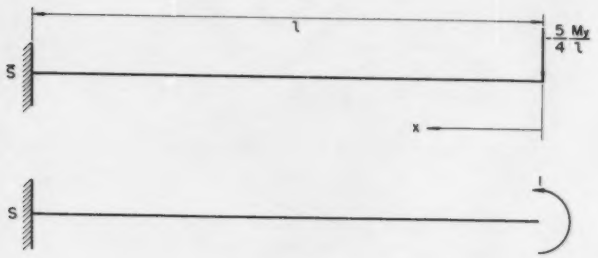

FIG. 7

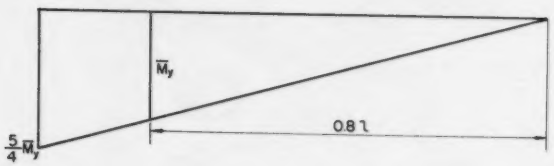

FIG. 8

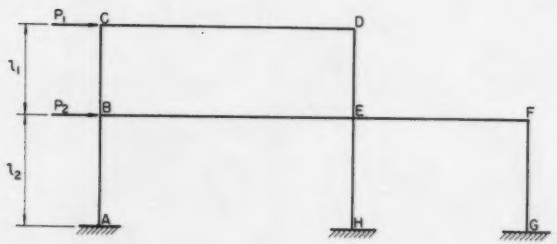

FIG. 9

In particular, let it be required to find the rotation at the free end of a cantilever beam acted upon by a concentrated downward force $P = -5\,M_y/4\,l$ at that end. The appropriate structures $\bar{S}$ and S are shown in Fig. 7. Thus, $M = +1$ and $\bar{M} = 5\,\bar{M}_y\,x/4\,l$ is shown diagramatically in Fig. 8.

Referring to Eqs. 40, Eq. 38 becomes, for the moments of Fig. 8,

$$K = \frac{5}{4}\,K_y\,\frac{x}{l} \qquad 0 \leq x \leq .81 \quad \ldots\ldots\ldots \quad (44a)$$

$$K = \frac{K_y}{\sqrt{3 - \frac{5}{2}\,\frac{x}{l}}} \qquad .8 \leq x \leq 1 \quad \ldots\ldots\ldots \quad (44b)$$

Substituting Eqs. 44 into Eq. 39, with η replaced by η', the rotation at the free end is obtained as

$$y'(0) = \frac{5}{4}\,K_y\,l \int_0^{0.8} z\,dz + K_y \int_{0.8}^{1} \frac{dz}{\sqrt{3 - \frac{5}{2}\,z}} \quad \ldots\ldots \quad (45)$$

or, integrating

$$y'(0) = 0.634\,K_y\,l \quad \ldots\ldots\ldots\ldots\ldots\ldots \quad (46)$$

Equilibrium Equations.—It is often necessary in structural analysis (for instance in applying slope deflection equations in elastic analysis or in applying the lower bound theorem in plastic analysis) to obtain equilibrium relations relating external loads and particular internal moments with no other internal stress resultants appearing. This is often done by applying the equations of statics directly to various free bodies and eliminating from these the undesired shears and thrusts. By choosing virtual displacements (consisting of straight lines that violate the slope continuity constraints at the sections in which pertinent moments act and that violate no other constraints), these equations are derived directly from the principle of virtual work, Eq. 8, in the form (since $\eta'' = 0$)

$$\int W\,\eta\,dx + \sum_i P_i\left(x_{p_i}\right) = \sum_j M\left(x_{S_j}\right)\theta_{S_j} \quad \ldots\ldots\ldots \quad (47)$$

It is to be noted that the sign on the right hand side of Eq. 47 will change depending on the sign convention used for moments.

Consider, as an illustrative example, the rigid frame and loading shown in Fig. 9. Suppose it is desired to obtain all equilibrium equations relating end moments and external loads (excluding those involving only joint equilibrium). Assuming joint equilibrium, there are eleven end moments necessary to completely specify the moment diagram (that must consist of straight lines). Since the structure is statically indeterminate to the ninth degree, two such equilibrium equations must exist. These may be obtained by assuming as virtual displacements any two independent sidesway mechanisms, such as, those of Fig. 10.

Applying Eq. 47 to Mech. I, using the usual slope-deflection sign convention that makes a moment positive if it acts clockwise on the end of a member, and then dividing through by θ,

$$\left(P_1 + P_2\right) l_2 = -\left(M_{AB} + M_{BA} + M_{EH} + M_{HE} + M_{FG} + M_{GF}\right). \quad \ldots \quad (48)$$

Similarly, using Mech. II as a virtual displacement,

$$P_1 l_1 = -(M_{BC} + M_{CB} + M_{DE} + M_{ED}) \quad \ldots\ldots\ldots\ldots (49)$$

Note that Eqs. 48 and 49 are obtained directly without having to eliminate undesired shears. In this particular example, it would have been as easy to apply the equations of statics directly, but for gabled frames or frames with sloping

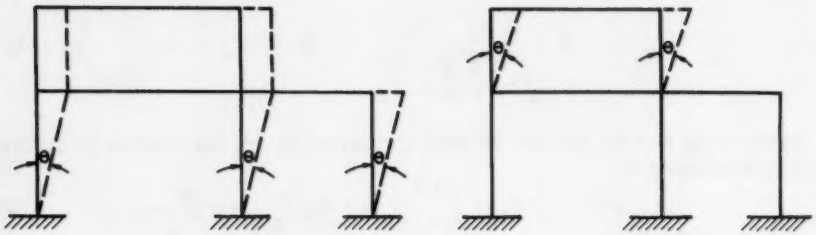

FIG. 10

columns, application of virtual work is the most efficient technique for obtaining the desired equations.

It is to be emphasized that application of the method requires the use of virtual displacements that violate constraints.

APPENDIX I. LONGITUDINAL FORCES

If distributed longitudinal forces act on the beam of Fig. 1, the thrust $T(x)$ satisfies the equilibrium equation (see Fig. 11).

$$T'(x) = -t(x) \quad \ldots\ldots\ldots\ldots\ldots\ldots (50)$$

Multiplying both sides of Eq. 50 by an arbitrary function $u(x)$, and integrating over the span length yields

$$\int_A^B T' u \, dx = -\int_A^B t u \, dx \quad \ldots\ldots\ldots\ldots (51)$$

If no concentrated longitudinal forces act, and u is assumed to be continuous, integration by parts gives

$$\int_A^B t u \, dx + T_B u(B) - T_A u(A) = \int_A^B T u' \, dx \quad \ldots\ldots\ldots (52)$$

If the left and right hand side of Eq. 8 are added to the left and right hand side of Eq. 52, a principle applicable to the computation of deflections including the effect of thrust is obtained. The function u may be handled with the same freedom as η. To find the displacement in a direction m of joint i of an

ideal truss, for instance,

$$u' = g(\bar{T}) \quad \ldots\ldots\ldots\ldots\ldots\ldots (53)$$

in which g depends on the material of the truss (for elastic members $g = \bar{T}/AE$) and

$$y_m(i) = \sum_{S} T\, g(\bar{T}) \quad \ldots\ldots\ldots\ldots\ldots\ldots (54)$$

in which S is a statically determinate truss obtained from $\bar{S}$ by eliminating bars, reactions or a combination of them, and loaded at joint i by a unit load in the

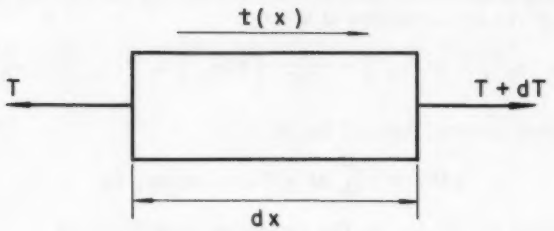

FIG. 11

m direction (so that its reactions do no virtual work with respect to the displacements in $\bar{S}$ unless there is a known support settlement there).

APPENDIX II. SHEAR AND THERMAL DEFLECTIONS

If the effect of shear or temperature gradients is to be included in the determination of deflections, then the moment curvature relationship must include these effects.

For instance, if a linear temperature gradient is applied to a symmetrical elastic beam, the appropriate relation is

$$y'' = -\left(\frac{M}{EI} + \alpha \frac{\Delta T}{h}\right) \quad \ldots\ldots\ldots\ldots\ldots (55)$$

in which α is the coefficient of thermal expansion, 2h is the beam depth, and $\Delta T/h$ is the temperature gradient. By substituting Eq. 55 into Eq. 13, thermal deflections will be included.

The determination of elastic deflections due to shear may be handled in either of two ways. Assuming no warping, the slope caused by shear alone is given by

$$y'_V(x) = \frac{k\, \bar{V}(x)}{AG} \quad \ldots\ldots\ldots\ldots\ldots (56)$$

in which k is a numerical factor depending on the cross section, A is the cross-sectional area, and G is the shear modulus. If no concentrated forces act, Eq.

56 may be differentiated and combined with the corresponding expression for flexure alone to give

$$y'' = -\frac{M}{EI} - \frac{k\,\bar{W}}{A\,G} \quad \ldots\ldots\ldots\ldots (57)$$

since

$$V' = -W \quad \ldots\ldots\ldots\ldots\ldots (58)$$

and substituted into Eq. 15 to give

$$y(\bar{x}) = \int_S M\left(\frac{\bar{M}}{EI} + \frac{\bar{W}k}{AG}\right)dx \quad \ldots\ldots\ldots\ldots (59)$$

If, however, a concentrated force P acts at $x = x_p$, then, since $\bar{V}$ is discontinuous there, y' is discontinuous at $x = x_p$;

$$y'(x_p^+) - y'(x_p^-) = \frac{k}{AG}\left[V(x_p^+) - V(x_p^-)\right] = -\frac{kP}{AG}\Big]_{x_p} \quad \ldots (60)$$

Using the more general form of Eq. 8,

$$\eta(\bar{x}) = -\int_A^B M\,\eta''\,dx - M(x_S)\,\theta_S \quad \ldots\ldots\ldots\ldots (61)$$

and substituting Eq. 60 for θ_S, the deflection is obtained as

$$y(\bar{x}) = \int_S M\left(\frac{\bar{M}}{EI} + \frac{k\bar{W}}{AG}\right)dx + \frac{kP}{AG}M_{x_p} \quad \ldots\ldots (62)$$

that could also have been obtained by considering the concentrated force as the limiting case of a distributed load.

The more familiar expression for elastic deflections due to shear may be obtained by not differentiating the right hand side of Eq. 4 by parts. Then the expression for deflections becomes, instead of Eq. 13,

$$\eta(\bar{x}) = -\int_S V\,\eta'\,dx \quad \ldots\ldots\ldots\ldots\ldots (63)$$

Substituting Eq. 56 into Eq. 63, the deflection due to shear alone is obtained as

$$y_V(\bar{x}) = \int_S k\,\frac{V\bar{V}}{AG}\,dx \quad \ldots\ldots\ldots\ldots (64)$$

that may be added to the flexural deflection to give

$$y(\bar{x}) = \int_S \frac{M\bar{M}}{EI}\,dx + \int_S k\,\frac{V\bar{V}}{AG}\,dx \quad \ldots\ldots\ldots (65)$$

ACKNOWLEDGMENT

The writer wishes to thank William Spillers for carefully and critically reading the manuscript.

An excellent paper[11] which, although just published, has been available to the writer for a long time is responsible for his awareness of the possibility of generalizing the interpretation of the virtual displacement.

---

11 "Virtual Work," by T. Kane and S. Shore, Bull. Pol. Inst. Jassy, Vol. 6(10), 1960.

2645 November, 1960 ST 11

Journal of the
STRUCTURAL DIVISION
Proceedings of the American Society of Civil Engineers

LOAD DISTRIBUTION IN COMPOSITE GIRDER-SLAB SYSTEMS

By G. Hondros,[1] M. ASCE and J. G. Marsh[2]

SYNOPSIS

A series of simply supported composite girder-slab systems embracing five and ten girders interconnected by a reinforced concrete slab was tested, from which confirmation of certain assumptions made in the design of a prototype bridge was sought. Comparisons between actual and theoretical behavior are made and the effect of skew angle of the bridge and torsional stiffness of the griders is assessed. The work brought to light the fact that the neutral planes of the girders are neither coplanar nor stationary and an attempt is made to explain this phenomenon, particularly from the point of view of induced distributed longitudinal forces in the slab, which undoubtedly occur in these structural types.

Primarily, the experimental work was aimed at providing an assessment of assumptions made with regard to distribution of loads and the effect of a 30° skew angle on a ten girder, 130-ft composite steel girder and concrete deck bridge span. Following the examination of the first model, two additional types were tested in which all properties were retained except that in the second model the torsional stiffness of the beams was reduced by 50%, and in the third model

Note.—Discussion open until April 1, 1961. To extend the closing date one month, a written request must be filed with the Executive Secretary, ASCE. This paper is part of the copyrighted Journal of the Strucutral Division, Proceedings of the American Society of Civil Engineers, Vol. 86, No. ST 11, November, 1960.

1 Senior Lecturer in Civ. Engrg., The Univ. of Western Australia, Nedlands, W. A.
2 Bridge Engr., Main Roads Dept., Western Australia.

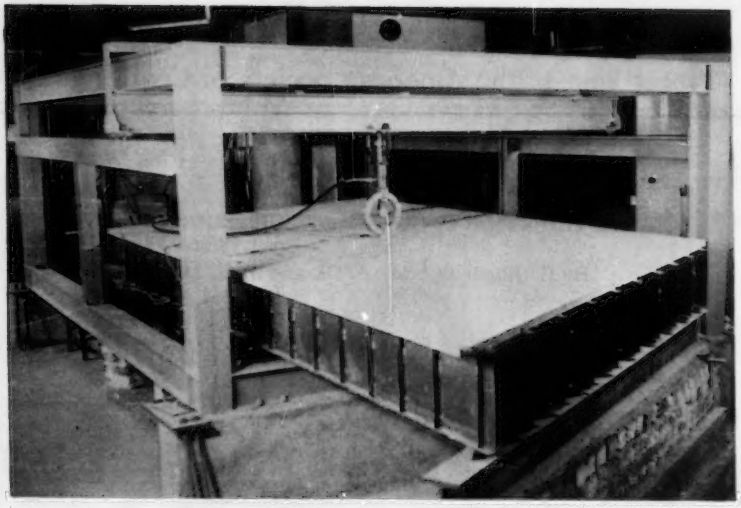

FIG. 1.—LOADING FRAME WITH SKEW-MODEL UNDER TEST

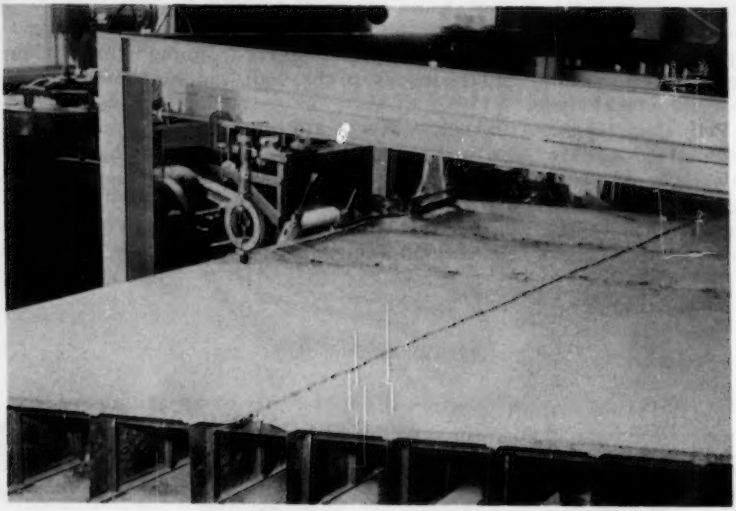

FIG. 2.—SLAB FORMWORK AND REINFORCEMENT

the span was not skewed. From each of these main models, two 5-girder systems, cracked and uncracked, were obtained by cutting the former along their longitudinal center line.

DESCRIPTION OF MODELS

Notation.—The letter symbols adopted for use in this paper are defined where they first appear, in the illustrations or in the text, and are arranged alphabetically, for convenience of reference, in Appendix II.

Identical variations in flexural stiffness ratios of composite girder to slab occurring in the prototype, along the length of its girders, were used in the

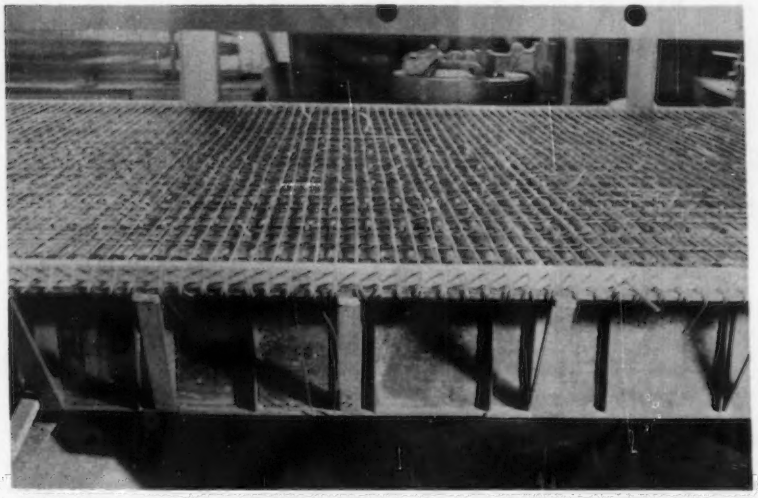

FIG. 3.—MODEL AFTER CENTRAL LONGITUDINAL CUT

models. Limitations of laboratory space and finance dictated the scale of plan dimensions while the vertical scale was governed by what was considered a reasonable minimum slab thickness ($1\frac{1}{4}$ in.). The scales chosen were 1/10 of prototype for plan dimensions and 1/6 of prototype in elevation.

Shear connectors were not scaled down from the prototype but were designed specifically for the attendant effects as developed in the models. Channel-section connectors were employed and proportioned according to the theory of Viest and Siess[3] (Figs. 1 through 6). Clamping devices were provided whereby the ends of the girders were held down onto the bearings to prevent uplift, but, at the same time, to furnish little or no bending restraint at these points. Fig. 1 shows the loading frame that allowed transverse and longitudinal movement

[3] "Design of Channel Shear Connections for Composite I-Beam Bridges," by I. M. Viest and C. P. Siess, Public Roads, Vol. 28, No. 1, April, 1954.

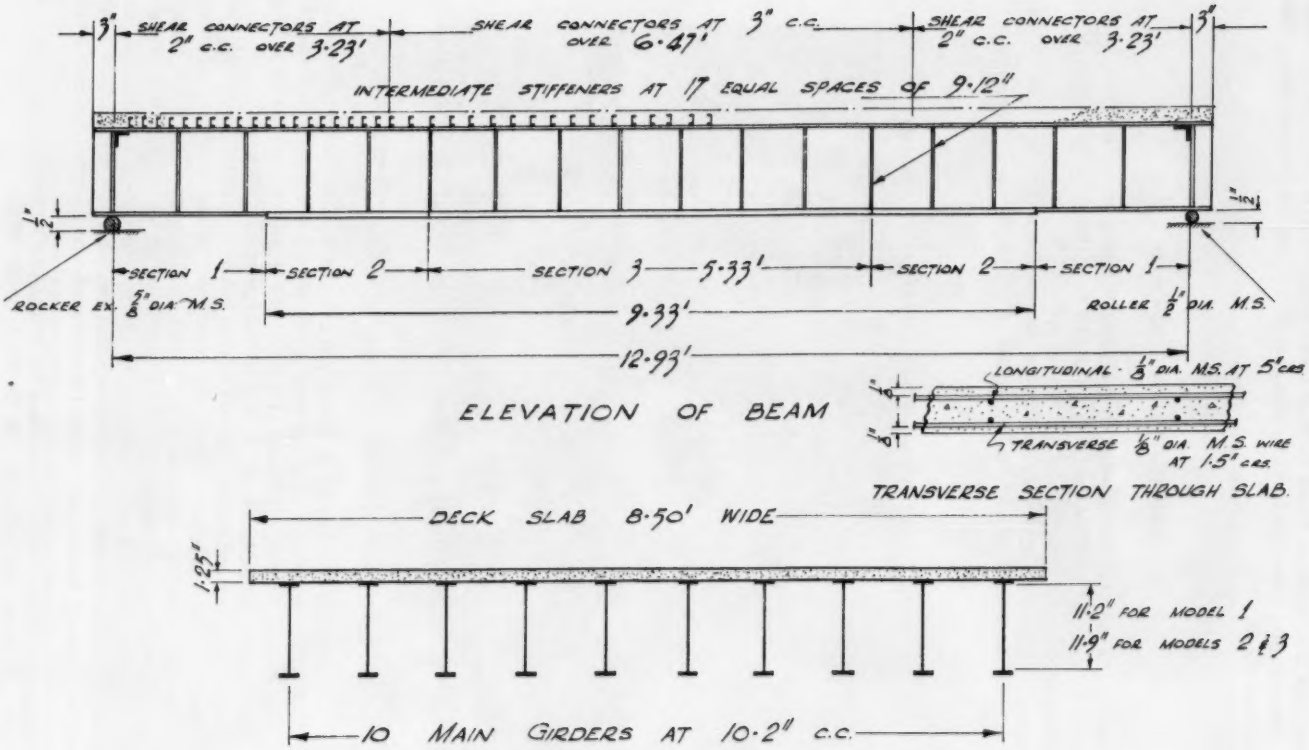

FIG. 4.—CROSS SECTION THROUGH MODEL

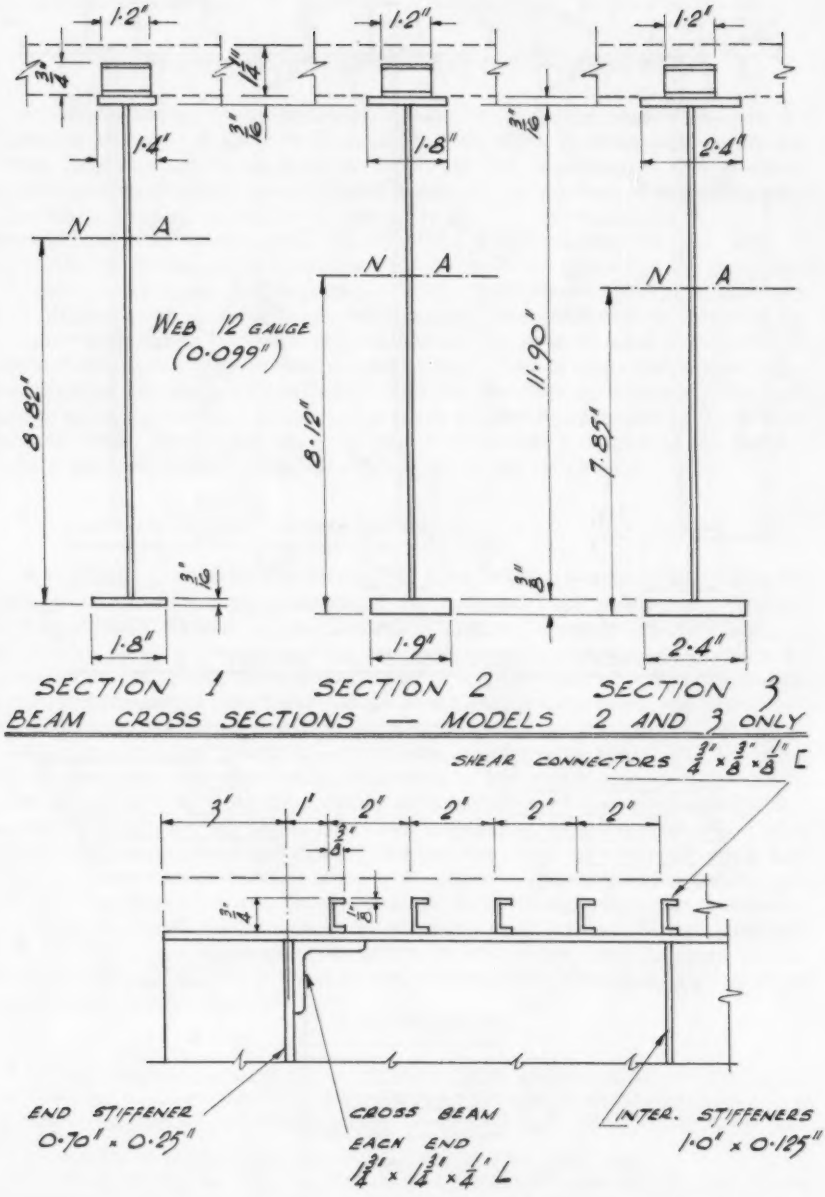

FIG. 5.—END DETAIL PART ELEVATION OF BEAM TYPICAL FOR ALL MODELS

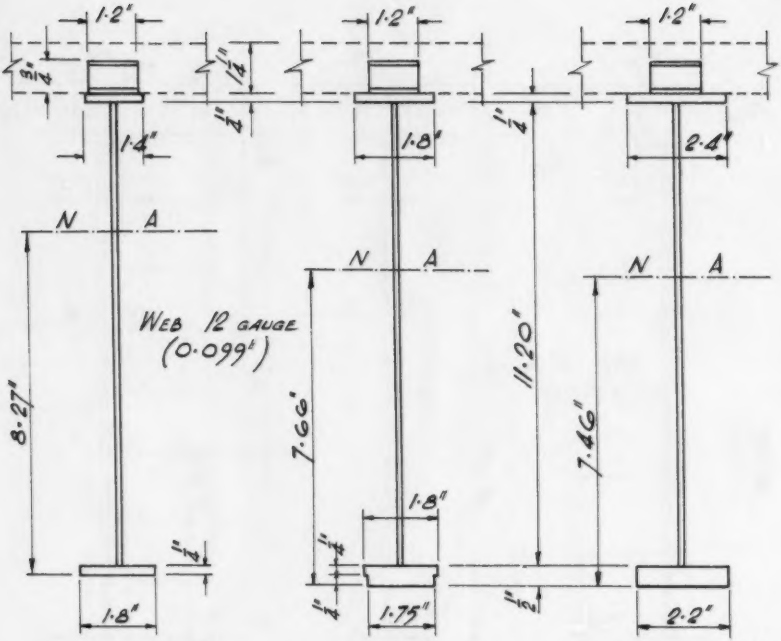

BEAM CROSS SECTIONS — MODEL 1 ONLY

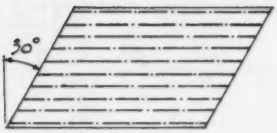

MODEL 1 (KENDALL)

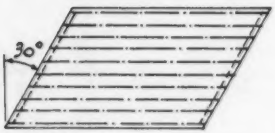

MODEL 2 (WELLS)

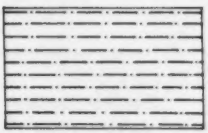

MODEL 3 (BARON HAY)

FIG. 6

of the jack whereby any point on the surface of the model slabs could by subjected to point loadings.

EXPERIMENTAL TECHNIQUE AND INSTRUMENTATION

Strains were measured by electric-resistance strain gages (SR 4) of the bonded-wire type. A total of 78 gage stations were present in each model. These gage stations were selected to permit the construction of a comprehensive series of influence surfaces of strain and, in addition, some gages were situated on the webs of selected girders to provide information as to the progressive position of the neutral planes of the girders during the test. (Fig. 7) Manipulation of the gages conformed to the methods described by Hondros.[4] The gages were connected through a suitable switch box in groups of twelve to a multichannel D. C. bridge. Notwithstanding calibration of the electric resistance gages (gage factor check), mechanical gages were used to confirm the electric strain readings at selected points from time to time. Deflections were measured by dial gages (Ames type; 0.0001 in. per division) mounted under each girder at the appropriate point. Loads were applied by hydraulic jacks through proving rings, Fig. 1, for accurate load measurement, except in the tests to failure when such measurements were made by pressure gage.

TESTS ON CONCRETE

A modular-ratio of 10 was chosen for the live-load design of the composite beam of the prototype. Accordingly, it was necessary for the elastic properties of the concrete of the model to conform to this requirement. In the absence of any direct means of predicting this, the concrete mix was varied until tests for modulus indicated that the nominal value of E_c, the elasticity modulus of concrete, had been achieved. Three independent methods were employed to measure E_c (indirectly via specimens); the electrodynamic,[5] the Brazilian[6] and by embedding gages at the "heart" of a 6 in. cube compressive specimen. As was to be expected, the cube specimens, wherein load and strain distributions are indeterminate and variable, gave rather erratic results. Generally, between zero and working stress, E_c on the cube was impossibly high but above this limit, E_c tended to be constant and agreed with the results of the electrodynamic test. At about three times working stress, E_c began to fall as plastic deformation set in. The Brazilian and electrodynamic methods agreed and gave constant values of E_c, which, in the case of the former, remained so to failure. The high value of E_c at low stresses is thought to be due to the establishment of non-uniform states of stress in the cube and, consequently, different rates of strain at different points within the cube.

---

4 "The Protection and Manipulation of Electric-Resistance Strain Gauges of the Bonded Wire Type for Use in Concrete, particularly for Internal Strain Measurement," by G. Hondros, Magazine of Concrete Research, London, Vol. 9, No. 27, November, 1957, pp. 173-180.

5 "Methods of Testing Concrete," British Standard No. 1881, 1952.

6 "The Evaluation of Poissons Ratio and the Modulus of Materials of a Low Tensile Resistance by the Brazilian (Indirect Tensile) Test with Particular Reference to Concrete," by G. Hondros, Australian Journal of Applied Science, Vol. 10, No. 3, September, 1949, pp. 243-268.

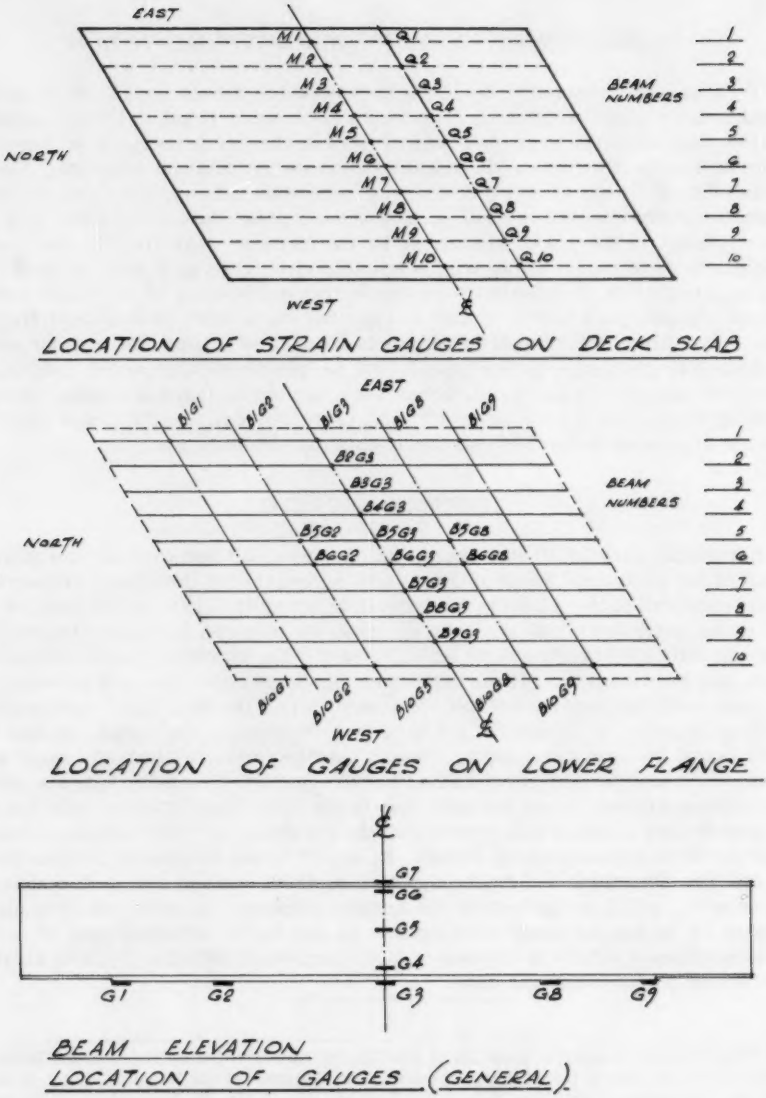

FIG. 7.—LOCATION OF GAUGES

The ultimate 28-day strength of 6 in. cube test specimens taken from the concrete of the slabs was in the range 3,000 to 4,000 psi.

TESTS OF MODELS

Preliminary Tests on Steel Beams.—Before the model was assembled, the steel beams, provided with suitable temporary lateral bracing, were tested individually. Principally, these tests were meant to check the degree of agreement in the beams' behavior compared to the theoretical, that is, to prove that the stiffness of the beams agreed closely with the computed value. Secondly, the tests were used to bring to light any faults due to imperfect preparation and fabrication. The beams were loaded at mid-span with temporary lateral bracing on the top flange which was introduced to eliminate lateral instability. Strains and deflections were observed during several load increments.

The Girder-Slab Models.—

Loading.—A load of 4 tons was selected and this was applied to the model at points over the girders and on transverse lines at $\frac{1}{8}$, $\frac{1}{4}$, and $\frac{3}{8}$ of the span as

TABLE 1.—TEN GIRDER MODEL—UNCRACKED

Load at	Strain Measured At	Gages Read
Center-line	Center line and 1/4 span	All gages
3/8 span	"	Bottom flange only
1/4 span	"	All gages
1/8 span	"	Bottom flange only

Deflection Readings

Load at	Dial Gages Read
Center-line	Center line and 1/4 span
1/4 span	"

well as at mid-span. The load on the cantilevered sections of the slab beyond the edge beams was reduced to a figure that avoided the possibility of damaging the concrete.

Strain Gages.—Gages were attached to the lower and top flanges of the beams and to the concrete surface at the center and one-quarter lines (Fig. 7).

Dial Indicators.—Deflection observations were taken at the center and quarter lines on the underside of the girders by Ames dial indicators.

Test Sequence.—Generally, positions on the slab at which the load was applied and points where strain measurements were recorded, as well as test details, conformed to the pattern indicated in Table 1 for the ten girder model - uncracked.

For the ten girder model - cracked test, the slab over five adjacent girders between the edge beam and the center line, was systematically and extensively cracked between the girders in an attempt to simulate the effect of tensile cracking of a bridge slab in service. Exactly one half the model was treated in this way for the following reasons: (1) This would give a reasonable assessment of the effect of cracking provided loading was confined to the cracked side. The remote, stiffer, uncracked half does not have a great deal of effect. (2) By cutting the ten girder model along its longitudinal center line, it was desired

to obtain two five girder models for testing, one cracked and one uncracked, thus sustaining the elastic and stiffness properties of the models. In the case of ten girder-cracked model loads were applied and effects measured as indicated in Table 2. At the end of this test, the ten girder model was cut along its longitudinal center line into cracked and uncracked halves. This was done by using a electric hammer to sever the concrete, heavy-duty wire cutters being used for the steel. A reasonably neat cut was obtained (Fig. 3).

For the five girder model - uncracked, loads were placed at girder centers across the center line and one quarter span. Strains in the bottom flanges and the beam deflections were observed at the center line and the one quarter span.

For the five girder model - cracked, the test sequence was similar to that of the five girder - uncracked case. However, in addition, attempts were made to load this system to failure.

In the test on the single - composite beam, one edge beam together with its section of the slab was separated from its model and tested as a composite item.

RESULTS AND ANALYSIS

Preliminary Tests on the Bare Steel Beams.—Mention has already been made of the provision of lateral restraints to reduce the inherent lateral instability of the steel sections and to permit singular tests to be done on them. However, this support, provided in the plane of the top flanges, was not entirely successful

TABLE 2.—TEN GIRDER—UNCRACKED

Load at	Strain Observed	Deflections Observed
Center line	Center line and 1/4 span	Center line and 1/4 span
1/4 span	Center line and 1/4 span	Center line and 1/4 span

and some lateral movement was observed both in the top flange and in the web between stiffeners. The beams behaved elastically and identical readings were obtained for repetitive loading for top flange stresses up to 20,000 psi. However, stresses in the top flange were generally somewhat higher than their theoretical equivalents, the neutral plane lower and the deflections greater.

These departures from theory were thought to be due to buckling of the web and the movements consequent on lateral instability of the flanges. Significantly, readings taken on each side of the web indicated that the mean stresses in the web were often less than the theoretical values, whereas the mean stress in the top flange gave no such variation.

The Girder-Slab Models.—

Migration (Vertical Shift) of the Neutral Plane.—The neutral planes of the beams were observed to alter their position with movement of load across the slab and, in general, there were large downward displacements of these planes as the load moved away from the beam in question. This hitherto unrecorded phenomenon is considered to be a characteristic of T-beam bridges and is of distinct importance. The two major factors considered to act in determining the magnitude and direction of the vertical shift of the neutral planes of the girders in composite systems are distributed longitudinal forces in the slab, and slab shrinkage.

In a system in which the slab is supported on flexible beams with which it does not interact no resultant forces (additional to M/Z effects) are induced in the slab by bending and the load is distributed to beams by means of vertical shear, torsion, and bending resistance of the slab. In T-beam composite systems, the slab, considered as a transformed steel area, becomes a thin membrane and, together with the girders, forms a type of cellular network. The interconnection of the girders by this thin skin withdraws from them the freedom to develop top flange stresses with a distribution identical to that in the former case (that is, slab resting on elastic beams). Consequently, there will be some modification of the normal forces in the slab by means of lateral distribution from horizontal shear action.

Accordingly, a modifying system of longitudinal forces in the slab will be produced. It is important to note that these forces constitute an internal self-equilibrating system and, as static equilibrium must be satisfied across any transverse plane, they must equate to zero because the load system has not altered.

These distributed components are designated P_1, P_2 . . . , the subscripts referring to the corresponding girders in the structure. Each is assumed to act at the centroid of that portion of the slab regarded as the flange of the composite section. They are, in effect, eccentric forces with respect to the neutral planes of the composite sections and must, when acting, cause a shift in the position of the neutral plane of pure flexure. If this distributed force is tensile, it will induce both a direct and bending tension in the upper fibers of the steel girder, while in the lower fibers the direct tension may be partially or completely balanced by the induced bending compression (from the P force). The net result is that the neutral plane of the beam is raised. Similarly, if the distributed force is compressive, the neutral plane of the beam will be lowered.

To put this theory to quantitative test the stresses at any point in the composite beam were assumed to be resolved into three components satisfying

$$f = \pm \frac{P}{A} \pm \frac{P\,e}{Z} \pm \frac{M}{Z} \quad \ldots\ldots\ldots\ldots\ldots\ldots (1)$$

Provided two stresses f_B, the bottom flange steel stress, and f_T, the top flange steel stress, are measured at any cross section, P, the distributed longitudinal force in the slab at a girder, and M the bending moment can be computed by the solution of the two simultaneous equations obtained by equating the measured stresses to the theoretical values expressed as functions of P and M. The function e is the eccentricity of force P with respect to the neutral plane of pure flexure of the composite girder, A is the cross sectional area of the composite section, and Z is the section modulus at the fiber at which the stress is required. Some hope was entertained that the values of M could be compared to theoretical values computed according to the accepted elastic theories of either Hendry and Jaeger[7] or Morice and Little.[8] Unfortunately, as may be seen subsequently, due to breakdown of the slab in bending from transverse distribution, no strict comparisons could be made in this regard.

However, it was possible to accurately assess (it is claimed) the effect of the distribution of the "P" forces in spite of large variations in the effective

---

[7] "The Load Distribution in Highway Bridge Decks," by A. W. Hendry and L. G. Jaeger, Proceedings, ASCE, No. ST 4, July, 1956, pp. 1–48.

[8] "The Analysis of Right Bridge Decks Subjected to Abnormal Loading," by P. B. Morice and G. Little, Cement and Concrete Assn., London, D. B. 11.

value of E_c, or the actual rates of strain occurring in the concrete. Initially, E_c was taken as 4×10^6 psi, but when values of P were computed on this basis ΣP did not equal zero. It was then clear that for this to be so, E_c should be in the order of 1.5×10^6 psi. The effective value of E_c was then investigated.

In the experimental work under review, the only complete set of recorded steel strains in the top and bottom flanges were for the ten girder-uncracked square model and of these, the readings at midspan for load at midspan were analyzed. Concrete strain measurements were inconsistent and none of the observed values were used in the analysis.

By eliminating M from the two equations for stresses f_B and f_T mentioned previously and by expressing the section properties as functions of E_c, a relationship was obtained for P in terms of E_c and the stresses by summing effects for all girders (see Appendix I).

$$\Sigma P = \left\{\left(1.07 + 0.454\, E_c\right) \Sigma f_T + \left(1.45 - 0.0283\, E_c\right) \Sigma f_B\right\}$$

By equating this expression to zero a value of E_c was found for each load position. This value of E_c is a weighted mean for all girders and, generally, it was found to vary from 1.5 to 2×10^6 psi, depending on which beam was loaded. One "detached" value was as low as 1×10^6 psi. It will be shown subsequently that these values are reasonably consistent with the results obtained in the single composite beam test. Further, with reference to the distribution of forces in the slab induced by composite T beam action, the values of M found by eliminating P from the expressions for f_T and f_B (Appendix I), indicate a less favorable transverse distribution of load than that indicated by the recorded lower flange strain readings. In other words, the effect of composite or monolithic T-beam action is to improve the load distribution that would occur in a structure incorporating separate slab and beams. The following reasons would support this conclusion. For values of E_c, certainly down to 1.5×10^6 psi and possibly as low as 1.0×10^6 psi, the expression for M in terms of observed stresses at the top and bottom flanges of the steel beams was practically constant, as was the modulus of section for stress in the lower flange. That is, these are practically independent of the value of E_c (see Appendix I and Figs. 18 and 19).

Therefore, the stress values in the lower flanges computed from the values of M could be compared to the actual values computed from the strain measurements and any differences, justifiably, could be attributed to the redistribution of the forces in the slab. In the ten girder models the greatest value of such difference was in the order of 9%, resulting in an increase of 4% (from 43% to 47%) in the distribution coefficients, as may be seen from Fig. 8.

Further demonstration of the validity of the theory stems from the fact that ΣM for the indicated value of E_c of 1.5×10^6 psi for the composite beams is 373,740 in.-lbs for model 3 whereas the measured static moment from the 4.175 ton load acting on the span at 3 in. off center was equal to 362,200 in.-lbs, a 3.2% disagreement. The summation of the lower flange strains gave 403,000 in.-lbs as the moment value for $E_c = 1.5 \times 10^6$ psi, assuming that the beams acted according to their section properties. This moment does not closely approach the static value. With regard to the variable nature of E_c revealed by a consideration of the "P" forces, it was apparent after a little thought, that the movement of the neutral planes is partly influenced by such variations in the value of E_c. As the bridge is subjected to load, shrinkage cracks in the slab begin to close up, as a result of which the neutral plane of the composite beam tends to rise an amount depending on the degree to which the cracks have closed.

This can be considered to be a rise in the value of the effective E_c. Thus, as observed in the relatively heavily loaded beam, under a load the neutral plane would occupy a higher position than in the less heavily loaded remote beams. Significantly, it was observed that the position of the neutral planes of the remote beams fell far below that of the composite beam for which $E_c = 0$, or that for the steel section alone with the slab non-existent. Thus, indicating the existence of the "P" forces.

If E_c varies with load, as described previously, strains should not exhibit a linear relationship with load in the lower stress ranges, that is, before cracks have completely closed. In the case of the single composite beam cut from the model, the expected effect due to changing E_c was pronounced in the top flange but to a lesser extent in the bottom flange. In the latter case, the section modulus (Z) would be kept reasonably constant because, as the cracks in the slab

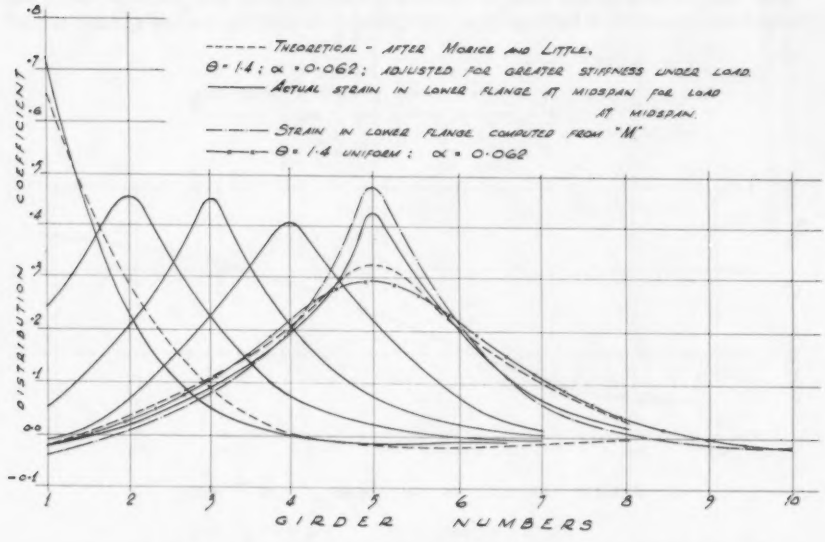

FIG. 8.—TEN GIRDER UNCRACKED SLAB DISTRIBUTION COEFFICIENTS

close up the neutral plane would rise correspondingly. Some additional and indeterminate cracking in the concrete, caused by the hammer used in cutting out the composite beam, may have made the effect more marked as compared to the model bridge.

The value of E_c deduced from strain readings for various loads in the single beam test showed a variation of from 0.49×10^6 psi at $\frac{1}{4}$-ton load to 2.38×10^6 psi at 3-ton load. The values were confirmed by agreement between computed and actual deflections. E_c in these calculations was taken to vary according to the strain at the center of the slab and, hence, varied along the length of the beam as well as with the load. The variation of E_c with strain was determined as an approximate mean line drawn through points computed from the one quarter line and midspan strain readings, the section properties in terms of E_c and the theoretical bending moments for the applied load (Fig. 9).

It is of interest to note that as the load tended to a zero value, E_c tended to zero, indicating that at zero load the slab contributed nothing to the strength of the composite section. Thus, the indicated low and variable nature of E_c is confirmed.

Summarizing the preceding analysis one can say that there are strong reasons leading to the conclusion that the two important factors that govern the shift of the neutral planes of the girders in composite systems are (1) the distribution of additional longitudinal forces in the slab, and (2) the changing value of the effective E_c of the concrete slab as the load moves across the slab causing shrinkage cracks in the concrete to close or open.

Altered Lateral Distribution of Load Due to Systematic Load Cracking of the Slab.—Cracking of the slab reduced its stiffness resulting in increases of the lower flange stresses of the interior girders of the ten girder model by about 15% and approximately 7% for the edge-girders.

The comparison in the case of the five girder models was made between the cracked and uncracked half-models obtained from cutting the ten girder model

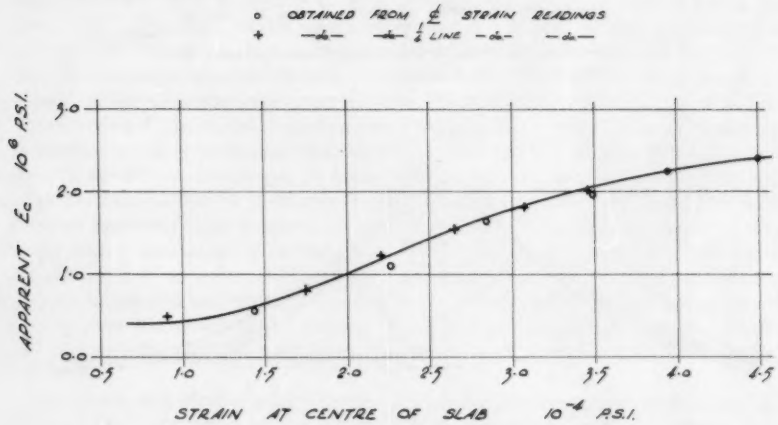

FIG. 9.—SINGLE BEAM TEST RELATION OF APPARENT E_c TO STRAINS AT CENTRE OF CONCRETE SLAB

in half. Possibly, added variables entered into the comparison in this case. The mean increase in the interior girders was about 14% and the mean for the exterior girders about 6%.

Comparison of Five and Ten Girder Behavior with Each Other and with Theory.—Comparison with theory can be made with greater facility in the case of the square model than the skew models. The strains in the lower flanges for the five girder-uncracked model were, on the average, 8% greater, and the edge girder strains possibly 3% greater than the corresponding strains for the uncracked ten girder system. For the five girder-cracked model the lower flange strains were up to 5% greater for the interior beams but not significantly different for the exterior beams.

Actual distribution of lower flange stresses on the transverse center line, compared to theoretical values deduced from charts prepared by Morice and Little[8] after Guyon and Massonet, appear in Figs. 10 and 11.

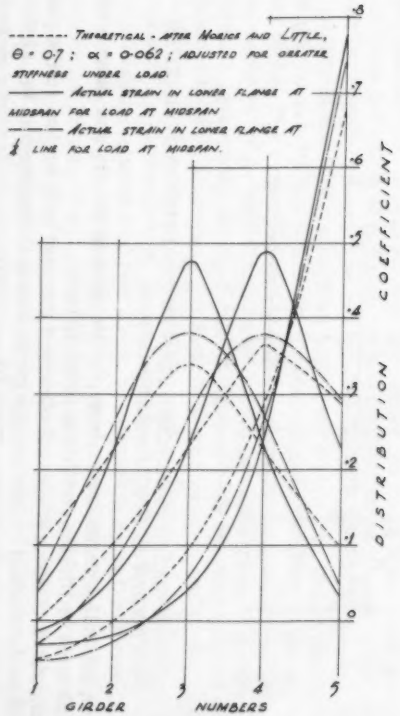

FIG. 10.—FIVE GIRDER UNCRACKED SLAB DISTRIBUTION CO-EFFICIENTS

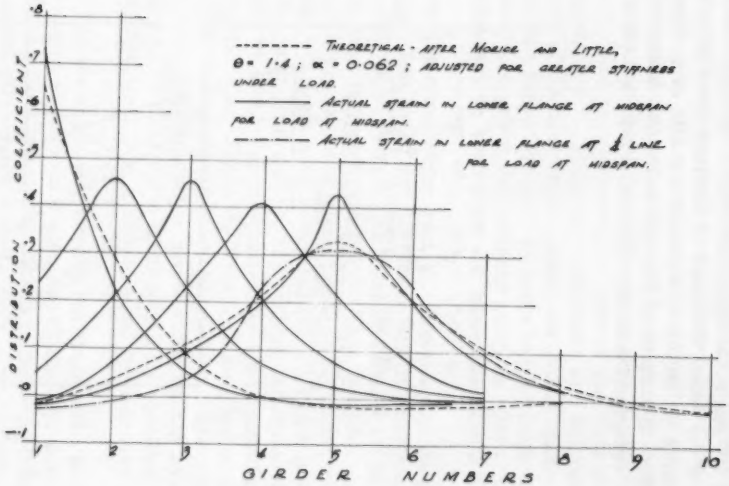

FIG. 11.—TEN GIRDER UNCRACKED SLAB DISTRIBUTION COEFFICIENTS

In the evaluation of stiffnesses, E_c was taken as 4 x 10^6 psi transversely, and 1.5 x 10^6 psi in the composite beam. An equivalent uniform I, moment of inertia, for the beam was used to compute the stiffness factor, calculated to give the same deflection at midspan for load at midspan, as the model beam.

The effect of torsion of the slab in the two theories[7,8] was approximately the same, reducing the no-torsion coefficients by 20% of the difference between

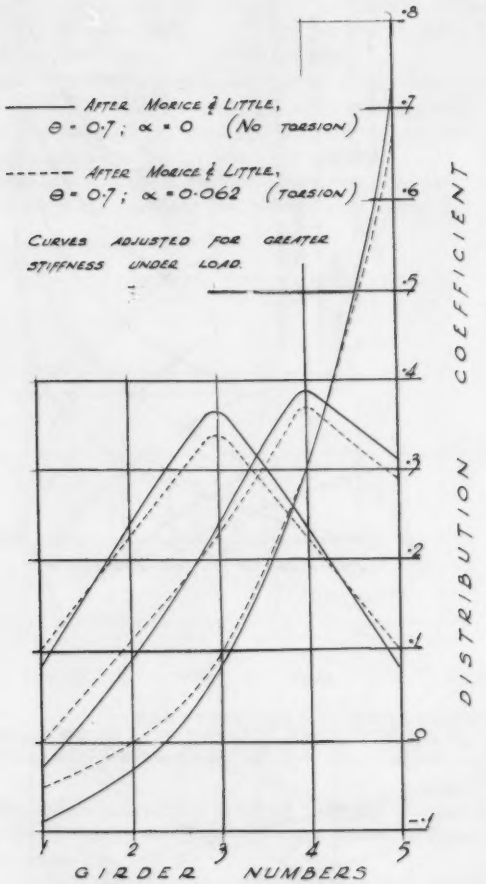

FIG. 12.—FIVE GIRDER UNCRACKED SLAB DISTRIBUTION COEFFICIENTS AT MIDSPAN FOR LOAD AT MIDSPAN

no-torsion and full-torsion coefficients, in the case of Hendry and Jaeger, and 25%, in the case of Morice and Little (Fig. 12).

A comparison of theoretical and observed results, with regard to the proportion of load absorbed by the various girders in both the five and ten girder-uncracked models, is presented in Figs. 10, and 11 for the center and one quarter transverse lines.

Considering the ten girder model, it was apparent that a high degree of agreement between the theoretical and observed results can be achieved by increasing the value of E_c for the composite beam. However, this would negate the previous conclusions drawn with regard to the low effective average value of E_c for the composite beams. This objection can be overcome if the average value of E_c is maintained for all girders while the value of E_c for the girder under load is increased. This is consistent, in view of the findings with the single composite beam, wherein E_c is shown to increase with increasing load. Accordingly, in the case of the complete system, the girder under the load would, in fact, be stiffer than the others as it is more heavily loaded. Such increased stiffness would in turn cause the girder to carry an even greater proportion of the load, which can be seen from an inspection of the theoretical curves in Fig. 8.

In the case of the interior beam under load, an allowance for the increased stiffness of the girder to conform to the E_c-strain relation observed for the single composite beam caused an increase of from 29.5% to 32.5% in the theoretical proportion of the load taken by such beam. This, however, is still far below the observed value (being assumed proportional to the strain in the lower flange) of 43% in the case where the load is applied and the strain is measured at midspan. On the other hand, it is close to the value of 31% observed for the proportion of strain taken by the girder in question, for load applied and strain measured at the one quarter line (Fig. 15). This indicates the possibility of a breakdown of transverse slab-stiffness toward midspan. Accordingly, the theoretical transverse slab moments were investigated on the basis of the transverse E_c equalling 4×10^6 psi and the longitudinal E_c equalling 1.5×10^6 psi and the yield stress in the steel having a value equal to the measured stress of 24,000 psi.

Indeed, it was found that the maximum theoretical transverse bending moments exceeded the computed moment of resistance of the slab at the yield of the steel (Figs. 13 and 14). This was more marked in the five girder models and was reflected in a more unfavorable distribution of load therein.

Distribution curves for lower flange stresses at the one quarter and center lines for loads in turn at the one quarter and center lines (Figs. 11 and 15) indicate that the slab broke down in transverse bending at the one quarter line for load applied at the one quarter line. An observation made from the fact that the curve at the center line for load at the one quarter line is very different from the curve at one quarter line for load at one quarter line and yet very similar to the curve for the one quarter line for load at the center line.

Mention must be made of an apparent omission in the investigation, which is that no results are available for incremental loads up to the value used in the tests. The reason for this is that the strain gauges and the models generally were subjected to "exercising runs" before the actual recorded tests were performed, by applying load at discreet points over the one quarter and center lines. Probable systematic but inextensive cracking of the slab in positive and negative bending occurred at certain regions from such loadings thereby decreasing the slab stiffness. Incremental loadings were then applied and a linear relationship between load and strain was observed up to the design load of 4.19 tons. Accordingly, it was decided to apply this load only during tests. Had graduated loading been applied and results recorded from commencement, a non-linear relation between load and strain may have been observed.

Fig. 16 indicates the satisfactory agreement of the two theoretical approaches, namely those of Hendry and Jaeger, and Morice and Little, especially

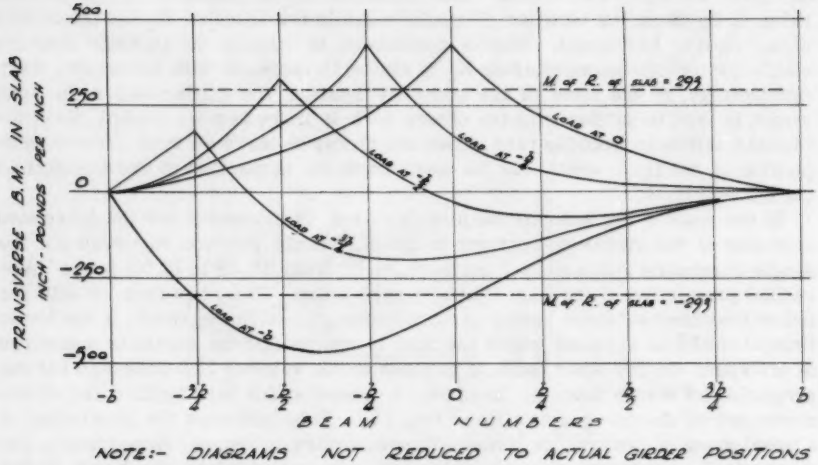

FIG. 13.—FIVE GIRDER SPAN THEORETICAL TRANSVERSE BENDING MOMENT IN SLAB AFTER MORICE AND LITTLE.

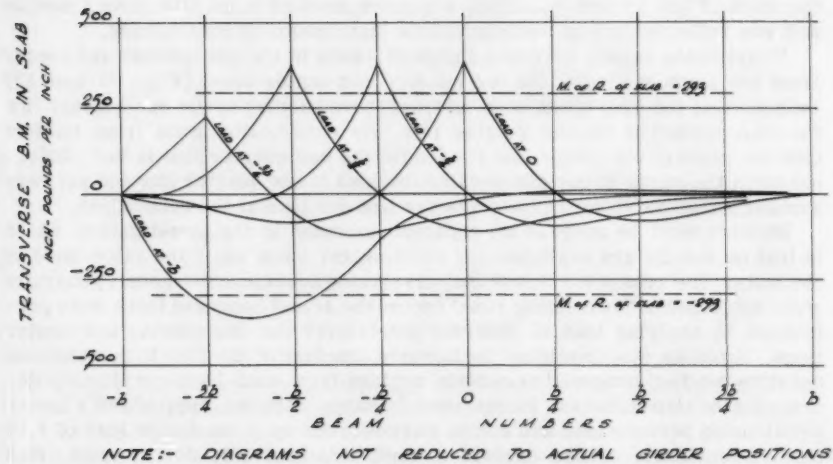

FIG. 14.—TEN GIRDER SPAN THEORETICAL TRANSVERSE BENDING MOMENT IN SLAB AFTER MORICE AND LITTLE

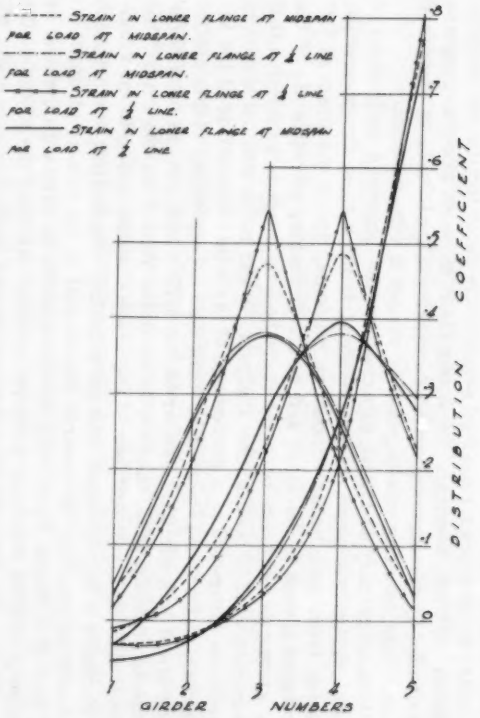

FIG. 15.—FIVE GIRDER UNCRACKED SLAB DISTRIBUTION COEFFICIENTS

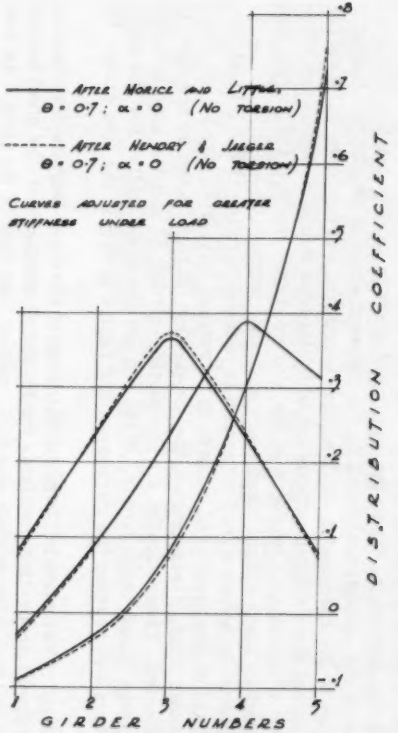

FIG. 16.—FIVE GIRDER UNCRACKED SLAB DISTRIBUTION COEFFICIENTS AT MIDSPAN FOR LOAD AT MIDSPAN

in the case of the five girder model. Greater divergence occurs in the ten girder instance, which could be due to the fact that data for the five girder span were transformed for use in the ten girder case with the method of Hendry and Jaeger. With regard to the treatment of the edge-girder by these theoretical methods an important qualitative difference must be recorded which favors the Morice-Little approach. When the number of girders incorporated in the system exceeds the number embraced by the present scope of Hendry and Jaeger's method (as in the case under review) the theoretical curves have to be extrapolated beyond the girder-positions for which figures would be available (without tedious computation) whereas in the Morice-Little method, the curves are interpolated—a much simpler and more accurate procedure.

Quantitatively, however, this objection is reduced because (Figs. 10 and 11), generally, when the number of girders is increased, say, from five to ten (with an increased width of structure), the proportion of load taken by the edge is hardly affected. Theoretically, for the outside-girder, 66% of the load is taken by this girder (load over girder) in the ten girder case, whilst for the same girder sizes and spacing the corresponding figure is 67% in the five girder instance.

The Effect of Variation in Torsional Stiffness of the Steel Beam.—Maintaining other sectional properties constant, the torsional stiffness of the steel beams in the second and third models was 50% smaller than that of the first. As was expected, no significant differences in behavior or the models was directly caused by this change.

The effect of 30° skew.—Except that model 2 was skewed at 30° and model 3 was square, the two systems were identical in all other respects. Generally, strains and deflections for the skew case were 20% less than those observed to occur in the square model. This margin can be taken as a measure of the increase in stiffness of this model due to skew. However, the proportion of the load distributed to each beam remained sensibly the same for the two models. In the authors' opinion, however, the comparison between skew and square models is clouded by the unknown degree of cracking in the former as compared to the latter. This cracking was impossible to assess experimentally.

Deflections.—Contrary to initial expectations, the observed deflections of the beams of the models were not proportional to the bottom flange strains. This variation from anticipated conduct is, no doubt, due to the effect of "P" (the distributed forces in the slab) and to the increasing effective E_c of the composite girder as the beam becomes more heavily-loaded—a situation that has not been subjected to quantitative analysis. It was noted that the observed beam deflections expressed as a percentage of the total (summation of the individual girder) deflections, is greater than the corresponding strain coefficients (expressed in a similar manner to the deflections), in the case of the girders remote from the load, than for those in the vicinity of the load. This is consistent with the lower stiffness of the remote beams due to lower effective E_c. Further, it is consistent with an eccentric longitudinal compression in the slab causing sagging (downwards movement) of the remote girders.

Deflections of a Single Beam.—E_c has been known to vary with the load or more precisely with the strain, or perhaps the mean strain at the center of the slab. Along the length of the beam, the strain varies in the concrete hence E_c and I also vary. For the theoretical evaluation of deflections it is necessary to establish the M/E I curve and for this purpose it was necessary to find how E varied with this strain at the center of the slab.

The empirical relationship (Fig. 8) was deduced from the one quarter line and center line strain readings of the top and bottom flanges for various load-

ings in the following manner. From the computed bending moments and the observed stresses, I was obtained, and for the section in question, the E_c necessary to give this value of I was computed. The values of E_c so found were plotted against the strain at the center of the concrete and a smooth curve drawn through these points. The strain at the center of the concrete was found by assuming a linear strain distribution across the composite section and utilizing the top and bottom flange strain readings on the steel section. For the purposes of computing deflections, E_c was then determined for each load at each change of section and at midspan and a simple mean E_c taken for lengths of the beam wherein the cross section remained constant.

The value of E_c at each change of section was found by plotting for each load some values of computed strain (M/Z) against E_c, Z of course being a known function of E_c. Where a line joining such points intersected the empirical E_c-strain curve, the relevant value of E_c was indicated. Corresponding I values were computed for the mean values of E_c so selected and deflections were evaluated from the resulting M/E I diagrams. Computed and observed deflections

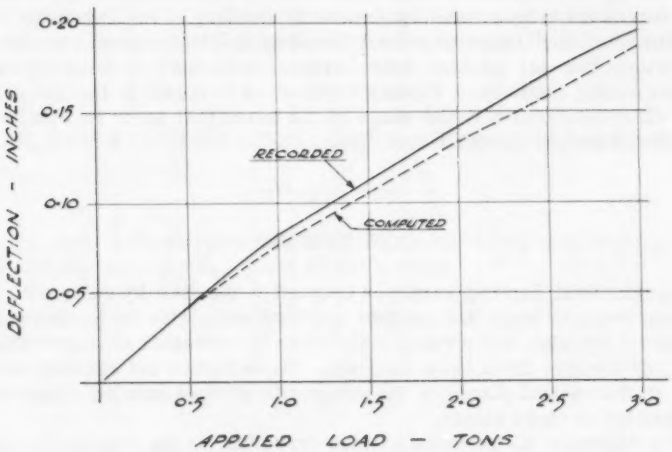

FIG. 17.—SINGLE BEAM TEST DEFLECTIONS

agreed well, diverging by a maximum of about 7½%. Superior results and improved agreement would result if the actual strains and the computed E_c for the one quarter and center lines are applied to points rather than the smooth curve. Thus, the values of E_c found from the strain readings are confirmed by the close agreement between actual and computed values for deflections (Fig. 17).

Tests to Failure.—Attempts to induce failure of the models by loading over a beam-line were not successful. The capacity of the hydraulic jack proved to be 9 tons at which load the stress in an edge beam was 44,000 psi in the steel and 10,300 psi in the concrete. These calculations are in accordance with the ultimate load theory wherein constant stress exists across the steel and concrete sections, due regard being given to the position of the neutral plane. Neither concrete nor steel showed signs of failure, though, when the measured strains in the lower flange exceeded 100×10^{-5} (stress of 30,000 psi) the neutral plane began to rise indicating yielding in the steel. The shear connectors

showed no sign of yield up to the maximum load applied, which means that there had not occurred any relative movement between slab and steel girders.

Punching failure was induced in the slab by about 10,000 lb on a 3 in. diam disc. The failure surface was inclined at 45° to the slab surface diverging downwards. Total failure area was 24 sq in.

Practical Implications Suggested by the Tests.—The tests suggest certain practical considerations, particularly in the case of precast-prestressed system, which are worthy of note.

1. If the effect of longitudinal slab shrinkage can be offset, the lateral-distributing capacity of a composite T-beam bridge may be increased. This can be achieved by longitudinally prestressing the slab either by propping the beams before casting the slab in-situ or by allowing shrinkage to occur in precast slabs before placing and jointing to prefabricated beams. However, longitudinal joints, if used in this case, can reduce the flexural stiffness of the slab and hence impair its capacity to transfer load.
2. When precast slabs are used, the loss in flexural stiffness of the slab may be partly or fully offset by the effect of the distribution of the slab longitudinal forces initially induced by composite bending of the T-beam.
3. The need for transverse load distributing diaphragms, a doubtful economic proposition for medium span bridges, is further reduced by the extra load distributing capacity of T-beam bridges, as revealed in the foregoing analysis. Careful attention to the shape of the beam, that is, to its section properties, may serve to increase this effect.

CONCLUSIONS

1. Longitudinal bending stresses induced in the slab by composite action, vary from beam to beam in a manner not consistent with the horizontal shear properties of the slab, and consequently there is a transfer of longitudinal slab forces ("P" forces) from beam to beam. These forces act eccentrically with respect to the neutral planes of the composite girders causing displacements in the position of these planes.
2. The effective E_c assumes a value depending on the degree of loading of the composite beams, and the position of the neutral planes of the girders fluctuates with the changing value of E_c.
3. The moment of inertia of the composite beams is reduced by the effect of slab-shrinkage in the working stress range, and the reduction may be larger than is generally assumed in composite I-beam and concrete slab systems and can be taken as a gage of similar effects that would occur in the case of systems utilizing precast girders surmounted by a cast-in-place slab.
4. Breakdown of the slab in transverse bending made it difficult to compare the theoretical and actual distribution curves. However the distribution curves at transverse lines remote from the load, although still colored, to some extent, by slab breakdown near the load, showed reasonable agreement with the theoretical.
5. Transverse distribution of deflections bears no resemblance to the distribution of strains in the lower flanges. This is because of the variable nature of the effect of (a) the effective value of E_c, and (b) the lateral distribution of slab compressions.

6. The effect of the variation in the torsional strength of the steel section is negligible.

7. The effect of skew was to stiffen the structure and a 30° skew of the deck caused a general reduction of strains of about 17% from those observed in the corresponding square model. This was no doubt influenced by the degree of transverse slab breakdown, but no attempt was made to assess this quantitatively. The distribution coefficients, however, were the same for the skew and square systems.

8. The analysis of Hendry and Jaeger gave similar distribution curves to that of Morice and Little.

ACKNOWLEDGMENTS

It is desired to acknowledge the important contribution to this paper of E. C. Wells, H. A. Kendall, J. K. Baron-Hay, senior students of the Civil Engineering Department of the University of Western Australia, who enthusiastically accepted the responsibility of conducting the tests. These tests were done in a most efficient manner. Grateful acknowledgment is made of the liberal financial assistance received from the Main Roads Department of Western Australia.

APPENDIX I.—DERIVATION OF EXPRESSIONS FOR M AND ΣP

Z_T, Z_B, and A are computed in terms of an equivalent steel section and are functions of the variable E_c. Then at any section

$$f_T = \frac{M}{Z_T} + \frac{P\,e}{Z_T} + \frac{P}{A} \quad \ldots\ldots\ldots\ldots\ldots\ldots (2)$$

$$f_B = -\frac{M}{Z_B} - \frac{P\,e}{Z_B} + \frac{P}{A} \quad \ldots\ldots\ldots\ldots\ldots\ldots (3)$$

in which P may be either positive or negative.

Eliminate P from Eqs. 2 and 3

$$M = -\left\{ \frac{Z_T\left(e\,A - Z_B\right)}{Z_T + Z_B} f_T + \frac{Z_B\left(e\,A + Z_T\right)}{Z_T + Z_B} f_B \right\} \quad \ldots\ldots (4)$$

Also, eliminate M from Eqs. 2 and 3

$$P = \frac{A\,Z_T}{Z_T + Z_B} f_T + \frac{A\,Z_B}{Z_T + Z_B} f_B \quad \ldots\ldots\ldots\ldots\ldots (5)$$

Values of the coefficients of f_T and f_B in the preceding expressions for various values of E_c are shown in Table 4.

It can be seen from Table 4 that the coefficients of f_T and f_B in the expression for M are practically constant, that is, M is not influenced by variations in the value of E_c. Hence M can be derived accurately from values of g_T and

g_B (galvanometer readings) at any beam in the model. Taking an approximate mean for the coefficients we find

$$M = (3.46\ g_T + 16.44\ g_B) \quad \ldots\ldots\ldots\ldots\ldots\ldots (6)$$

The coefficients of g_T and g_B in the expression for P, when plotted against E_c reasonably give straight lines (Fig. 19). The equations of these lines were derived with the coefficients expressed as functions of E_c. Substitution of the approximate functions in Eq. 5 gives

$$P = \left\{(1.07\ \ 0.454\ E_c) f_T + (1.45 - 0.0283\ E_c) f_B\right\} \quad \ldots\ldots\ldots (7)$$

$$P = (1555 + 658\ E_c)\ g_T + (2108 - 41.1\ E_c)\ g_B \quad \ldots\ldots\ldots\ldots (8)$$

But $\Sigma P = P_1 + P_2 + \ldots\ldots = 0$. Hence, if the value of E_c is assumed to be the same at each beam then

$$\left\{(1.07 + 0.454\ E_c)\ \Sigma f_T + (1.45 - 0.0283\ E_c)\ \Sigma f_B\right\} = 0 \quad \ldots\ldots\ldots (9)$$

and

$$(1555 + 658\ E_c)\ \Sigma g_T + (2108 - 41.1\ E_c)\ \ \Sigma g_B = 0 \quad \ldots\ldots\ldots (10)$$

Tables 5 and 6 were used in computations of P and M except for the top flange readings at girder 8 for load positions 9 and 10 as these were obviously in error.

TABLE 3.—CONVERSION OF STRAIN METER READINGS

Table Reference	3 to 11	12 and 13
Gage Factor	2.07	2.20
Circuit Sensitivity	10	7
To get strain multiply by	4.83×10^{-5}	6.50×10^{-5}

Tables.—The proving ring calibration (Table 3); 150 units on the Dial Indicator corresponded to 4.18 tons or 9,360 lb.

The galvonometer reading Conversion (Table 3) is as follows: For Tables 5 to 13 inclusive (MODEL 3), g x 1,450 = psi at $E_s = 3 \times 10^7$ psi (Gauge factor = 2.07, Sensitivity = 10). For Tables 14 and 15 (MODEL 2) g x 1,950 = psi at $E_s = 3 \times 10^7$ psi. (Gauge factor = 2.20, Sensitivity = 7).

APPENDIX II.—NOTATION

E_c = the modulus of elasticity of concrete

E_s = the modulus of elasticity of steel $(3 \times 10^7$ psi)

f = stress at any point in a cross section

f_T = top flange steel corresponding to observed strain

TABLE 4.—VALUES OF COEFFICIENTS f_T AND f_E

E x 10^{-6}	Coefficients of $-M=Af_T+Bf_B$		Coefficient of $P=Cf_T+Df_B$	
	A	B	C	D
0.5	3.47	16.43	1.30	1.44
1.0	3.47	16.43	1.53	1.43
1.5	3.47	16.43	1.81	1.41
2.0	3.47	16.43	1.98	1.40
3.0	3.46	16.44	2.43	1.37
4.0	3.46	16.44	2.89	1.34
5.0	3.45	16.45	3.34	1.31
6.0	3.45	16.45	3.79	1.29
7.0	3.44	16.46	4.25	1.25

TABLE 5.—STRAINMETER READINGS[a] 10 GIRDER - SQUARE MODEL (UNCRACKED)

Position of Strain	Position of Load (Load 150 Divisions)									
	1	2	3	4	5	6	7	8	9	10
1	13.20	4.54	0.98	-0.10	-0.35	-0.20	-0.09	-0.05	-0.05	.0
2	4.20	8.45	4.06	1.36	0.30	0	-0.16	-0.06	-0.10	-0.05
3	1.01	4.25	9.08	4.50	1.67	0.50	-0.03	-0.08	-0.06	0
4	0	1.40	3.93	7.60	3.60	1.45	0.33	0	0	0
5	-0.09	0.48	1.52	4.03	8.00	4.21	1.37	0.39	-0.01	+0.02
6	-0.06	0	0.35	1.52	3.88	8.26	4.08	1.49	0.43	-0.18
7	0	-0.09	0.16	0.26	1.25	3.87	7.63	4.02	1.21	0.05
8	-0.05	-0.08	0.14	-0.04	0.31	1.61	4.20	8.85	4.05	0.80
9	-0.03	0	-0.07	-0.16	-0.10	0.30	1.38	4.04	8.42	4.47
10	-0.14	-0.05	-0.18	-0.12	-0.10	-0.37	-0.20	0.88	4.30	14.20

[a] Strain Observed on Bottom Flange at Center Line Load Applied at Center Line.

TABLE 6.—STRAINMETER READINGS[a] 10 GIRDER - SQUARE MODEL (UNCRACKED)

Position of Strain	Position of Load (Load 150 Divisions)									
	1	2	3	4	5	6	7	8	9	10
1	-3.74	-3.65	-2.92	-1.83	-0.85	-0.23	0.12	0.52	0.90	1.29
2	-4.24	-4.30	-2.91	-2.14	-1.12	-0.65	-0.19	0.16	0.51	0.88
3	-4.26	-3.96	-4.25	-3.41	-2.20	-1.61	-0.46	0.34	0.10	0.58
4	-2.57	-2.73	-3.10	-3.65	-2.53	-2.11	-0.54	-0.78	-0.43	-0.10
5	-1.11	-1.59	-1.99	-2.40	-3.00	-2.20	-1.59	-0.34	-0.97	-0.56
6	-0.47	-0.85	-1.38	-1.92	-1.12	-3.62	-2.44	-2.09	-1.66	-1.34
7	0.15	-0.34	-0.61	-1.21	-1.11	-2.31	-3.42	-2.71	-2.26	-2.35
8	0.67	0.19	-0.08	-0.97	-0.78	-1.25	-0.63	-3.07	-	-
9	0.93	0.72	0.21	-0.23	-0.50	-1.24	-1.79	-2.62	-4.13	-4.37
10	1.58	1.20	0.60	0.12	-0.24	-1.25	-1.95	-2.92	-4.02	-5.96

[a] Strain Observed on Top Flange at Center Line Load Applied at Center Line.

TABLE 7.—STRAINMETER READINGS[a] 10 GIRDER - SQUARE MODEL (UNCRACKED)

Position of Strain	Position of Load (Load 150 Divisions)									
	1	2	3	4	5	6	7	8	9	10
1	8.20	3.61	0.74	-0.19	-0.20	-0.14	0	0	0	0
2	3.60	4.80	3.16	1.21	0.18	0	-0.10	-0.08	-0.11	-0.10
3	1.01	3.76	4.25	3.41	1.39	0.27	-0.19	-0.10	-0.06	-0.02
4	0.15	1.39	2.90	3.97	3.04	1.20	0.21	-0.03	-0.04	-0.03
5	-0.14	0.24	1.29	3.18	4.10	2.99	1.00	0.19	0	-0.04
6	-0.17	-0.06	0.22	1.27	3.25	4.20	3.37	1.27	0.33	-0.04
7	-0.38	-0.14	-0.20	0.34	1.19	2.95	4.08	2.97	1.22	0.02
8	-0.14	-0.19	-0.17	-0.18	0.20	1.21	3.36	4.60	3.30	0.65
9	-0.10	-0.12	-0.14	-0.09	-0.03	0.17	0.75	3.22	4.66	3.38
10	-0.08	0.02	-0.04	-0.12	-0.14	-0.15	-0.17	0.70	3.61	8.49

[a] Strain Observed on Bottom Flange at Center Line Load Applied at Quarter Line.

TABLE 8.—STRAINMETER READINGS[a] 10 GIRDER - SQUARE MODEL (UNCRACKED)

Position of Strain	Position of Load (Load 150 Divisions)									
	1	2	3	4	5	6	7	8	9	10
1	-3.65	-3.19	-2.47	-1.58	-0.95	-0.37	0.19	0.61	0.84	1.13
2	-3.38	-2.43	-2.25	-1.67	-1.15	-0.54	-0.11	0.20	0.55	0.70
3	-3.77	-3.37	-2.40	-2.47	-2.07	-1.37	-0.76	-0.20	0.20	0.48
4	-2.22	-2.46	-3.01	-1.42	-2.73	-1.46	-0.82	-0.68	-0.30	0
5	-1.13	-1.39	-1.59	-1.60	-1.24	-1.40	-1.51	-1.05	-0.81	-0.59
6	-0.55	-0.82	-1.11	-1.55	-1.46	-0.80	-1.43	-1.79	-1.62	-1.23
7	0.06	-0.20	-0.56	-0.99	-1.37	-1.45	-1.34	-1.88	-2.27	-2.01
8	0.47	0.17	-0.06	-0.18	-	-	-	-	-	-
9	0.88	0.63	0.20	-0.18	-0.61	-1.25	-1.95	-2.40	-2.80	-3.62
10	1.36	1.09	0.60	0.10	-0.44	-1.26	-2.04	-2.89	-3.74	-3.85

[a] Strain Observed on Top Flange at Central Line Load Applied at Quarter Line.

TABLE 9.—STRAINMETER READINGS[a] 10 GIRDER - SQUARE MODEL (UNCRACKED)

Position of Strain	Position of Load (Load 150 Divisions)									
	1	2	3	4	5	6	7	8	9	10
1	7.71	3.77	1.12	-1.07	-	-0.20	-0.10	-0.06	-0.07	-0.06
2	3.38	3.57	2.92	-	0.29	0	-0.07	-0.11	-0.11	-0.12
3	0.83	3.29	4.00	3.18	-	0.35	-0.01	-0.10	-0.02	-0.03
4	-0.05	1.20	3.30	3.80	2.91	1.22	0.20	-0.08	-0.12	0
5	-0.20	0.18	1.22	3.16	3.55	3.06	1.28	0.25	-0.03	-0.06
6	-0.20	-0.06	0.25	1.39	3.02	3.89	3.12	1.40	0.18	-0.18
7	-0.07	-0.13	-0.22	0.20	1.23	3.02	3.43	3.22	1.20	-0.02
8	-0.12	-0.13	-0.11	0	0.36	1.39	2.85	3.60	2.93	0.80
9	-0.02	-0.10	-0.12	-0.10	-0.33	0.24	1.27	2.93	3.50	3.47
10	0	0.08	0.09	-0.06	-0.40	-0.41	-0.20	1.02	3.33	7.44

[a] Strain Observed on Bottom Flange at Quarter Line Load Applied at Center Line.

TABLE 10.—STRAINMETER READINGS[a] 10 GIRDER - SQUARE MODEL (UNCRACKED)

Position of Strain	Position of Load (Load 150 Divisions)									
	1	2	3	4	5	6	7	8	9	10
1	-2.69	-2.01	-1.51	0	-0.47	-0.14	0.02	0.26	0.42	0.72
2	-2.27	-1.62	-1.50	-1.12	-	-0.53	-0.08	0.11	0.34	0.63
3	-2.46	-1.21	-1.06	-0.91	-0.75	-0.64	-0.46	-0.10	0	0.07
4	-1.01	-1.08	-1.08	-0.91	-0.80	-0.67	-0.54	-0.39	-0.15	0.19
5	-0.53	-0.68	-0.80	-1.03	-0.63	-0.88	-0.78	-0.62	-0.38	-0.31
6	-0.15	-0.33	-0.52	-0.70	-0.64	-0.70	-0.78	-0.86	-0.65	-0.58
7	0.03	-0.19	-0.28	-0.41	-0.62	-0.64	-0.47	-0.84	-0.90	-0.97
8	0.22	0.15	-0.02	-0.22	-0.53	-0.66	-0.79	-0.78	-1.01	-1.37
9	0.42	0.37	0.03	-0.06	-0.06	-0.73	-0.94	-1.16	-1.28	-2.00
10	0.62	0.56	0.32	0.08	-0.18	-0.56	-0.94	-1.39	-1.74	-2.40

[a] Strain Observed on Top Flange at Quarter Line Load Applied at Center Line.

TABLE 11.—STRAINMETER READINGS[a] 10 GIRDER - SQUARE MODEL (UNCRACKED)

Position of Strain	Position of Load (Load 150 Divisions)									
	1	2	3	4	5	6	7	8	9	10
1	13.59	4.0	0.59	-0.09	-0.24	-0.06	0	0	0	-0.03
2	3.82	9.17	3.43	0.86	0.06	-0.07	-0.16	-0.05	-0.12	-0.03
3	0.71	4.47	8.76	3.83	1.10	0.22	-0.14	-0.03	-0.02	-0.01
4	-0.06	1.11	3.58	8.78	3.82	0.87	0.10	0.10	-0.05	-0.02
5	-0.13	0.20	0.98	3.72	8.57	3.57	0.95	0.18	-0.10	-0.05
6	-0.20	0	0.20	1.09	3.77	8.49	3.78	0.90	0.14	-0.15
7	-0.05	0.46	-0.02	0.24	1.08	3.60	8.44	3.65	0.97	0
8	0	-0.07	-0.13	-0.02	0.20	0.96	3.42	7.94	3.62	0.57
9	-0.10	-0.13	-0.10	-0.14	-0.15	0.11	0.82	3.59	8.84	3.64
10	0	0.01	0	-0.02	-0.09	-0.23	-0.34	0.41	3.76	13.17

[a] Strain Observed on Bottom Flange at Quarter Line Load Applied at Quarter Line.

TABLE 12.—STRAINMETER READINGS[a] 10 GIRDER - SQUARE MODEL (UNCRACKED)

Position of Strain	Position of Load (Load 150 Divisions)									
	1	2	3	4	5	6	7	8	9	10
1	-4.62	-2.82	-1.67	-0.81	-0.34	-0.02	0.11	0.30	0.53	0.72
2	-3.19	-4.22	-2.14	-1.36	-0.64	-0.30	0	-0.16	0.40	0.62
3	-1.68	-1.87	-3.13	-1.49	-1.00	-0.59	-0.33	-0.10	0.07	0.21
4	-0.93	-1.27	-1.64	-3.08	-1.58	-0.99	-0.62	-0.38	-0.17	0
5	-0.40	-0.79	-1.04	-1.82	-3.41	-1.43	-1.01	-0.73	-0.47	-0.21
6	-0.11	-0.30	-0.59	-0.88	-1.39	-3.02	-1.47	-1.17	-0.80	-0.53
7	0.09	-0.04	-0.26	-0.54	-0.87	-1.23	-2.40	-1.36	-1.11	-0.93
8	0.31	0.19	0	-0.22	-0.53	-0.79	-1.27	-2.67	-1.62	-1.41
9	0.49	0.32	0.18	-0.03	-0.23	-0.66	-1.03	-1.66	-3.75	-2.83
10	0.61	0.59	0.26	0.19	0	-0.40	-0.80	-1.55	-2.43	-4.61

TABLE 13.—STRAINMETER READINGS[a] 10 GIRDER - SQUARE MODEL (CRACKED)

Position of Strain	Position of Load (Load 150 Divisions)									
	1	2	3	4	5	6	7	8	9	10
1	14.05	4.27	0.78	-0.16	-0.20	-0.12	-0.01	-0.06	-0.07	-0.10
2	4.03	9.19	4.21	1.21	0.16	-0.15	-0.17	-0.10	-0.04	-0.14
3	0.80	4.19	8.64	4.39	1.48	0.15	-0.03	-0.16	-0.10	0
4	0.20	(1.20)	-	-	(4.02)	1.28	0.20	-0.03	-0.17	0
5	-0.03	0.31	1.22	4.03	9.00	4.18	1.36	0.28	0	0.07
6	-0.02	-0.08	0.02	1.30	3.96	8.66	4.43	1.33	0.18	0
7	-0.08	-0.16	0	0.21	1.15	3.81	9.00	4.11	1.23	0.13
8	-0.07	-0.03	-0.06	-0.06	0.14	1.18	4.20	10.15	4.30	0.63
9	-0.13	-0.06	-0.03	-0.03	-0.03	0.16	1.00	4.08	9.78	4.31
10	-0.02	-0.15	0	0	0	-0.04	-0.18	0.58	4.05	15.07

[a] Strain Observed on Bottom Flange at Center Line Load Applied at Center Line.

TABLE 14.—STRAINMETER READINGS[a] 10 GIRDER - SKEW MODEL (UNCRACKED)

Position of Strain	Position of Load (Load 150 Divisions)									
	1	2	3	4	5	6	7	8	9	10
1	-9.00	2.98	0.71	0.05	-0.19	-0.08	-0.13	-0.12	-0.11	-0.02
2	3.18	5.52	2.64	0.95	0.14	-0.14	-0.22	-0.06	-0.11	-0.04
3	0.75	2.66	5.20	2.40	0.99	0.42	-0.01	-0.14	-0.09	-0.03
4	-0.03	1.18	2.30	4.70	2.44	1.00	0.35	0.03	-0.02	-0.12
5	-0.18	0.31	1.03	2.42	4.78	2.38	0.97	0.32	-0.02	-0.10
6	-0.18	-0.01	0.35	1.19	2.74	4.95	2.44	0.97	0.29	-0.14
7	-0.16	-0.09	0.05	0.39	1.13	2.39	5.30	2.33	1.00	-0.02
8	0	-0.10	-0.04	0	0.23	1.05	2.71	5.52	2.72	0.75
9	-0.02	0	-0.15	-0.17	-0.02	0.22	0.97	2.69	5.84	2.69
10	-0.01	0	-0.05	-0.17	-0.14	-0.36	0	0.59	2.88	9.26

[a] Strain Observed on Bottom Flange at Center Line Load Applied at Center Line.

TABLE 15.—STRAINMETER READINGS[a] 10 GIRDER - SKEW MODEL (UNCRACKED)

Position of Strain	Position of Load (Load 150 Divisions)									
	1	2	3	4	5	6	7	8	9	10
1	-	-	-	-	-	-	-	-	-	-
2	-1.51	-1.53	-1.10	-0.65	-0.40	-0.24	-0.09	-0.12	0.12	0.23
3	-1.00	-1.36	-0.65	-1.00	-0.80	-0.44	-0.39	-0.07	-0.09	0.13
4	-0.50	-0.65	-0.69	-1.06	-0.64	-0.43	-0.38	-0.18	-0.16	-0.02
5	-0.30	-0.50	-0.61	-0.77	-0.78	-0.57	-0.63	-0.45	-0.34	-0.18
6	-0.16	-0.36	-0.38	-0.51	-0.79	-0.40	-0.80	-0.63	-0.52	-0.43
7	-0.02	-0.17	-0.21	-0.38	-0.61	-0.70	-0.82	-1.00	-0.88	-0.77
8	0.18	0.07	-0.13	-0.22	-0.43	-0.68	-1.11	-1.62	-1.52	-1.53
9	0.34	0.28	0.03	-0.18	-0.36	-0.68	-1.10	-1.78	-1.87	-2.56
10	0.34	0.30	0.23	0	-0.15	-0.62	-1.03	-1.89	-1.88	-2.10

[a] Strain Observed on Top Flange at Center Line Load Applied at Center Line.

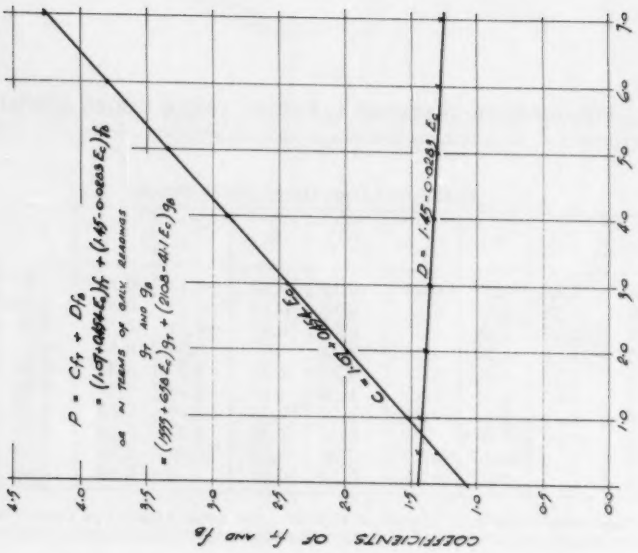

FIG. 19

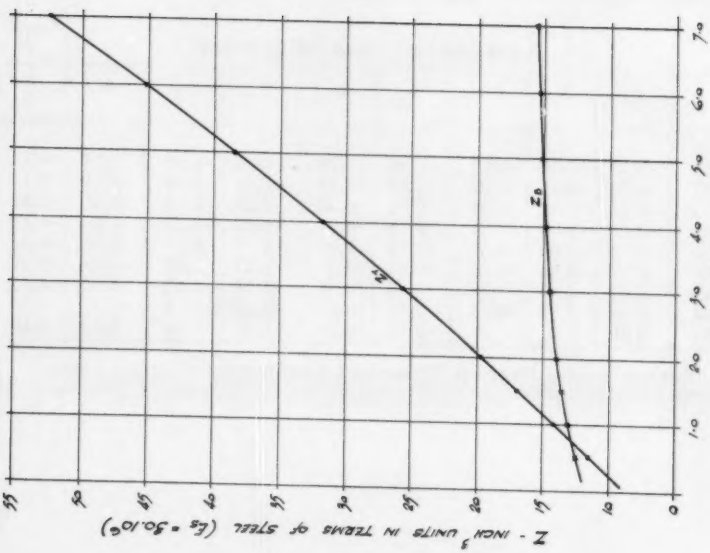

FIG. 18.—NO. 3 MODEL—SQUARE VALUES OF SECTION MODULUS OF COMPOSITE BEAM VERSUS E_c

f_B = bottom flange steel stress corresponding to observed strain

g_T = strainmeter-galvanometer reading at the extreme fibre of the top flange of the steel section

g_B = strainmeter-galvanometer reading at the extreme fibre of the bottom flange of the steel section

P = distributed longitudinal force in the slab at a girder

A = cross sectional area of the composite section

e = eccentricity of force P with respect to the neutral plane of pure flexure of the composite girder

Z = section modulus at the fiber at which the stress is required

Z_T = modulus of the composite section at a position corresponding to f_T

Z_B = modulus of the composite section at a position corresponding to f_B

M = bending moment induced in a girder as given by the ordinary theory of flexure of a slab on flexible beam supports

ton = 2,240 lb.

θ = stiffness coefficient (Morice and Little[8])

α = torsion coefficient (Morice and Little[8])

Journal of the
STRUCTURAL DIVISION
Proceedings of the American Society of Civil Engineers

SHEAR DIAPHRAGMS OF LIGHT GAGE STEEL

By Arthur H. Nilson,[1] M. ASCE

SYNOPSIS

It is recognized that the diaphragm strength of floor and roof elements of buildings can be utilized to resist horizontally-applied loads, eliminating the need for separate bracing systems. With proper attention to welding details, floors and roofs of light gage steel panels, designed primarily to carry vertical loads, will be effective as shear diaphragms. Extensive full-scale tests of light gage steel diaphragms are described and test results are interpreted.

INTRODUCTIONS

Buildings may be subjected to horizontal loads from a variety of causes. Those most commonly considered are wind forces, blast forces, and seismic or earthquake forces. Consider first a simple one-story building acted upon by wind forces (Fig. 1). Assume that the wind exerts a positive pressure on the windward side of the building. The wall sheathing, if properly designed, functions as a uniformly loaded slab spanning vertically, supported at the bottom by the wall foundation, and at the top by the beams FJ, JI, and IB. The roof surface BCFG is loaded in its own plane along its edge BF. The roof system must, in some manner, transmit this horizontal edge load from the line of application to stiff vertical shear walls or vertically-braced bents ABCD and EFGH, which in turn transmit the loads to the building foundations.

Note.—Discussion open until April 1, 1961. To extend the closing date one month, a written request must be filed with the Executive Secretary, ASCE. This paper is part of the copyrighted Journal of the Structural Division, Proceedings of the American Society of Civil Engineers, Vol. 86, No. ST 11, November, 1960.

[1] Asst. Prof. of Civ. Engrg., Cornell Univ., Ithaca, N. Y.

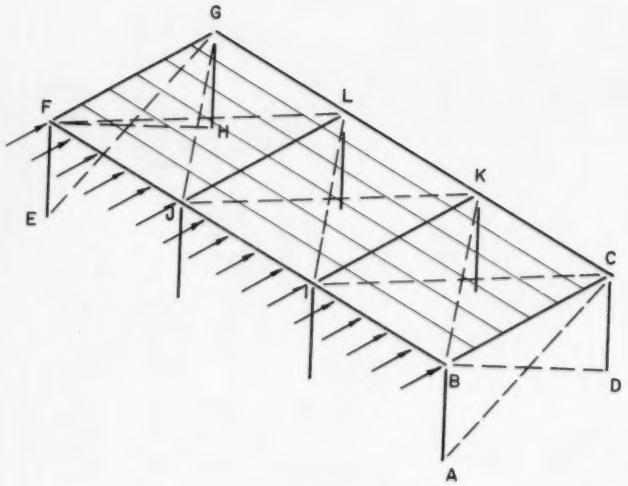
G
F
L
H
K
E
J
C
B
D
A

FIG. 1

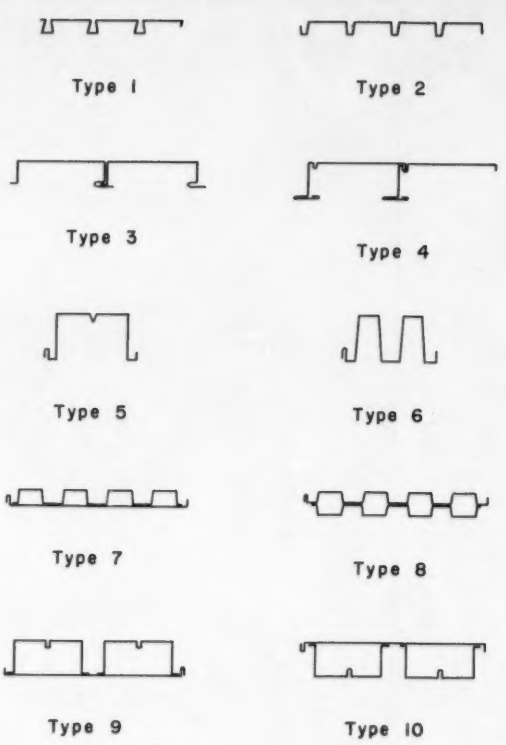
Type 1
Type 2
Type 3
Type 4
Type 5
Type 6
Type 7
Type 8
Type 9
Type 10

FIG. 2

The effect of a blast on such a building is similar to that of wind, except that, in the case of blast, one must consider the dynamic response of the building itself, as well as the exposed surface area and pressure. In the case of seismic action, one is concerned primarily with the dynamic response of the building, and not directly with surface area. Regardless of the cause of the horizonatal force, however, the behavior of the resisting structure is very much the same in each case. The load can be considered to act horizontally in the plane of the roof, which must transmit it to the top edge of the vertical shear walls.

This can be done by providing a system of horizontal X-bracing in the plane of the roof or floor. This, in effect, creates a horizontal truss, with members BF and GC as chord members, FG, JL, IK, and BC as posts, and with the X-bracing itself as diagonals. This may be undersirable architecturally, however, and in any case is wasteful, because the roof sheathing can, with proper attention to fastening details, be made to act as the shear-resisting web of what exactly corresponds to a plate girder, with BF and GC as flanges, loaded along the edge BF, and supported at its ends by shear walls ABCD and EFGH. The separate system of X-bracing may, therefore, be dispensed with, and the sheathing, designed primarily for vertical loads, will carry the horizontal loads as well.

Such shear diaphragms have been successfully constructed of wood, concrete, and light gage steel, in addition to various patented fibrous roof sheathing materials. The behavior of wood diaphragms has been established by extensive tests by the United States Forest Products Laboratory, the Oregon Forest Products Laboratory, and the Douglas Fir Plywood Association. Such diaphragms may be constructed using diagonal planking, or more usually, using plywood sheets, securely nailed and sometimes glued as well. Allowable shears as high as 820 ppf have been recommended for plywood diaphragms.[2] (Note that the strength of such elements is controlled by shear capacity, and is usually expressed in pounds per foot of diaphragm depth in the horizontal direction parallel to the load. It could as easily be expressed in pounds per square inch of web area, as is usual in ordinary steel design.)

The behavior of concrete diaphragms is more easily predicted by theory, since the shear web is, in this case, composed of one monolithic member. Many such diaphragms have been tested. When properly reinforced along the long edges with tensile steel bars, and when properly secured to the supporting structure, such diaphragms of concrete are the strongest and stiffest obtainable.

LIGHT GAGE STEEL DIAPHRAGMS

Shear diaphragms of light gage steel panels are more complex in their action under load. The use of such steel panels over a steel frame to carry vertical loads has become widespread in recent years because of economy, light weight, and speed of installation. A few of the many cross sections that are presently available are shown in Fig. 2. The steel sheet used in fabricating such panels is usually in the range from 20 gage (0.0359 in.) to 12 gage (0.1046 in.). When more than one sheet is used to make up a cross section, the components are generally resistance spot welded along the linear joint.

For installations designed to resist vertical load only, welding systems are nominal, and serve only to secure the panels to the supporting frame to

[2] "Fir Plywood Diaphragms," Douglas Fir Plywood Assn.

prevent shifting and to resist uplift, and to prevent differential vertical movement between adjacent panels that might damage the roofing or insulation. When designed also to resist the horizontal shear loads described previously, the welding pattern must be somewhat more complex. In this case, the welds must (a) secure adjacent panels to one another at intervals along the joints so that relative horizontal movement between panels is prevented, thus insuring that the deck will act as one integral shear web rather than as a large number of individual parts; (b) secure marginal panels to supporting steel frame so that horizontal loads may be transmitted into and out of the diaphragm along the lines FG, JL, IK, and BC (Fig. 1); and (c) secure marginal panels to the steel frame along the long edges BF and CG so that these marginal beams can function as "flanges" for the plate girder for which the deck functions as web, and thus carry bending stress. The welds in this case are loaded in logitudinal shear.

Welding.—A number of different welds unique to the installation of light gage steel panels have been developed and refined in experimental work. The basic types are shown in Fig. 3. In securing panels to supporting structural steel, most frequently a "puddle" weld is used, shown in Fig. 3(a). These are similar to the conventional plug weld, except that no pre-punching of the light gage steel sheet is involved, the hole being burned and the weld made in one continuous operation. Such welds are commonly from 1/2 in. to 1 in. in diameter, the size depending on the required strength. It has been found that the effective diameter of fusion, at the level of the under surface of the panel steel, is about 1/4 in. less than the nominal and apparent diameter at the top surface of the steel. A representative group of such welds is shown after failure in Fig. 4.

If the panel edges terminate in a stiffened (upturned) lip, it is possible to fillet weld the structural steel successfully to the panel at the base of the lip (Fig. 3(b) and 5). This has the advantage over the puddle weld in that less slag is generated in making the weld, since one need not burn through the panel steel to fuse to the structural beam. Consequently, a better weld is more easily obtained. It has been found, however, in a number of tests, that edge fillet welds to unstiffened edges are notably deficient in strength because deformation of the panel adjacent to the weld results in premature failure. Such welds to unstiffened edges should be avoided in favor of welds that are surrounded by panel steel on all sides, thus minimizing distortion and premature tearing action.

Along the seams between the panels, in the event that the panels terminate in a down-turned edge (one side of which is usually a hooked edge as seen in several of the typical sections in Fig. 2), it is convenient to place a welding bead along the joint between the panels. Such welds are usually 1 in. to 2 in. in length, and spaced 12 in. to 48 in. o.c. depending upon the required shear strength, and are designated somewhat loosely as fillet welds (Fig. 3(c) and 6). If the panels are used such that the concave part of the hook joint is downward (Fig. 3(d)), it becomes necessary to use a modified form of the puddle weld described earlier, in which an elongated hole is burned through the top of the hook, fusing the hook to the upper portion of the upstanding lip of the adjacent panel. One of these welds is visible in Fig. 4.

Several manufacturers have developed clinching tools by means of which a button-type indentation is made through the hook portion of an edge joint, engaging the upstanding lip of the adjacent panel. A typical took of this type is shown in Fig. 7. Tests indicate that such mechanical joint fastenings will

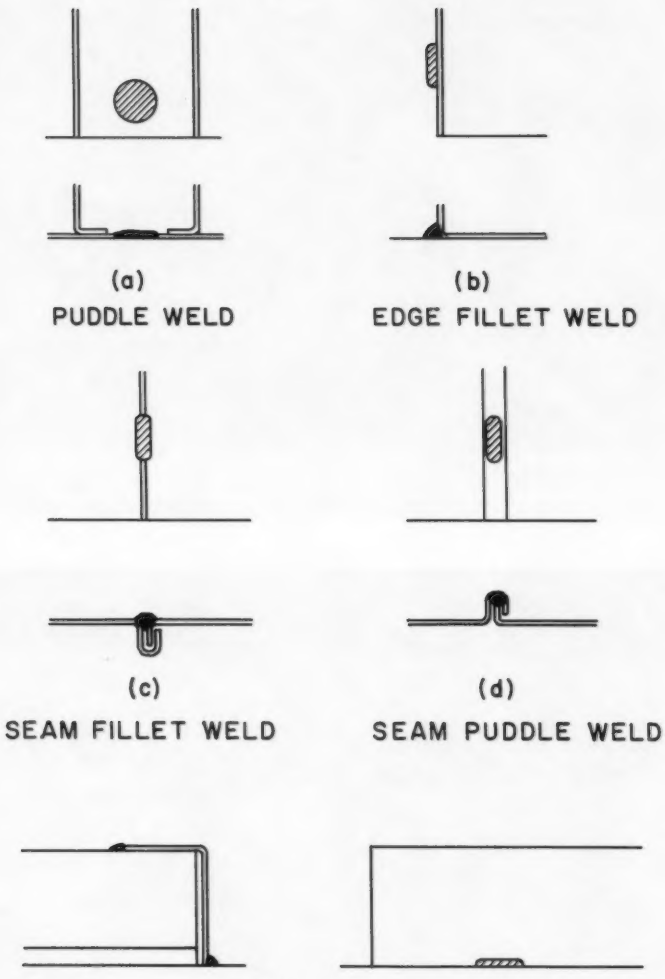
(a)
PUDDLE WELD
(b)
EDGE FILLET WELD
(c)
SEAM FILLET WELD
(d)
SEAM PUDDLE WELD
(e)
CLOSURE ANGLE WELDS

FIG. 3

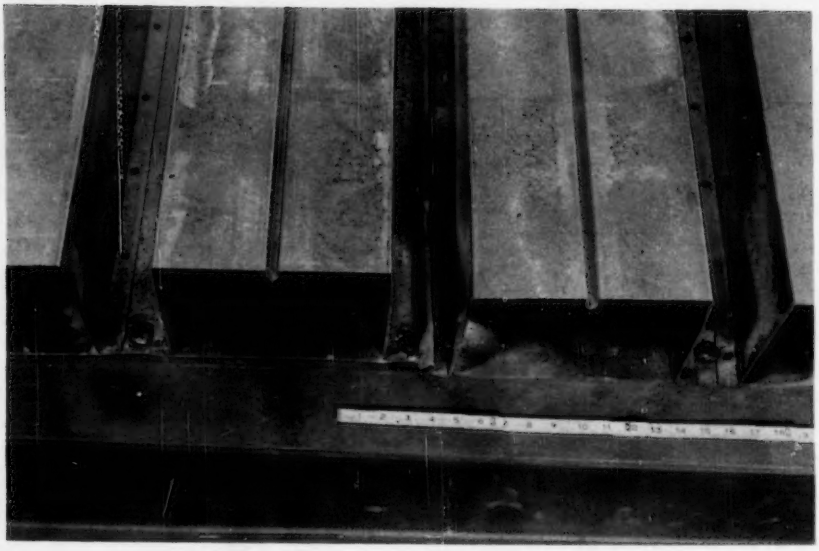

FIG. 4.—DETAIL OF PUDDLE-TYPE END WELDS AND SEAM WELDS

FIG. 5.—DETAIL OF FILLET-TYPE EDGE WELDS

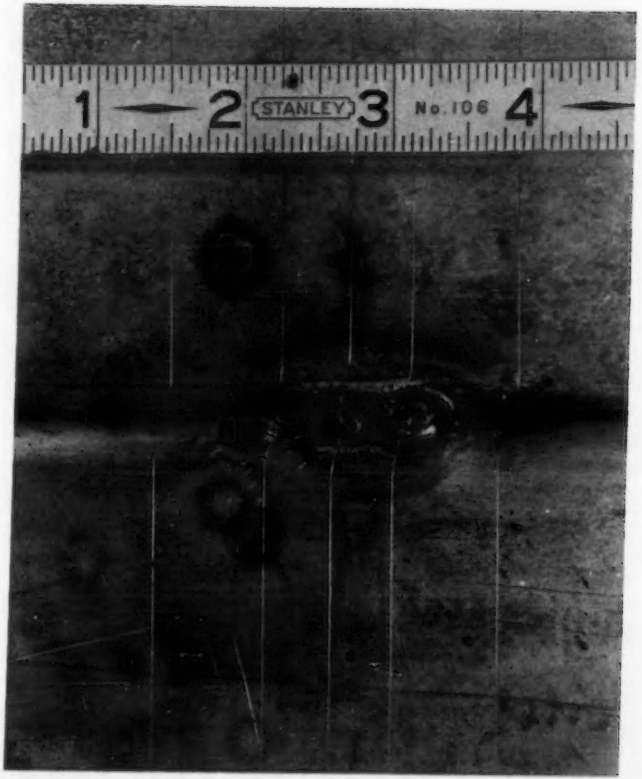

FIG. 6.—DETAIL OF FILLET-TYPE SEAM WELDS

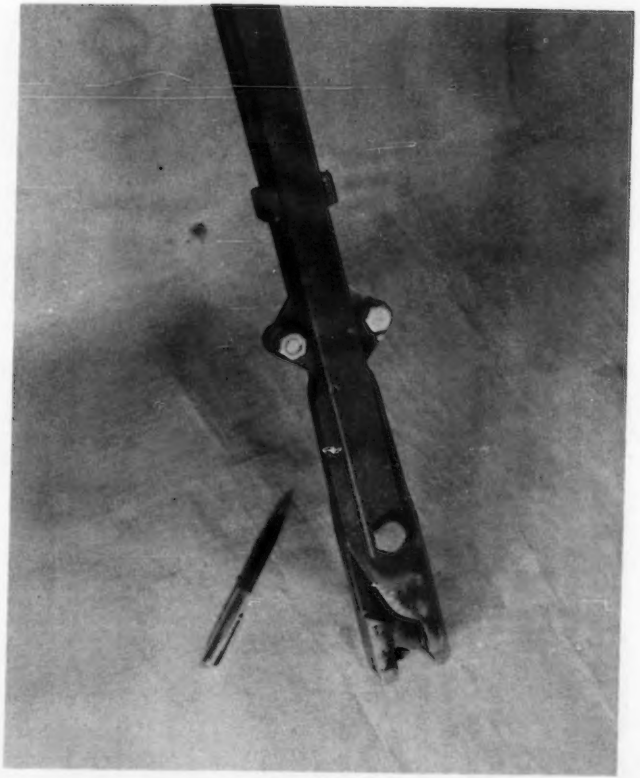

FIG. 7.—SEAM CLINCHING TOOL

develop substantial shear values before spreading of the hook permits the inner lip to disengage. It should be noted that such seam clinching devices were originally designed for the purpose of controlling differential deflection between adjacent units under vertical load. In shear diaphragms, their function is more critical. Since the effectiveness of seam clinching for shear diaphragms depends upon precision of joint engagement, its use should be restricted to applications where precise vertical alinement can be obtained.

Considerable experimentation in welding indicates that good results can be obtained in welding light gage steel panels to structural steel by using the American Welding Society (AWS) Specification E-6013 rod of 1/8 in. diameter. In making fillet-type welds, for which no burning-through is required, a current of 150 amp to 175 amp at approximately 35 DC (burn-off rate of 9 in. to 11 in. per min) will be satisfactory. For forming puddle-type welds, a current of 200 amp to 225 amp at approximately 45 DC (burn-off rate of 13 in. to 15 in. per min) will be necessary. (These values were developed for panel steel of 16 gage thickness; lighter thicknesses of panel steel would dictate the use of somewhat lower amperages.)

End Closures.—When panels of type 4 or 10 are used for shear diaphragms, it becomes necessary to provide some means for transferring the shear force from the plane of the deck flat plate to the plane of the top flange of the supporting steel beams, Unstiffened vertical webs would permit large horizontal movement between the deck and the supporting beams. Various methods and devices have been developed for accomplishing this, perhaps the simplest being the continuous light gage steel closure angle, installed as shown in Fig. 3(e) and Fig. 8, intermittant fillet welded to the deck plate and to the top flange of the supporting beam. The fillet welds shown in Fig. 8 were 1 in. in length and spaced 24 in. o.c., or one set per panel end.

The performance of diaphragms using panels of Types 1, 2, and 3, all usually of 1-1/2 in. depth, could be improved by the use of such a closure angle, both in stiffness and strength. However, for these shallow sections such accessories are usually omitted.

Marginal Beams and Marginal Beam Connections.—In the case of a floor system acting as a diaphragm in conjunction with a steel frame, the marginal beams running perpendicular to the direction of the applied loads are subject to axial stresses, as are the flanges of a plate girder. The magnitude of these axial stresses is usually quite small, and the 33 1/3% increase in permissible stresses allowed by most building codes for wind, seismic, and blast effects is usually sufficient to cover the increase in actual stresses, so that marginal beams designed conventionally for vertical loads will, in most cases, prove adequate to function as diaphragm flanges as well, with no increase in area necessary.

The force acting on a marginal beam in an actual structure is primarily axial, being applied through end connections that are largely unable to transmit moments acting in the plane of the beam web. It is true that small moments will be developed, as the load of any given segmental marginal beam is applied eccentrically, more or less uniformly along the surface of the top flange by the welds joining beam to light gage steel panels. However, for the most highly stressed marginals, near the midpoint of the "plate girder" span between shear walls, the largest part of the load on the beam is applied axially from the adjacent beams, and bending stresses are small.

It has been found to be sufficiently accurate for design purposes, if the bending moment resulting from plate girder action is considered to be resisted by the full area of the marginal beams, conservatively neglecting the

contributing area of the deck panels in computing flexural stresses. Values so obtained are sufficiently on the safe side that the small effect of eccentricity of the load applied along the top flange surface can be neglected. Thus, the total axial force in the marginals will be equal to the total applied moment at the section divided by the horizontal distance between marginals. Dividing this force by the full area of the marginal will then give an average value of stress. Values so obtained agree closely with experimentally obtained maximum stress values for a large number of tests.

The connection detail between adjacent sections of marginal beam should be checked for adequacy. It should be apparent that all of the flange forces,

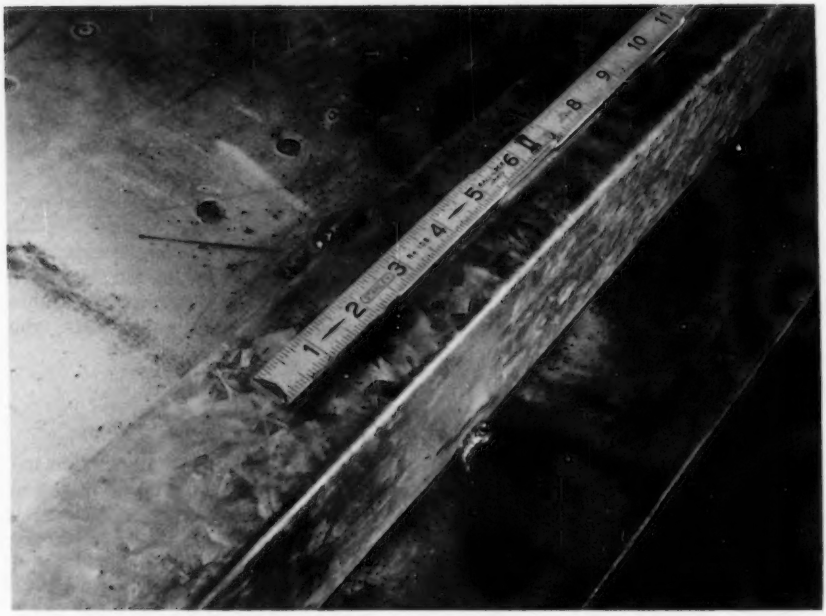

FIG. 8.—END CLOSURE ANGLE

tension or compression, must be transmitted across these joints. It will usually be found that the stress increase allowed by specification will be more than adequate to provide for the combined stress situation that results, but the number of bolts or rivets or size of weld may have to be increased slightly at the outer marginals. It should be noted that crimping-type deformation of the framing angles in transmitting axial tension could have a detrimental effect. Standard methods of review are satisfactory, and may indicate the need for either a stiffener or the use of a heavier-than-normal framing angle.

BACKGROUND OF DIAPHRAGM TESTING

The behavior of light gage steel panel diaphragms does not yield nicely to analysis. The large number of relatively small parts involved, with possible

individual movement, and the stress concentrations that are present near the welds as horizontal load is applied, prevent the application of the results of analysis with any large degree of confidence. Accordingly, a considerable number of isolated tests have been performed by a number of persons and institutions over a period of time.

The first tests to come to the author's attention were performed in California in 1947, by C. B. Johnson and F. J. Converse. These tests utilized panels of Type 2, and were performed by pulling with cables on a full sized building. A second group of tests was performed in 1949 and 1950 by S. B. Barnes, who used panels of Type 10. These tests were described in detail in an unpublished report that included much interpretive material of interest.

Mr. Johnson has presented[3] some interesting structural theory pertaining to diaphragm action. He summarized the information available at that time (1950), and discussed some of his earlier tests. He concluded that he had "demonstrated the usefulness and structural adequacy of light gage steel shear diaphragms for building construction," and he hoped that his work would provide "the stimulus for continued research and experimentation along these lines." The second part of this statement reflects the evident fact that test information was needed as a basis for the responsible design of such structural elements.

Following Mr. Johnson's work, a number of tests of light gage steel diaphragms were made by James M. Fox of Los Angeles, S. B. Barnes, Jepson and Styer Engineers of Seattle, Wash., and others, in addition to the extensive tests at Cornell University. While little or no information or test data has been published in the usual technical journals up to this time, a very considerable amount of data is available from the manufacturers of the panel units, who have been the sponsors of most of these tests.

DESCRIPTION OF CORNELL TESTS

In July, 1955, the first Cornell University tests of full-scale diaphragm installations were initated at Thurston testing laboratory, under the direction of George Winter, F. ASCE, and the author. There followed an extended series of more than fifty diaphragm tests, utilizing many types of panels, steel thicknesses, patterns of welding, panel spans, and panel depths. Information that has evolved from these tests has provided a firm basis for the design and installation of light gage steel diaphragms in many parts of the country. Ultimate strength and working strength values have been established for many different systems, and the performance of such diaphragms under load has been accurately cataloged.

Three-Bay Tests of Type 9 and Type 10 Panels.—The early tests at Cornell in 1955 and 1956 made use of a three-bay steel frame exactly analogous to the area BCFG shown in Fig. 1. Fig. 9 shows the arrangement for testing the type 10 panels. Three 10 ft-by-12 ft bays were established, forming a deck area 12 ft-by-30 ft (Fig. 10). 12 WF 27 beams framed in the short direction of each bay, into 10 WF 33 jacking beams running east-west at the third points of the test area, and into 10 WF 21 reaction beams running east-west at the extreme ends. The frame was supported on eight short columns located at the ends of the 10 in. beams. The columns under the two jacking beams were

[3] "Light Gage Steel Diaphragms in Building Construction," by Carl B. Johnson, Presented at the February 1950 ASCE meeting in Los Angeles, Calif.

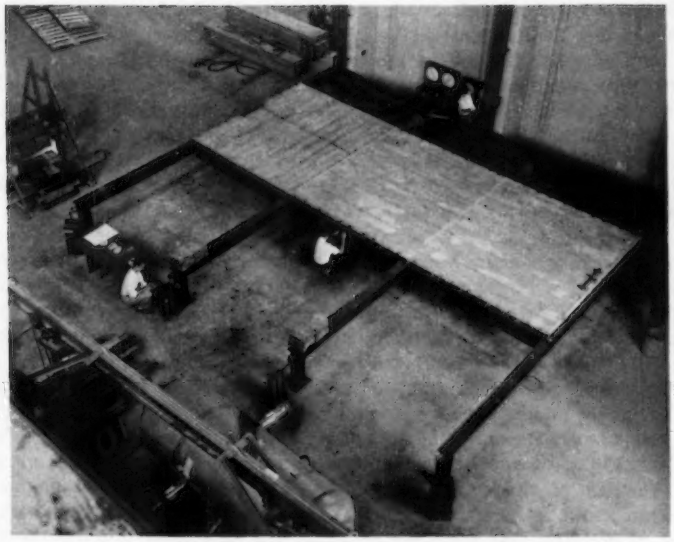

FIG. 9.—THREE BAY DIAPHRAGM TEST OF TYPE 10 PANELS

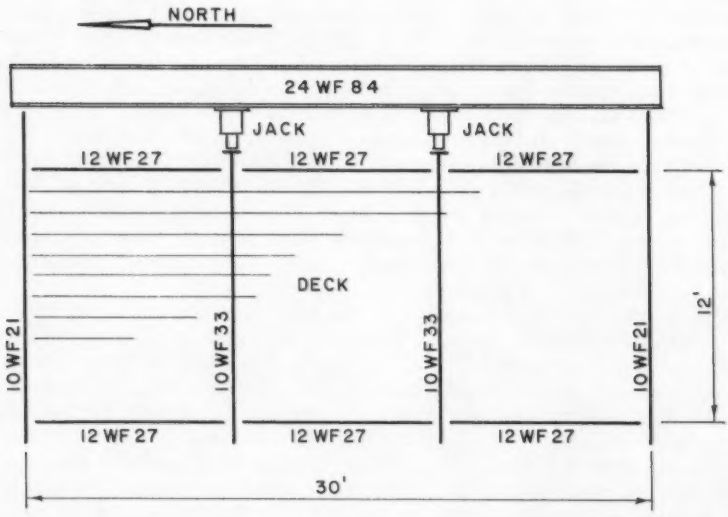

FIG. 10

set on rollers to minimize frictional resistance. A 24 WF 84 beam was provided, to the east of the decked area, running in the north-south direction, and set with the web horizontal. Loads were applied to the test structure by jacking between this 24 in. beam and the jacking beams previously described, using two 50 ton hydraulic jacks. The reaction beams at the north and south ends of the deck area were connected to the 24 in. beam, and in turn to the laboratory columns at the extreme ends. The deck panels were laid on top of the beams, and suitably interconnected along the seams and welded to the beams to form a diaphragm. In this manner, the test installation of Fig. 10 duplicated the action of the structure of Fig. 1 in every respect, except that instead of the distributed load, two concentrated loads were used.

The frame was loaded preliminary to the placing of the steel deck, and it was found that a jack load of only 500 lb resulted in third-point deflection of the deck area of as much as 3/4 in. Considering the very small magnitude of deflections with the deck panels in place and welded, it was apparent that virtually all of the resistance to horizontal movement was provided by the deck itself, with very little resistance provided by the stiffness of the frame.

Loads were applied to the diaphragm installation in increments using hydraulic jacks, and at each increment, observations were made of horizontal movements of various parts of the installation, tensile and compressive strains in the marginal beams, and relative movement between adjacent panels.

The results of these early tests indicated clearly that strong and stiff diaphragms could be constructed of light gage steel roof or floor panels, with patterns of welding that were not prohibitively expensive and that would still permit that form of construction to be competitive. Panels of Types 9 and 10 were tested, with light gage sheet of 16 or 18 gage. The strongest of these systems reached an ultimate shear strength of 3,550 lb per ft; the net deflection at 50% of that failure load was only 0.11 in. in 30 ft. The results of the more important of these original tests are summarized in Table 1, and typical load-deflection curves shown in Fig. 11. Only the most essential data has been included in the summary tables. Details of closure angle configuration and welding, for example, have been omitted, but it is felt that sufficient information is given elsewhere in this report to permit the engineer to arrive at a satisfactory detail, with the assistance of manufacturers' test data.

Cantilever Tests of Type 9 Panels.—Upon completion of the tests described above, an expansion of the program was planned to include tests of long span panels, up to and including 30 ft in length. The construction of a third-point loading frame of 30 ft-by 90 ft dimension, similar to the smaller test frame, would have proved prohibitively expensive and cumbersome. Therefore, a different scheme for these long-span tests was developed.

It is easily seen by inspection of the shear diaphragm for the three-bay third-point loaded frame that the center bay is completely inactive in resisting shear. In fact, it was included in the earlier tests only because of the relative convenience of introducing load to the diaphragm along two lines rather than one. It is obvious also that the two outer bays are symmetrical, and identical in structural action. Although bending moments exist in the center bay and have an effect on deflection, for a system that is shear-critical the presence or absence of the center bay will have no effect on strength. On this basis, then, it was proposed to test a single "end" bay, loaded as a cantilever, that would yield the same strength values as the three-bay frame, and from which the deflection of an equivalent three-bay frame could be computed.

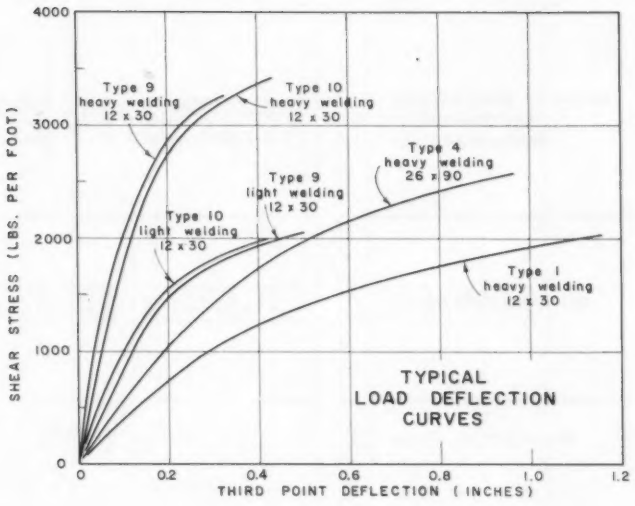

FIG. 11

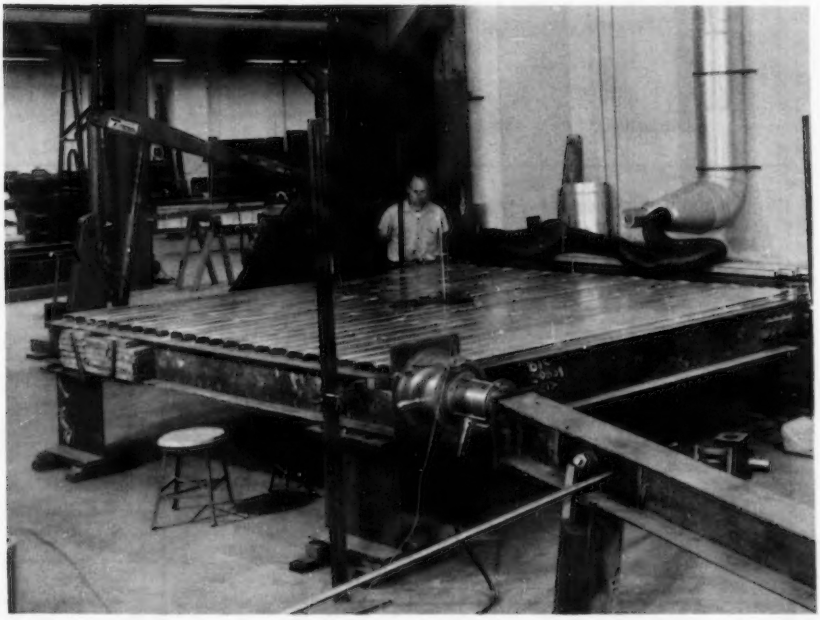

FIG. 12.—CANTILEVER DIAPHRAGM TEST OF TYPE 1 PANELS

TABLE 1.—SUMMARY OF LIGHT GAGE STEEL PANEL DIAPHRAGM TESTS

Test No.	Panel Depth, in inches	Gage of Shear Plate[a]	Panel Span, in feet	End Welds,[a] in inches	End Weld Spacing, in inches	Edge Welds,[a] in inches	Edge Weld Spacing	Seam Welds,[a] in inches	Seam Weld Spacing	Failure Shear, in ppf	Net Deflection at 50 per cent of Failure Load, in inches
Tests of Type 9 Panels											
2a	3	16	12	1"P	8	1P	48	Cl	24	2030	0.122
57-3	3	16	12							2150	0.091
57-5	3	16	12							1770	0.081
5	3	16A	12							1460	0.087
58-3	6	16A	30							970	0.415
11	3	18	12							1480	0.116
59-5	3	18A	15							1230	0.375
58-7	4½	18A	22							900	0.530
59-3	3	16A	15	3/4"F	8	3/4F	36	1P	36	1650	0.225
59-1	6	16A	30							1490	0.168
1c	3	16	12	1"P	8	1P	24	1 P	18	3230	0.070
57-2	3	16	12							3220	0.050
58-8	4½	16	22							2910	0.231
58-5	6	16	30							2670	0.145
58-6	6	16	30							2570	0.156
59-4	3	16A	15							3190	0.319
58-4	6	16A	30							2290	0.167

58-2	7½	16A	30								2130	0.167
58-2a	7½	16A	30								2730	0.188
9	3	18	12								2080	0.070
59-2	4½	18	22								2380	0.214
Tests of Type 10 Panels												
4c	3	16	12	3/4F	6	3/4F	48	3/4F	48		2000	0.100
3d	3	16	12	3/4F	6	1F	24	1F	24		3420	0.096
12	6	16	12								3550	0.109
10	3	18	12								2300	0.065
Tests of Type 4 Panels												
58-1	7½"	18	30	1"P	12	1P	18	1F	18		1740	0.175
58-2	6	18	26								1730	0.182
58-3	4½	18	20								2380	0.306
58-4	6	18	26								2590	0.265
58-5b	6	18	26								2500	0.250
58-5c	6	18	26								2150	0.343
Tests of Type 1 Panels												
59-6	1½"	16	10	3/4P	6	3/4P	18	1P	18		3580	0.300
59-7	1½	18	10								2320	0.402
59-8	1½	20	10								1330	0.407
59-10	1½	16A	10								3330	0.132
59-11	1½	18A	10									
59-9a	1½	20A	10								1540	0.119
59-12	1½"	16	10	3/4P	9	3/4P	24	1P	24		2630	0.449
59-13	1½	20	10								1000	0.477

[a] A = acoustic perforations in shear-carrying plate
P = puddle weld
F = fillet weld
Cl = clinched seam joint

In order to compute the deflection of the equivalent three-bay frame from information obtained from testing one end panel as a cantilever frame, it is apparent that two corrections must be made. First, one must eliminate the deflection effect of small unavoidable movements of the cantilever support points. The effect of such movements on the deflection at the jack in the direction of the applied load is easily determined using the known aspect ratio of the particular test, in conjunction with recorded dial gage readings of such support movement. Second, one must introduce an additive correction to account for the missing center bay. By means of statics one can determine the axial forces in the center span marginal beams resulting from the application of a given third-point load, and by Hooke's law determine the total tensile and compressive strains. On the basis of the geometry of the equivalent frame, the deflection at the third points in the direction of the jacking force, due to the axial deformation in the center bay, is readily computed.

In order to provide experimental verification of the argument just presented, a pilot series of tests was performed on a single bay 10 ft-by-12 ft cantilever test area, and which used identical panels, spans, and weld systems as had been tested on the three-bay 12 ft-by-30 ft test frame. The frame used for these pilot tests is shown in Fig. 12. These tests showed remarkable agreement with the earlier three panel tests, both with respect to shear at failure and to load-deflection characteristics. This close agreement provided a firm basis for proceeding with cantilever tests of long-span panels.

A square frame was built measuring 30 ft on each side, using 16 in. wide flange beams. (It will be helpful in following the description to refer to Fig. 13. The north direction in the photograph is toward the left background.) This frame rested on rollers permitting essentially unrestrained shear deformation to occur. At the southeast corner of the test area, the frame was connected to a 24 in. wide flange beam in such a manner as to permit vertually no movement at that point in any direction. The 24 in. beam was rigidly connected in turn to the laboratory columns. At the northeast corner the frame was restricted against east-west movement, but north-south movement was permitted by means of a sliding greased plate connection. The southwest and northwest corners of the frame were supported on rollers and were free to displace in any direction. At the northwest corner of the frame the load was applied in a northerly direction using a drawbar and yoke arrangement in conjunction with two fifty-ton capacity hydraulic jacks. The marginal 16 in. wide flange beam on the south edge of the deck could be repositioned using alternate sets of bolt holes to form test areas of 26 ft, 22 ft, 20 ft, and 15 ft in the north-south dimension, in addition to the basic 30 ft dimension. The east-west dimension of the frame remained constant at 30 ft for all tests.

Prior to testing any diaphragm, an experiment was made to determine how much resistance to horizontal movement was provided by the stiffness of the frame and its connections. With no panels in place, a force was applied to the frame by means of the jacks. A total horizontal displacement of 1-1/4 in. was observed at the jacks with no measurable jacking force. At a total of 1-1/2 in. a pressure of 100 lb was recorded. Since these displacements are of the same order of magnitude as the largest deflections recorded during actual testing of loads of many thousands of pounds, it was concluded that the resistance of the frame itself to shear deformation was a negligible quantity.

A total of thirteen tests was made using Type 9 panels with the large cantilever frame. Spans ranged from 15 ft to 30 ft, and panel depths from 3 in. to 7-1/2 in. Both perforated and non-perforated shear plates were tested, and

weld patterns ranged from heavy to very light, including clinched-seam systems. The results of these tests are summarized in Table 1, and typical load-deflection curves are shown in Fig. 11.

Cantilever Tests of Type 4 Panels.—A total of seven tests were conducted using Type 4 panels on the large cantilever frame. The presence, in some panels of this type, of intermediate and edge stiffeners, while improving the performance of such panels in resisting vertical loads, tends to increase the flexibility of diaphragms because of the somewhat longer stress path involved. Also a consideration was the fact that the stiffening elements consisting of the vertical ribs were more widely spaced as compared with panels of Type 9 and Type 10. In scheduling the tests, an attempt was made to use each depth panel

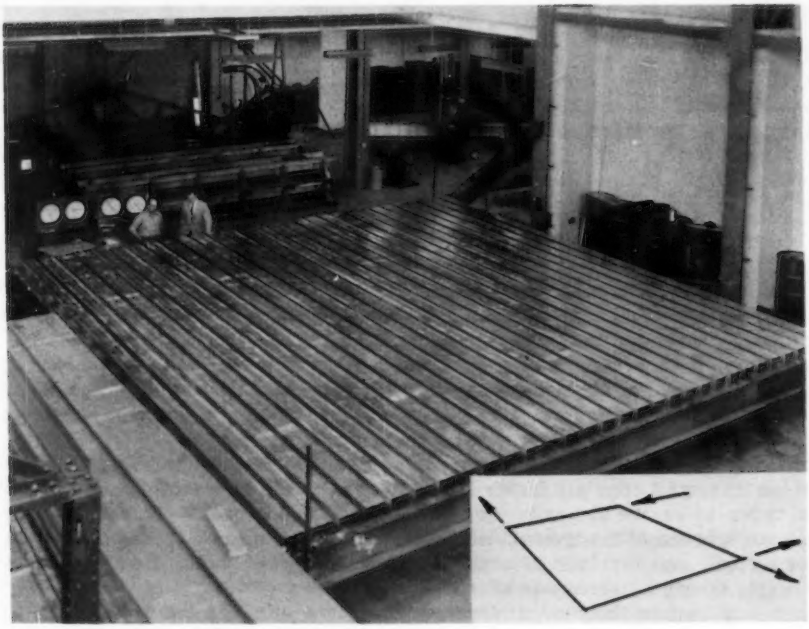

FIG. 13.—CANTILEVER TEST OF TYPE 9 PANELS

on the longest span that would reasonable result from vertical load design for that depth. In all cases the thickness of the steel was 18 gage. The results of the seven tests of this type of panel are summarized in Table 1, and typical load-deflection curves obtained are shown in Fig. 11. Failure loads range from 1,730 lb per ft to 2,590 lb per ft, with very small deflections.

Cantilever Tests of Type 1 and Type 2 Panels.—Panels of this general configuration, meeting the specifications of the Metal Roof Deck Technical Institute, are widely used at the present time for carrying gravity-type loads. These panels are generally used on spans of 8 ft or less. In spite of their lack of a

continuous flat plate element, tests indicate that such panels will carry very substantial shear loads, even with relatively light patterns of welding.

Panels of this type tested at Cornell were of 10 ft span, and of thicknesses ranging from 16 gage to 20 gage. A cantilever test frame 10 ft-by-12 ft in size was used, with loads applied at one corner by a single jack, parallel, to one edge of the diaphragm. Panels spanned perpendicular to the jack force in each case. Panels were tested both flat side down, the flat plate being welded directly to the frame, and flat side up, with the bottom of the ribs welded to the frame. No end closure devices were used with the latter installations, the shear being transferred to the plate level by the flexural resistance of the panel ribs. In general, puddle type welds were used at panel edges, ends, and seams. These were found to be superior to edge fillet welds in resisting deformation, even when the panel configuration permitted the use of fillet welds.

Diaphragms using these panels were tested to failure loads as high as 3,580 lb per ft. While rather severe distortion was evident near failure, particularly at the ends of panels, application of the usual safety factor of three would result in a working load at which distortion was well within acceptable limits. The strongest of the tested diaphragms of this type utilized 16 gage panels of Type 1, on a 10 ft span, and reached the load of 3,580 lb per ft noted above. At 50% of the ultimate load, the net cantilever deflection was only 0.30 in. A summary of test results for these diaphragms is included in Table 1.

ANALYSIS OF TEST RESULTS

Safe Working Values of Shear.—A number of different criteria have been proposed to establish safe working strength values of light gage steel diaphragms. It is evident that, for structural systems that are shear-critical, a maximum shear strength theory is the proper one. That is, when the shear load on the actual structure reaches the shear load present in the test specimen at failure, the failure of the actual structure will occur.

Early investigations into the strength of light gage steel diaphragms involved an attempt to apply a factor of safety to the yield strength of each system in order to arrive at a value of safe working load. Because of the non-linear characteristics of the typical load-deflection plot for shear diaphragms of light gage steel, and the lack of any clearly-defined yield point, this approach to working strength values was abandoned.

It has become the general practice to apply a safety factor to the ultimate load attained, this being a definitely established quantity for any system. Most authorities concerned are in agreement that a safety factor of 4 applied to the ultimate load is sufficiently conservative, but not overly so, in view of the variation in the skill of welding operators doing the work plus the large number of individual welded connections and the impossibility of investigating each for soundness. However, there is general agreement also that the increase in allowable stress values of 33 1/3% usually applied to wind, earthquake, and blast stresses, is applicable here as well, and so this results in an effective safety factor of 3 applied to the ultimate load. (For certain systems, it is more rational to apply a safety factor to the critical buckling load for the web, rather than to the ultimate load reached.)

It should be emphasized at this point that the strength of any particular diaphragm system must be established by test of that system, and not by tests

of individual welds, with an attempt to extrapolate this information. Several investigators in the past have attempted to arrive at generalized values of strength per weld for the several types of weld in common use, and to apply these values to different systems to arrive at failure loads. In countless tests it has been demonstrated that the strength of any particular weld in light gage steel diaphragms under horizontal load will depend to a very large extent on the configuration of the surrounding metal, particularly in those failures resulting from tearing of the panel steel around the weld rather than actual separation of the weld itself. The typical weld failure, in fact, is by tearing or buckling of the panel steel. In these cases it should be obvious that the configuration of the panel adjacent to the weld is of great importance. This is illustrated by tests in which 24 in.-wide panels were welded at their ends to supporting steel using three puddle welds per panel, for an average spacing of 8 in., while along the beams running parallel to the panel span, edge panels were welded with puddle welds of identical size but at a 24 in. spacing. In many instances the panel end welds failed and the edge welds did not, although it is easily shown that the shear per foot of panel is exactly the same along ends and edges of the panels.

Deflection.—Horizontal deflections permitted by floor or roof diaphragms must be held within certain limits in order to insure the safety of the structure. These allowable limits, logically, are less a function of the span of the diaphragm than of the unsupported height of the wall and the stiffness and strength properties of the wall material. Thus, predicted deflections at design load must be compared with maximum allowable values, which will depend upon the variables mentioned. An empirical formula proposed for masonry walls by the Structural Engineers Association of Southern California is:

$$\text{allowable defl.} = \frac{h^2 f}{.01 E t} \quad \ldots\ldots\ldots\ldots\ldots (1)$$

in which h is the unsupported height of the wall in feet, t is the thickness of the wall in inches, E is the modulus of elasticity of the wall material, and f is the allowable compressive stress of the wall material.

In addition to the consideration of deflection from the viewpoint of structural safety, under certain circumstances an analysis of shear reactions, shear, and bending moments may depend on a deflection study. For example, intermediate shear walls may be present in addition to the usual shear walls at the ens of a building, in which case a deflection analysis is mandatory in order to determine the distribution of reactions to the various resisting elements.

In an earlier unpublished paper,[4] the author has developed a method for predicting the deflection performance of light gage steel diaphragms. Briefly, it was found convenient to separate the various contributions to total deflection as follows:

(a) Deflection due to flexural stress;
(b) Deflection due to shear stress in an assumed solid web (flat plate);
(c) Deflection due to seam slip between adjacent panels; and

---

[4] "Deflection of Light Gage Steel Floor Systems Under the Action of Horizontal Loads," by A. H. Nilson, a thesis presented in partial fulfillment of the requirements for the M. S. degree, Cornell Univ.

(d) Deflection due to relative movement between marginal beams and shear web at end connections (negligible if proper shear transfer devices are installed, but substantial if they are omitted).

Conventional formulas permit determination of flexural deflection. In computing the moment of inertia of the diaphragm, it was found sufficiently accurate to consider only the moment of inertia of the marginal beams about the mid-depth of the diaphragm, neglecting the small contribution of the diaphragm web. Shear deflections likewise can be determined using conventional formulas, but making use of a "shape factor" which was determined from test data. Diaphragm deflection due to seam slip can be related entirely by geometry to the movement along the seams. The relation between seam fastener load and resulting seam slip was established by analysis of extensive test data, and both curves and approximate formulas were presented for design use. Additional test data correlated panel end shear and panel web deformation, permitting the computation of item (d).

In the light of increasing experience with such diaphragms, it has become apparent that actual deflections are of an extremely small order of magnitude, even for much larger diaphragm span-depth ratios than are presently contemplated. Investigation of typical load-deflection curves included with this paper will reveal the great rigidity of properly installed light gage steel diaphragms. For the most flexible of the diaphragms tested, a clinched seam system, used for a diaphragm of extreme span-depth ratio of 6-to-1 (15 ft-by-90 ft diaphragm), the deflection at 50% of the ultimate load was only 0.38 in., or 1/2800 of the 90 ft span.

It is felt that deflection of such diaphragms is so small that it will seldom be a factor in design, except for such special circumstances as already noted.

Effect of Panel Depth.—For panels having a continuous flat plate element, such as Types 3,4,7,9, and 10 (Fig. 2), the flat plate is the principal shear-carrying element. The principal function of the vertical ribs is to serve as a stiffener for the very thin shear web, preventing, or at least controlling, buckling of the shear web. Once the adequacy of a certain depth of panel has been demonstrated for a certain span to serve as a web stiffener, then increasing the depth of the section or increasing the thickness of the material forming the vertical ribs, should have no effect on the strength of the diaphragm. All test evidence indicated that, if the panels were designed in the usual manner for vertical loads, then the resulting depth and thickness of the vertical ribs would provide adequate web stiffening for horizontal plate girder action that was adequate to control shear buckling of the web. Panel depths and thicknesses were purposely chosen for test which would represent a reasonable minimum for the span involved, and in no case did a diaphragm fail by premature buckling of the flat plate element. Certain control tests were made keeping all variables constant except for the panel depth, to indicate whether any strengthening effect would be obtained by use of a deeper section. For example, Test No. 58-2 used 7 1/2 in. depth, Type 9 panels with 16 gage flat plate and 18 gage hat section, on a 30 ft span, and resulted in a failure load of 2,130 lb per ft. Test 58-4 on the other hand used 6 in. depth, Type 9 panels with 16 gage flat plate and 18 gage hat section, and resulted in a failure load of 2,290 lb per ft. All details of the two tests were identical except for the depth of the panels. The difference in failure load of 7% (which, in fact, is in favor of the shallower panels) is well within the range of experimental scattering.

For panels without a continuous flat plate element, such as Types 1, 2, 5, 6, and 8 (Fig. 2), the ribbed section must serve not only as the stiffener but as the shear carrying element itself. Changes in panel depth have several effects in this case. A certain minimum depth is required for adequate stiffening as mentioned previously. As the depth increases for this type of panel, however, the path that must be followed by the shear increases accordingly, and so shear deflection will likewise increase for the deeper panels, with the result that diaphragms using the deeper panels of this type will generally be somewhat more flexible than those using shallower sections.

A second effect of deepening the panel section is that distortion of the panel webs near panel ends is increased. Considering Type 4 section for example, the shear load is applied and taken out of the diaphragm by the supporting structural steel at the level of the top surface of the top flange of the beams. The shear is carried in the diaphragm at the level of the top of the panel. The resulting eccentricity, equal to the depth of the panel, causes the panel ribs to "sway" to the side, permitting relative movement between the top and bottom surface of the panels. This has an additive effect on overall diaphragm deflections, of course. It can be seen from Fig. 11 that this deflection increase is not serious in the case of the usual 1-1/2 in. roof deck of Type 1 or Type 2, but for the deeper sections of Type 6 for example, it would be a serious problem. It could be overcome by the use of some shear transfer device such as the continuous closure angle previously described.

Effect of Panel Span.—There is sufficient test evidence to indicate that there is a definite correlation between panel span and diaphragm shear strength expressed as pounds per foot of diaphragm depth. Diaphragms using shorter span panels tend to be stronger per foot of depth and stiffer, and those using longer span panels are not so strong and are more flexible. This relation is clearly seen by plotting failure load in pounds per foot against diaphragm panel span in feet for particular systems, as has been done in Fig. 14. (Note that these curves are interpolations from test data with considerable scatter, and are subject to revision in the light of additional experimental information.)

While there is sufficient test evidence to indicate that there is a definite inverse relation between span and failure load, it should be noted that failure load is not particularly sensitive to changes in span. In Fig. 14(c) for example, one notes that, even for an extreme variation in span from 12 ft to 30 ft for 16 gage plain panels, the variation of ailure loads was from 3,220 plf to 2,640 plf, a reduction of only 18%. One concludes that failure loads can be established by tests for panels used at a span that could be considered a reasonable maximum for the panels tested, and the resulting failure load could be used for all shorter spans without any serious loss in economy.

Relation of Material Thickness to Strength.—There is reason to believe that, for systems that do not depend upon the stiffness of panel vertical ribs for transmitting shear from support beams to the plane of the shear resisting element that is, for systems in which the continuous or near-continuous flat plate is welded directly to the marginal beams), the failure load is very nearly directly proportional to thickness of the panel steel. Referring to the summary data presented in Fig. 14(a), the failure load obtained for 16 gage unperforated panels at 20 ft span for Type 9 panels with clinched seams is 1,760 plf. Prorating this on the basis of flat plate thickness, one obtains an estimated value for 18 gage unperforated panels at 20 ft span of 1,410 plf, compared with a value from the curves of 1,270 plf, a difference of only 10%. Prorating the value of 16 gage acoustic panels at 20 ft span, 1,240 plf, one obtains

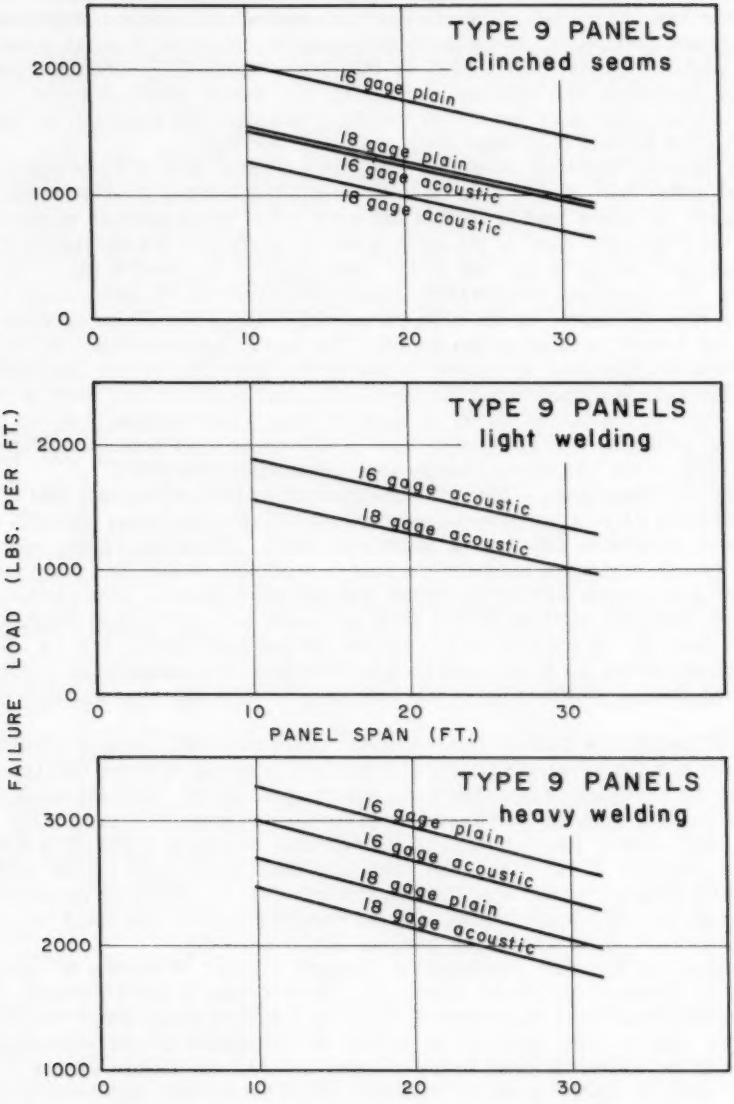

FIG. 14.—VARIATION OF FAILURE LOAD WITH SPAN

an estimated value for 18 gage acoustic panels at 20 ft span of 990 plf, compared with a value from the curve of 1,000 plf, a negligible difference. It is felt that the prorating of results in this manner could be done without serious error for the entire range of thicknesses presently used for diaphragms, say from 20 gage through 14 gage.

It should be noted that this realtion will be, roughly, directly proportional only for those systems that do not rely upon out-of-plane bending stiffness of the vertical panel ribs for transmitting shear force. For panels of Types 1, 2, 3, or 4, for example, when used without closure angles to transmit shear, prorating would not be valid, since the stiffness of the panel ribs in resisting bending caused by shear would be more nearly proportional to the third power of the thickness, whereas the strength of the welds and performance of the diaphragm as a whole would still be in the first power. No direct relation is readily obtainable for this situation.

Effect of Acoustic Perforations.—Certain manufacturers provide panels with a sound-absorbing element, which, with a perforated panel bottom surface, makes for improved acoustic characteristics of the deck when used as a ceiling surface as well as floor or roof deck. The perforations are usually about 1/8 in. in diameter, and spaced at about 3/4 in. centers. Although the actual shear stress in the diaphragm web is usually quite low at failure (4,770 psi on the gross section for the most highly stressed system tested at Cornell) the presence of the acoustic perforations does increase this shear stress and consequently increases the shear strain and overall deflection of the system. Considering the stiffness of the plate in a direction perpendicular to its own plane, the presence of the holes increases flexibility in this direction, permitting tension-field type buckling at a somewhat lower load value. This buckling in turn increases weld stresses.

Another important effect of perforations is the attendant difficulty in making proper welds, particularly puddle welds in material of 20 gage and lighter. With the higher currents necessary for fusion with this type of weld, the presence of the perforations tends to cause excessive burning of the light gage sheet around the edge of the welds, so that unsatisfactory welds may result.

Test data indicate conclusively lower values of failure load for perforated systems as compared with otherwise identical systems. For example, the average failure load of unperforated panel tests 58-5 and 58-6 was 2,620 plf, while the failure load of the corresponding perforated panel test 58-4 was 2,290 plf, a decrease in strength of 13%. The average failure load of unperforated panel tests 57-3, 2a, and 57-5 was 1,980 plf, while the corresponding peforated panel test 5a failed at 1,460 plf, a strength decrease of 26%. On the basis of 1/8 in. holes at 3/4 in. centers, the area reduction in the perforated plate is 17%.

Panel Orientation Relative to Load.—Elementary structural theory proves that, in a plate girder or beam web, the shear on the two perpendicular faces of a small element is equal in magnitude and opposite in sign. It follows directly from this that the orientation of the panels in a diaphragm relative to the direction of the applied horizontal load does not influence the strength or stiffness of the diaphragm, and that the panels will be equally effective whether they are laid perpendicular or parallel to the load direction. This point was demonstrated by Cornell laboratory tests in 1955, in which, using the three-bay test frame, the panels in one of the outer bays were placed parallel to the

load direction, while the panels in the other outer bay were placed perpendicular to the load direction. In all cases the deflection of the third points of the test frame were exactly identical, as were measurements of seam slip between adjacent panels.

In actual building installations, any one of several panel arrangements are common, as shown in Fig. 15. Fig. 15(a) shows a roof structure framed with trusses spanning in the short direction of the building between columns in the exterior walls. Light gage steel panels are frequently used to span directly between trusses as shown by panel "A" in the sketch. Considering, for example, that the horizontal wind or earthquake loads are applied as concentrations P along the column lines, the total shear wall reaction at either end of the building will be 3P, and the total shear force along all of the panels in the second bay will be 2P. Making the usual and very close approximation that the unit shear stress can be found by dividing total shear force by web area, one obtains a unit shear of 2P/L pounds per linear foot acting on the short ends of panel "A." Taking moments about any corner of the panel, one obtains the equal unit shear stress of 2P/L pounds per linear foot acting along the long edges of the panel.

It is easily seen that the corresponding panel "A" in the right half of Fig. 15(a), in which purlins have been used spanning between trusses, with panels supported by the purlins, is likewise loaded along each of its edges with a unit shear of 2P/L pounds per linear foot. It is evident that the direction of the panel span is of no significance, and that the shear per foot along any edge of the panel will be identical.

Fig. 15(b) shows a framing plan more common to multi-story buildings, in which floor panels are carried by beams which in turn are supported by girders framing to columns. It is easily shown that, as in the sketch previously considered, panel "A" is loaded with a shear of 2P/L plf along the edges parallel with the load direction. The summation of moments about any corner of the panel requires an equal unit shear 2P/L plf acting in the opposite sense along the other two edges of the panel.

If the spacing of supporting steel permits, it is not unusual for floor or roof panels to be continuous over two or in some cases three spans. This circumstance is shown as panel "B" in Figs. 15(a) and 15(b). In the case of Fig. 15(b) where the entire panel is subjected to a constant value of shear, welds along the intermediate supporting beam can actually be omitted or at least minimized since they carry no computed stress. In the case of Fig. 15(a), however, where the left and the right halves of the panel carry different unit shear load, it is necessary to weld along the intermediate beam. These welds need not be of sufficient strength to transfer the entire unit shear into or out of the panel, as the welds at either end of that panel must be, but need only suffice to introduce the unit load P/L into the diaphragm along that line.

Fig. 15(c) shows an installation of a type only recently (1960) possible, with the marketing by several of the larger manufacturers, of long span light gage steel panels, up to and including 30 ft in length. In this case intermediate framing is dispensed with altogether, and panels span from building wall to building wall. If these panels are carried by a light steel frame, they would be secured at their ends to this frame in the usual manner, and along their own edges by the customary seam welds. It should be noted that, if the panels are carried by a masonry wall rather than by a steel frame, and if diaphragm action is required, some provision must be made to provide "flange action" by tensile and compressive reinforcement along the tops of the walls.

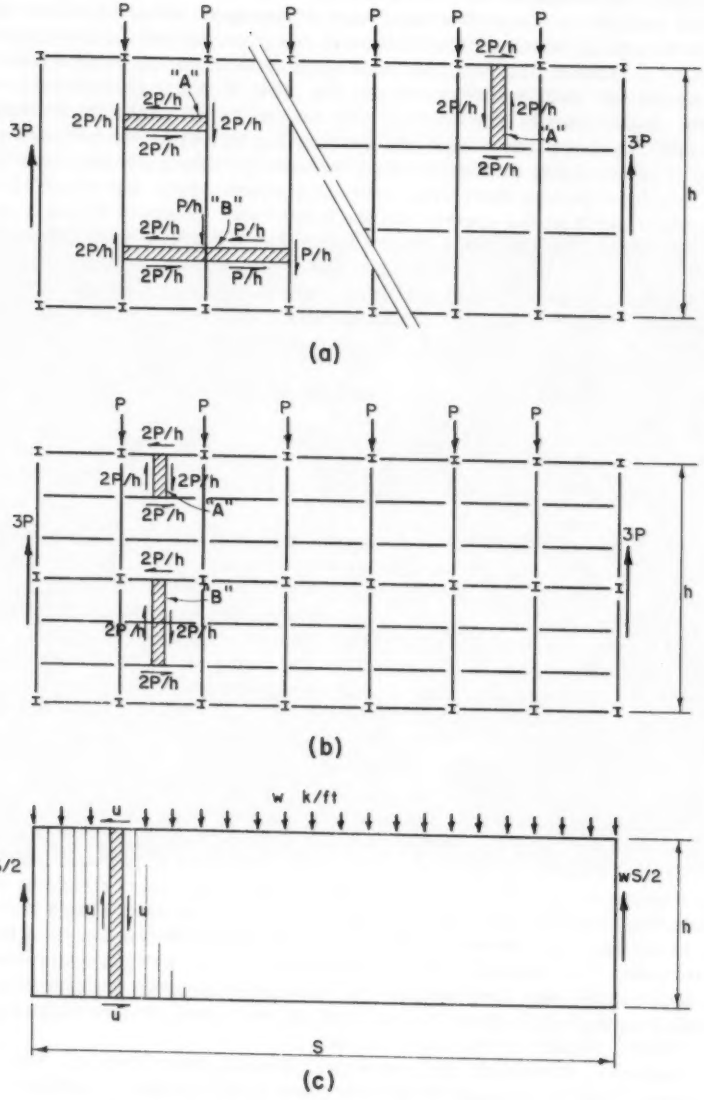

FIG. 15.—TYPICAL INSTALLATIONS

In addition, a reliable means must be devised to transfer longitudinal shear from the top of the walls into the light gage steel roof.

Application of Tension Field Theory.—It was observed that certain of the light gage steel diaphragms tested transformed into the tension field state prior to failure. It is self-evident that diaphragms using panels of Types 1, 2, 5, 6, and 8, which lack a continuous flat plate element, cannot function as part of a tension field web, because accordion action at the ribs prevents the transfer of tensile stress across the ribs. It is unlikely also that diaphragms using panels of Types 7, 9, and 10 would pass into the tension field state, because the close rib spacing has the effect of increasing the critical shear buckling stress (at which the web transforms from an ordinary shear web to a tension field web) above that stress which will result in failure of other parts of the system. On the other hand, panels of Types 3 and 4, having a continuous flat plate, when appropriately welded along the seams essentially in the plane of that flat plate, and with fairly wide spacing of vertical ribs, can and do develop tension field conditions. Fig. 16 shows such a diaphragm made up of Type 4 panels, which is clearly in the tension field state, although local failure had occurred at the near corner at the time the photograph was taken.

The critical stress for shear buckling of thin plates supported on four sides is computed, using the expression

$$f_{s_{cr}} = \frac{k \pi^2 E}{12\left(1 - \mu^2\right)} \left(\frac{t}{w}\right)^2 \quad \ldots\ldots\ldots\ldots\ldots (2)$$

in which $f_{s_{cr}}$ as the critical value of shearing stress that will produce buckling (in pounds per square inch); k denotes the constant, equal to 5.4 for plate areas with essentially an infinite aspect ratio of length to width; E is the modulus of elasticity; μ refers to Poisson's Ratio, taken equal to 0.3 for steel; t denotes the thickness of plate (inches); and w is the width of plate between stiffeners (inches). Conditions in the shear web of a light gage steel diaphragm depart from the ideal conditions assumed in the development of the foregoing expression to a certain extent. The edges of the plate areas are not perfectly supported, but have flexible supports along the stiffening ribs. In addition the shear load is applied by edge welds that may have some eccentricity with respect to the shear-carrying element. Consequently some deviation from the theoretical values should be expected. Nevertheless, such calculations of theoretical buckling stress will give at the very least an order of magnitude solution, and it must be realized that, once it is established that such a diaphragm will transform into a tension field, the exact stress at which this occurred will be irrelevent as far as determining the ultimate strength of the diaphragm is concerned. One can make use of the tension field theory to determine the diagonal tensile stresses in the web plate, the load on seam welds and edge welds, and the load per foot acting inward along the marginal beams, which must be resisted by the panel ribs as stiffeners or by the flexural rigidity of the marginal beams.

For example, examining the results of Cornell Test 58-4(LS), the computed shear buckling stress for the web plate area bounded by stiffeners and end marginal beams was 2,320 psi, or 1,330 lb per ft. The development of the diagonal buckling wave pattern seen in Fig. 16 occurred at a shear of 1,150 lb per ft. The small difference between these values is undoubtedly due to the imperfections noted previously. Having established that tension field action

will occur for this particular diaphragm, one can draw certain conclusions regarding the stress in the diaphragm near failure. At the failure load of 67.3 kips, or 2,590 lb per ft, the diagonal tensile stress in the buckled web, assuming complete tension field action, would be equal to twice the value of unit shear stress that would be present had the web not buckled. For this case, the resulting diagonal tension at failure is 9,040 psi. From this value, seam and edge weld loads could readily be computed.

An important characteristic of a tension field girder is that an inward component of force is present along the flanges of the girder, tending to pull the flanges together. The function of the stiffeners in such a web-buckled girder is to prevent this inward movement, and thus the stiffeners

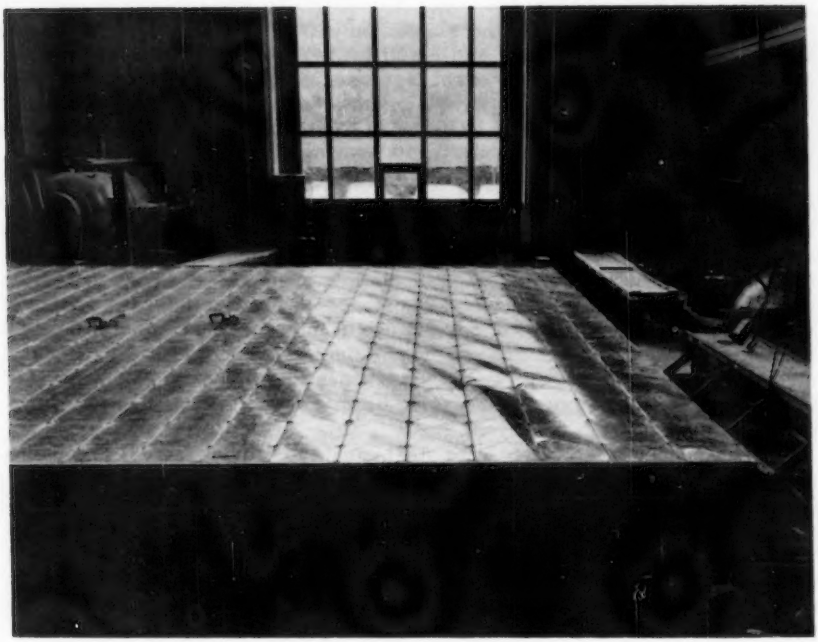

FIG. 16.—CANTILEVER DIAPHRAGM TEST OF TYPE 4 PANELS NOTE DIAGONAL BUCKLING PATTERN.

act as columns between flanges. The magnitude of this inward load along the girder flanges (marginal beams) in readily computed using the expression

$$w_h = 12\ t\ f_t \sin^2 a \quad \ldots\ldots\ldots\ldots\ldots\ldots \quad (3)$$

in which w_h is the load acting inward along the marginal beams (pounds per foot); t refers to the thickness of web plate (inches); f_t denotes the diagonal tension stress in the web plate (pounds per square inch); and a is the angle between marginal beam and lines of diagonal tension (usually taken equal to

45 degress). The inward force so computed may be of considerable magnitude. If panels are oriented parallel to the load direction (that is perpendicular to the marginal beams so loaded) then the column ribs can be checked for their capacity to serve as stiffeners between flanges to resist this force. If the panels are oriented perpendicular to the load direction, then no stiffening is possible from the panels, and the marginal beams themselves must be heavy enough to resist the computed lateral force by bending about the vertical axis. This requirement may in effect prohibit the utilization of the tension field strength of such diaphragms, and might require that the critical shear buckling stress be taken as the failure stress for the system.

OTHER APPLICATIONS

It is thus apparent that the diaphragm stiffness of roof and floor areas using light gage steel panels can be utilized to eliminate unnecessary horizontal bracing systems and to effect increased economy in building construction. Innumerable structures have been erected in many areas making use of this diaphragm stiffness to resist wind loads, and loads due to earthquake forces.

The practicing engineer will be quick to note that the characteristics involved in the performance of light gage diaphragms in resisting horizontal loads are exactly the same as those involved when such diaphragms are called upon to prevent the lateral buckling of beams and columns. G. Winter has illustrated[5] that even relatively weak diaphragm systems will prove to provide many times the required horizontal resistance to prevent lateral buckling of beams and girders in a floor system. The use of inter-beam struts and diagonal members is thus avoided, and yet the unreduced values of allowable flexural stress can be used. Rigid frames and trusses likewise obtain a condition of full lateral support along compressive flanges due to the presence of a properly welded light gage steel roof.

The proper use of light gage steel panels to provide lateral resistance would eliminate a great deal of the bracing usually associated with light steel frames such as are used for mill buildings. Not only would such members provide full lateral support for the compression chord of the roof trusses, but they would also prevent the several types of distortion of the building as a whole that are responsible for the installation of bracing in the plane of the roof, the plane of the end walls, and in a vertical plane perpendicular to the plane of the trusses.

Another interesting application is in the case of the "frameless" building, in which the rigidity of the roof and wall elements in their own plane is used to provide resistance to both vertical and horizontal forces. Such "folded plate" structures are coming into considerable popularity in concrete construction, although the utilization of the same principles in light gage steel buildings is only beginning. It is apparent that the in-plane shears, longitudinal and transverse, developed by bending of any one of these plate elements in its own plane, and the edge shears caused by one plate on those adjacent, are of

---

5 "Lateral Bracing of Columns and Beams," by George Winter, Proceedings, ASCE, Vol. 84, No. ST 2, March, 1958.

the same variety that were considered in the test program described, and the results can be applied directly to such construction.

CONCLUSION

This paper summarizes the results of an extensive series of tests of light gage steel roof and floor diaphragms. Such tests have proved conclusively that shear diaphragms constructed of light gage steel panels can, with proper welding, resist large horizontal loads, to the extent that the need for horizontal bracing systems in building using these panels is largely eliminated. Shear stress and marginal beam stress in such diaphragms are usually quite low, and it will be found that a building which has been properly designed for vertical loads will function also in diaphragm action with no increase in member or panel sizes, and without exceeding allowable stresses. Special attention must be given to welds joining panels to one another and to supporting steel.

The deflection of light gage steel panel shear diaphragms must be considered in order to avoid damage to the walls that are being supported. This is of particular importance in masonry buildings. However, in every one of a large number of tests of many types of building panels, the actual deflection under load was but a small fraction of that which would be allowed under present specifications.

ACKNOWLEDGMENTS

The experimental work described in this paper was done in Thurston testing laboratory at Cornell University by the author as a part of Cornell's long-term research on light gage steel structures, under the general direction of George Winter, head of the Structural Engineering Department. The work was sponsored by Fenestra, Inc., manufacturers of the sections tested. The full cooperation and objective viewpoint of the sponsoring organization is gratefully acknowledged.

Journal of the
STRUCTURAL DIVISION
Proceedings of the American Society of Civil Engineers

SIMPLY SUPPORTED CORNER PLATE

By Mario G. Salvadori,[1] F. ASCE and H. C. Reggini[2]

SYNOPSIS

A corner plate, simply supported on two parallel boundaries, each composed of two semi-infinite straight lines meeting at right angles, is uniformly loaded. Bending and twisting moments and shears and boundary reactions in the plate are determined by finite-difference integration of the corresponding boundary value problem. The penetration into the side strips of the disturbance represented by the corner is shown to be practically negligible at a distance from the inner corner of the order of the width of the side strips.

INTRODUCTION

In modern reinforced concrete design, flat slabs are often used as floors in buildings leaving an inner rectangular core with sides parallel to the outer boundaries of the building. The floor slabs may be either simply supported by or elastically built-in into the core and the outer walls, thus becoming a "corner plate" of widths a and b. (Fig. 1).

When the sides l and l' of the core are much larger than the widths a and b of the strips, the stresses away from the corner approach asymptotically, the values for infinite strips of widths a and b, respectively. It will be shown that the stresses due to a uniform load in the corner region of the plate considered simply supported are rather insensitive to the lengths l and l', so that they may be computed as l and l' were infinite as soon as $l \geq 2a$, $l' \geq 2b$.

Note.—Discussion open until April 1, 1961. To extend the closing date one month, a written request must be filed with the Executive Secretary, ASCE. This paper is part of the copyrighted Journal of the Structural Division, Proceedings of the American Society of Civil Engineers, Vol. 86, No. ST 11, November, 1960.

[1] Prof. of Civ. Engrg., Columbia Univ., New York, N. Y., and Assoc., Paul Weidlinger, Cons. Engr., New York, N. Y.

[2] Assoc. Prof., Buenos Aires Univ., Buenos, Aires, Argentina, and Assoc., H. Fernantezlong, Cons. Engr., Buenos Aires, Argentina.

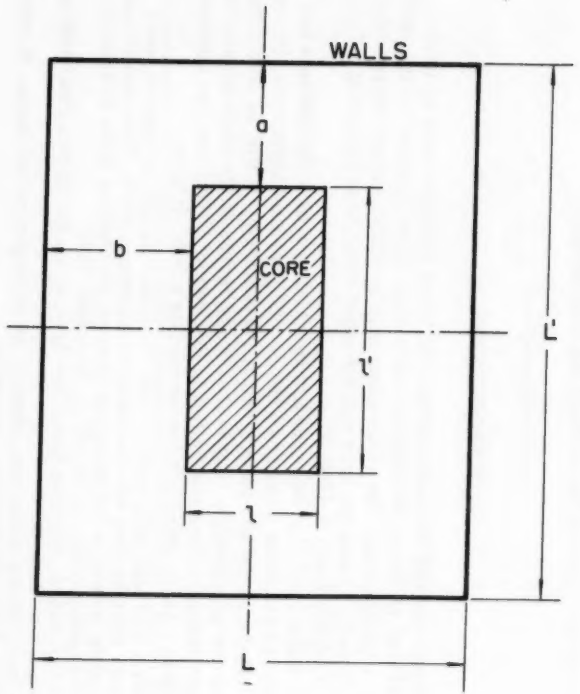

FIG. 1.—FLOOR SLAB

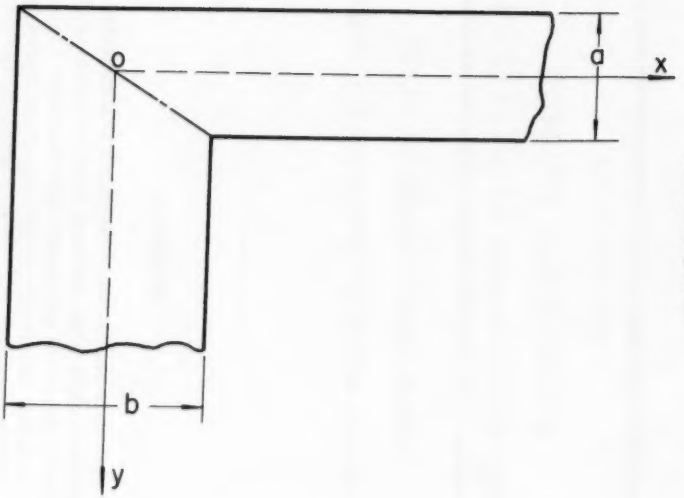

FIG. 2.—CORNER PLATE

The reentrant corner of the plate introduces a singular point in the solution of the plate equation, so that shears are infinite there. In practice, these theoretically infinite stresses do not arise, because they are relieved by plastic deformations due to diagonal tension.

The evaluation of stresses and displacements for the corner plate was obtained by numerical methods, using first-order central-difference operators and solving the corresponding equations in an electronic computer.

CORNER PLATE PROBLEM

The indefinite corner plate of Fig. 2 is simply supported on its boundary and loaded with a uniform load q. The plate deflections w are determined[3] by the following boundary value problem:

$$\nabla^2 M = q \quad \ldots\ldots\ldots\ldots\ldots\ldots \quad (1a)$$

$$\nabla^2 w = M/D \quad \ldots\ldots\ldots\ldots\ldots\ldots \quad (1b)$$

$$M = 0, \; w = 0 \text{ on the boundaries} \quad \ldots\ldots\ldots\ldots \quad (2)$$

$$\lim_{x \to \infty} \frac{\partial w}{\partial x} = \lim_{y \to \infty} \frac{\partial w}{\partial y} = 0 \quad \ldots\ldots\ldots\ldots\ldots\ldots \quad (3)$$

$$\lim_{x \to \infty} \frac{\partial M}{\partial x} = \lim_{y \to \infty} \frac{\partial M}{\partial y} = 0 \quad \ldots\ldots\ldots\ldots\ldots\ldots \quad (4)$$

in which

$$\nabla^2 = \frac{\partial^2}{\partial x^2} + \frac{\partial^2}{\partial y^2} \quad \ldots\ldots\ldots\ldots\ldots\ldots \quad (5a)$$

and

$$M = \frac{M_x + M_y}{1 + \nu} \quad \ldots\ldots\ldots\ldots\ldots\ldots \quad (5b)$$

Conditions 3 and 4 are equivalent to the conditions:

$$\lim_{x \to \infty} w = \frac{q a^4}{384 D} \left[5 - 24 \left(\frac{y}{a} \right)^2 + 16 \left(\frac{y}{a} \right)^4 \right] \quad \ldots\ldots\ldots \quad (6a)$$

$$\lim_{y \to \infty} w = \frac{q b^4}{384 D} \left[5 - 24 \left(\frac{x}{b} \right)^2 + 16 \left(\frac{x}{b} \right)^4 \right] \quad \ldots\ldots\ldots \quad (6b)$$

$$\lim_{x \to \infty} M = \frac{q}{2} \left(\frac{a^2}{4} - y^2 \right) \quad \ldots\ldots\ldots\ldots\ldots\ldots \quad (7a)$$

$$\lim_{y \to \infty} M = \frac{q}{2} \left(\frac{b^2}{4} - x^2 \right) \quad \ldots\ldots\ldots\ldots\ldots\ldots \quad (7b)$$

expressing the fact that the plate is bent into cylindrical surfaces away from the corner.

---

[3] "Theory of Plates and Shells," by S. Timoshenko and Voshorsky-Krager, McGraw Hill Book Co. Inc., New York, 1959.

n = 2

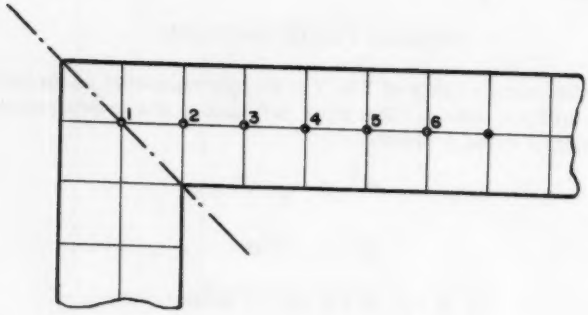

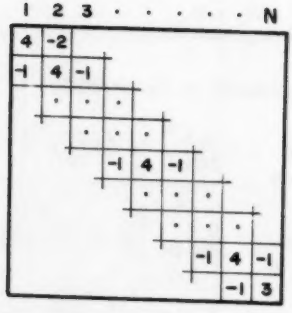

FIG. 3(a)

n = 4

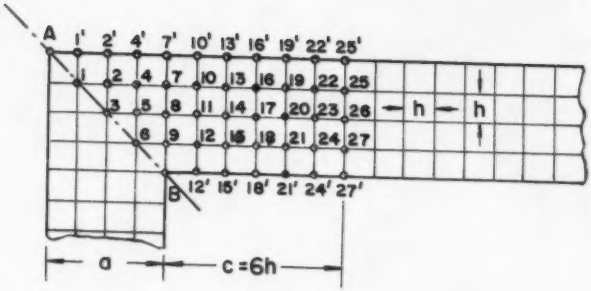
A
1' 2' 4' 7' 10' 13' 16' 19' 22' 25'
1 2 4 7 10 13 16 19 22 25
3 5 8 11 14 17 20 23 26
6 9 12 15 18 21 24 27
h
h
B
12' 15' 18' 21' 24' 27'
a
c=6h

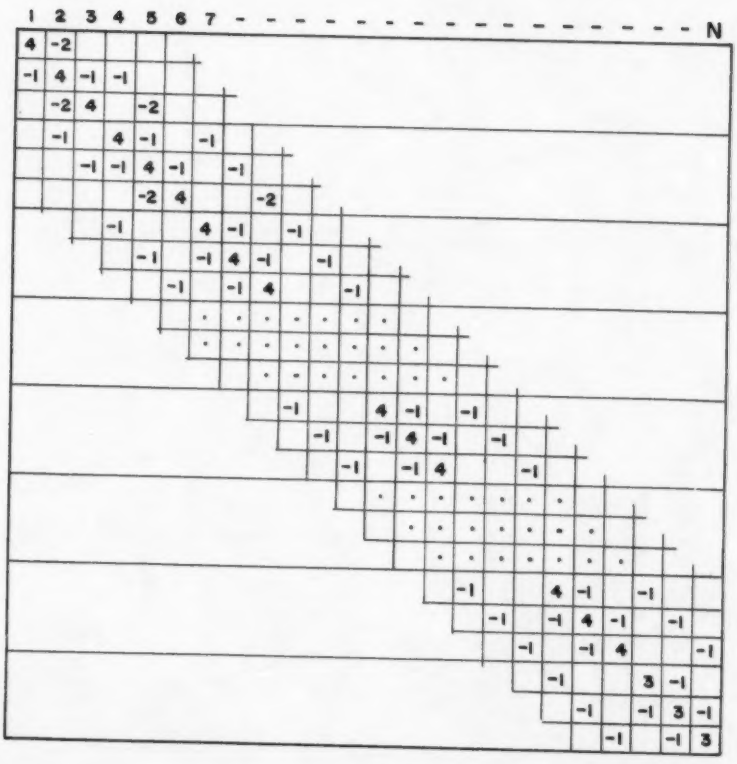
1 2 3 4 5 6 7 - - - - - - - - - - - - - - - - - - N

FIG. 3(b)

Once M and w are known, the stress resultants are given by:

$$M_x = -D\left(\frac{\partial^2 w}{\partial x^2} + \nu \frac{\partial^2 w}{\partial y^2}\right) \quad \ldots\ldots\ldots\ldots\ldots (8a)$$

$$M_y = -D\left(\frac{\partial^2 w}{\partial y^2} + \nu \frac{\partial^2 w}{\partial x^2}\right) \quad \ldots\ldots\ldots\ldots\ldots (8b)$$

$$M_{xy} = M_{yx} = -D(1-\nu)\frac{\partial^2 w}{\partial x\, \partial y} \quad \ldots\ldots\ldots\ldots (8c)$$

$$Q_x = \frac{\partial M}{\partial x} \quad \ldots\ldots\ldots\ldots\ldots\ldots\ldots\ldots (8d)$$

$$Q_y = \frac{\partial M}{\partial y} \quad \ldots\ldots\ldots\ldots\ldots\ldots\ldots\ldots (8e)$$

$$V_x = \frac{\partial M}{\partial x} + \frac{\partial M_{xy}}{\partial y} \quad \ldots\ldots\ldots\ldots\ldots\ldots (8f)$$

and

$$V_y = \frac{\partial M}{\partial y} + \frac{\partial M_{xy}}{\partial x} \quad \ldots\ldots\ldots\ldots\ldots\ldots (8g)$$

FINITE DIFFERENCE SOLUTION

Assuming a and b to be multiples of a spacing h, (if either a or b are not multiples of h, the problem may be solved for the two plates for which, for example:

$$b' = m\,n \leq b \leq (m+1)\,h = b''$$

and the solution for the width b may be obtained by interpolation):

$$a = n\,h \quad \ldots\ldots\ldots\ldots\ldots\ldots\ldots (9a)$$

and

$$b = m\,h \quad \ldots\ldots\ldots\ldots\ldots\ldots\ldots (9b)$$

and using first-order central-difference operators, and in particular:

$$\nabla^2 = -\frac{1}{(a/n)^2}\begin{bmatrix} & -1 & \\ -1 & 4 & -1 \\ & -1 & \end{bmatrix} \quad \ldots\ldots\ldots\ldots (10)$$

The problem is reduced to the solution of the two systems of linear algebraic equations:

$$A\,X = I \quad \ldots\ldots\ldots\ldots\ldots\ldots\ldots (11a)$$

and

$$A\,Y = X \qquad \ldots\ldots\ldots\ldots\ldots\ldots \quad (11b)$$

in which A is the matrix of the coefficients, I a unit column, and X and Y are related to M and w by

$$M = \frac{q\,a^2}{n^2}\,X \qquad \ldots\ldots\ldots\ldots\ldots\ldots \quad (12a)$$

and

$$w = \frac{q\,a^4}{n^4\,D}\,Y \qquad \ldots\ldots\ldots\ldots\ldots\ldots \quad (12b)$$

The matrices corresponding to n = 2, 4 together with the numbering of the corresponding pivotal points are given in Fig. 3, for the case a = b, when boundary conditions 3 and 4 are used.

TABLE 1

c/h	N	Point 1	2	3	4	5	6	7	8	9
		X								
2	12	0.95186	1.40372	2.09458	1.56844	2.28584	2.28238	1.58451	2.19638	1.77931
3	15	0.94965	1.39930	2.08621	1.56133	2.27312	2.26779	1.57291	2.17717	1.76245
4	18	0.94916	1.39831	2.08438	1.55972	2.27044	2.26474	1.57010	2.17292	1.75905
5	21	0.94905	1.39809	2.08397	1.55935	2.26984	2.26408	1.56948	2.17197	1.75831
6	24	0.94902	1.39804	2.08387	1.55927	2.26971	2.26393	1.56934	2.17176	1.75815
		Y								
2	12	1.44089	2.40585	3.95271	2.82609	4.45228	4.49235	2.87770	4.25253	3.39123
3	15	1.42590	2.37698	3.89970	2.78303	4.37931	4.40957	2.81450	4.15181	3.30594
4	18	1.42201	2.36944	3.88595	2.77148	4.36027	4.38852	2.79650	4.12469	3.28440
5	21	1.42100	2.36748	3.88239	2.76845	4.35531	4.38307	2.79164	4.11750	3.27880
6	24	1.42075	2.36698	3.88148	2.76767	4.35404	4.38168	2.79037	4.11563	3.27735

TABLE 2

	X				Y			
	Value of c/h							
Point	2	4	6	∞	2	4	6	∞
Upper	1.57358 (5%)	1.52017 (1%)	1.51381 (1%)	1.50000	2.84794 (14%)	2.61348 (5%)	2.57619 (3%)	2.50000
Middle	2.13645 (7%)	2.03129 (1%)	2.02169 (1%)	2.00000	4.09245 (17%)	3.67044 (5%)	3.61539 (3%)	3.50000
Lower	1.63849 (7%)	1.52478 (2%)	1.51745 (1%)	1.50000	3.04072 (22%)	2.62966 (5%)	2.58873 (4%)	2.50000

Table 1 gives the values of X and of Y at points 1 to 9 in the corner region of Fig. 3 (b) (h = a/4), when boundary conditions 3 and 4 are applied at a distance c = 2 h, 3 h, 4 h, 5 h, and 6 h from the reentrant corner. It is seen that for $c/h \geq 2$ the maximum difference between any X is less than 1.2%, and between any Y value less than 3.4%. For $c/h \geq 4$, these differences reduce to 0.5% and 2.1%. It is thus seen that as soon as $l \geq 2a$ the deflections and stress resultants may be considered practically independent of l and equal to those for $l = \infty$.

Table 2 gives the values of X and Y at the pivotal points farthest from the reentrant corner for various values of c/h and for $c/h = \infty$ (cylindrical deflection), together with the percentage difference from the values for $c/h = \infty$. It is seen that the corner disturbance is less than 2% in the moment M and less than 5% in the displacement as soon as $c/h \geq 4$.

TABLE 3

n	At the origin (c/h = 6)		At the middle of infinite strip	
	X	Y	X	Y
2	0.12500 (5%)	0.01562 (4%)	0.12500 (0%)	0.01562 (17%)
4	0.13024 (1%)	0.01516 (1%)	0.12500 (0%)	0.01365 (5%)
h^2-extrapolation n=2; n=4	0.13199	0.01501	0.12500 (0%)	0.01299 (0,2%)
∞	. . .	. . .	0.12500	0.01302

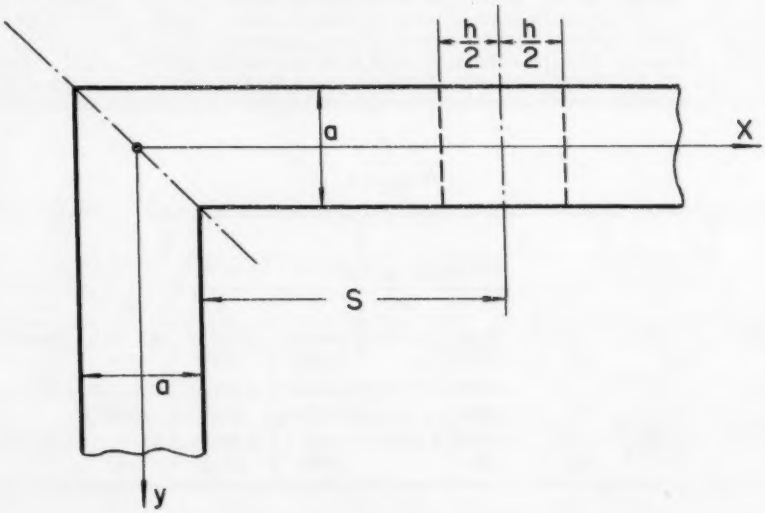

FIG. 4

In order to evaluate the influence of the spacing h on the numerical solution, the values of X and Y at the origin (center of corner) and at the point farthest from the corner at the middle of the strip were evaluated for c/h = 6, taking n = 2 and n = 4. Table 3 shows the results of this computation and the values obtained by h^2 extrapolations,[4] together with the percentage of error in comparison with the extrapolated values (the values for the cylindrical deflection are X = 0.12500, Y = 0.01302 and should be compared with the extrapolated values 0.12500 and 0.01299). It is seen that the values at the origin obtained with n = 4 are in error by 1% and that the values at the middle of the strip are in error by 5%. The extrapolated values may be considered practically correct.

FINITE CORNER PLATES

Boundary conditions 3 used in solving the case of the indefinite corner plate state the symmetry of the deflection about a line parallel to y at S (Fig. 4), since they make

$$X_{S-h/2} = X_{S+h/2} \quad \ldots\ldots\ldots\ldots \quad (13a)$$

and

$$Y_{S-h/2} = Y_{S+h/2} \quad \ldots\ldots\ldots\ldots \quad (13b)$$

Hence, the solutions thus obtained are also valid for symmetrical plates with l = l' = 2 S. Fig. 5 gives the dimensions of these plates (for n = 4).

STRESS RESULTANTS

The stress resultants of Eqs. 8 are easily evaluated by means of the pivotal values of M and w using first order central difference operators.[5] The bending and twisting moments become, (assuming, for simplicity, Poisson's ratio equal to zero):

$$M_x = p\,a^2 \frac{1}{n^2} [-1, 2, -1]\, Y \quad \ldots\ldots\ldots\ldots \quad (14a)$$

$$M_y = p\,a^2 \frac{1}{n^2} \begin{bmatrix} -1 \\ 2 \\ -1 \end{bmatrix} Y \quad \ldots\ldots\ldots\ldots \quad (14b)$$

and

$$M_{xy} = p\,a^2 \frac{1}{4\,h^2} \begin{bmatrix} -1 & 1 \\ 1 & -1 \end{bmatrix} Y \quad \ldots\ldots\ldots\ldots \quad (14c)$$

The principal moments along the diagonal of the corner (Fig. 6) are given by:

$$M_{1,2} = \frac{1}{2}\left(M_x + M_y\right) \pm M_{xy} = \frac{p\,a^2}{4\,n^2} \begin{bmatrix} \mp 1 & -4 & \pm 1 \\ -4 & 16 & -4 \\ \pm 1 & -4 & \mp 1 \end{bmatrix} Y \ldots\ldots\ldots \quad (15)$$

---

[4] "Numerical Methods in Engineering," by M. G. Salvadori and M. L. Baron, Prentice-Hall, New York, 1955, p. 75.

[5] Ibid., p. 63.

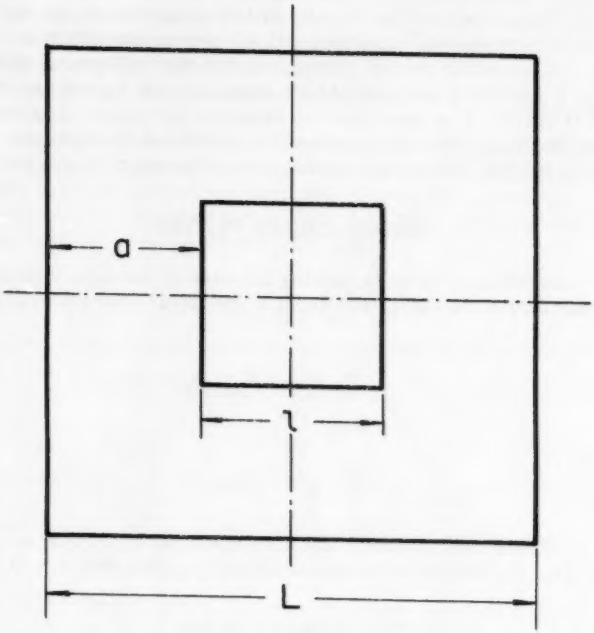

$\frac{C}{h} = 2$	$\frac{L}{l} = \frac{11}{3}$
$\frac{C}{h} = 3$	$\frac{L}{l} = \frac{13}{5}$
$\frac{C}{h} = 4$	$\frac{L}{l} = \frac{15}{7}$
$\frac{C}{h} = 5$	$\frac{L}{l} = \frac{17}{9}$
$\frac{C}{h} = 6$	$\frac{L}{l} = \frac{19}{11}$

FIG. 5.—SQUARE PLATES

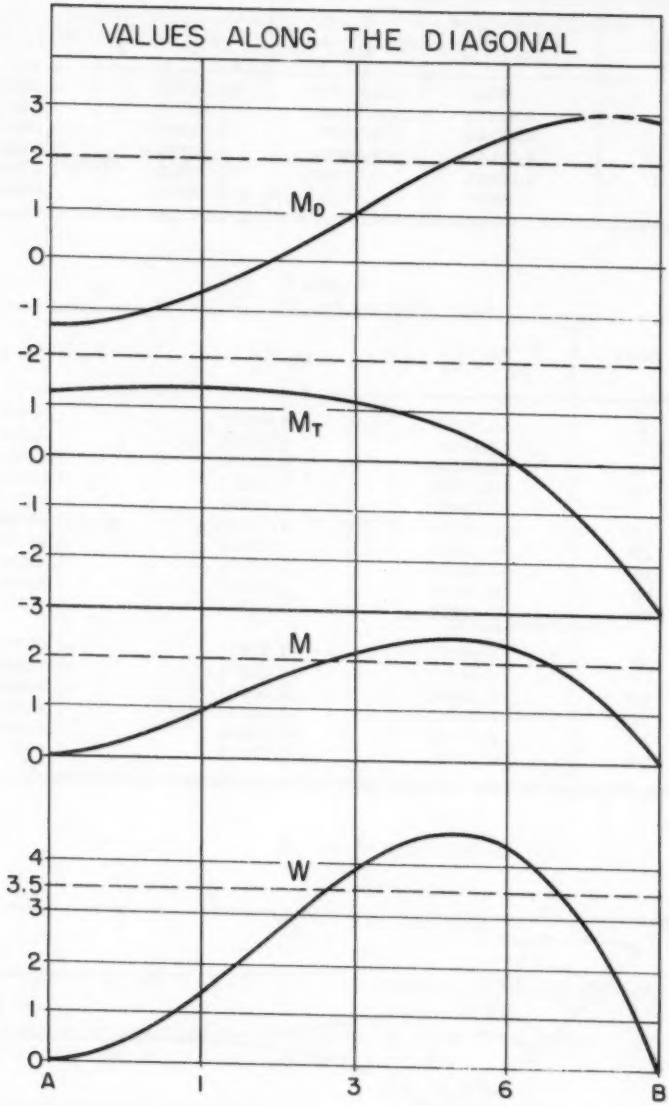
VALUES ALONG THE DIAGONAL
3
2
1
0
-1
-2
M_D
1
0
-1
-2
-3
M_T
2
1
0
M
4
3.5
3
2
1
0
W
A
1
3
6
B

FIG. 6

TABLE 4

Point	$w/\left(\frac{1}{256}\ \frac{p\,a^4}{D}\right)$	$M_D/\left(\frac{1}{16}\ p\,a^2\right)$	$M_T/\left(\frac{1}{16}\ p\,a^2\right)$	$M/\left(\frac{1}{16}\ p\,a^2\right)$
A	0,00000	(-1,42075)	(1.42075)	0,00000
1	1,42075	-0.51999	1.42075	0,94902
3	3,88148	0.98027	1.11381	2,08387
6	4,38168	2.44094	0.26605	2,26393
6-B	2,93035	2.95805	-1.38800	1,57006
B	0,00000	(2.85395)	(-2.85395)	0,00000

TABLE 5

Point	$\frac{\partial M_{xy}}{\partial x} / \left(\frac{1}{4}\ a\ p\right)$	$Q_y/\left(\frac{1}{4}\ a\ p\right)$	$V_y/\left(\frac{1}{4}\ a\ p\right)$
A	0.00000	0.00000	0.00000
1'	0.47452	0.94902	1.42354
2'	0.54554	1.39804	1.94358
4'	0.37799	1.55927	1.93726
7'	0.10421	1.56934	1.67355
10'	-0.00238	1.54632	1.54394
13'	-0.02560	1.52612	1.50052
16'	-0.02318	1.51381	1.49063
19'	-0.01702	1.50745	1.49043
22'	-0.01333	1.50484	1.49151
B	0.68093	-1.75815	-1.07722
12'	0.24197	-1.59691	-1.35494
15'	0.09764	-1.53967	-1.44203
18'	0.04463	-1.51745	-1.47282
21'	0.02346	-1.50844	-1.48498
24'	0.01570	-1.50517	-1.48947

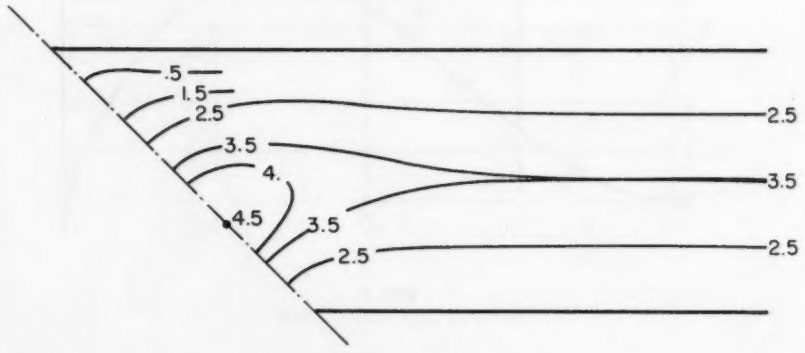

FIG. 7.—DEFLECTION

Table 4 gives the value of the displacements and of the bending moments at the pivotal points of the network for n = 4, c/h = 6.

Similarly, the reaction and shear along the outer and inner boundary are given in Table 5. They were computed by means of the following operators:

$$Q_y = \frac{\partial M}{\partial y} = p\,h\,\frac{1}{2}\begin{bmatrix}-1\\0\\1\end{bmatrix} X \quad \ldots\ldots\ldots\ldots\ldots (16)$$

assuming $M_{\text{outside}} = -M_{\text{inside}}$ at the boundary,

$$Q_y = p\,h\begin{bmatrix}0\\-1\end{bmatrix} X \text{ at the outer edge} \quad \ldots\ldots\ldots (17)$$

$$Q_y = p\,h\begin{bmatrix}1\\0\end{bmatrix} X \text{ at the inner edge} \quad \ldots\ldots\ldots (18)$$

$$M_{xy} = p\,h\,\frac{1}{2}\begin{bmatrix}1 & -2 & 1\\0 & 0 & 0\\-1 & 2 & -1\end{bmatrix} Y \quad \ldots\ldots\ldots\ldots\ldots (19)$$

assuming $W_{\text{outside}} = -W_{\text{inside}}$ at the boundary,

$$M_{xy} = p\,h\begin{bmatrix}0 & 0 & 0\\-1 & 2 & -1\end{bmatrix} Y \text{ at the outer edge} \ldots\ldots (20)$$

$$M_{xy} = p\,h\begin{bmatrix}1 & -2 & 1\\0 & 0 & 0\end{bmatrix} Y \text{ at the inner edge} \ldots\ldots (21)$$

The concentrated forces required to keep the corners at A and B down are:

$$S_A = 2.84\,p\,h^2 \text{ (down)}$$

and

$$S_B = -5.71\,p\,h^2 \text{ (up)}$$

The total load on the plate is $22.5\,p\,h^2$, the resultant of all the boundary forces is $23.7\,p\,h^2$.

Fig. 6 gives the values of w, M, M_1, and M_2 along the diagonal of the corner. Fig. 7 gives the contour lines of the plate deflections.

ACKNOWLEDGMENTS

The computations of this research were performed on the 650 IBM computer of The Watson Scientific Computing Laboratory at Columbia University. The writers are indebted to W. Eckart, director of the laboratory, for permission

to use the computer and to Kenneth M. King and Joyce Alsop, members of the laboratory staff, for advice and help in the programming and in the actual computation.

Journal of the
STRUCTURAL DIVISION
Proceedings of the American Society of Civil Engineers

DISCUSSION

Note.—This paper is a part of the copyrighted Journal of the Structural Division, Proceedings of the American Society of Civil Engineers, Vol. 86, No. ST 11, November, 1960.

LATERALLY DEFLECTED COLUMNS[a]

Closure by John Sherman

JOHN SHERMAN,[1] F. ASCE.—Appreciation is expressed to Messrs. Eremin and Koo for their discussion of this paper.

Mr. Eremin states that the quantity X_r is rather difficult to convert to the ratio L/r. This is because X_r contains the L/r for the portion of the column within the portal, and has no relation to the stiffness factor of the column below the portal. Eq. 24a which gives the value of X_r can be modified as follows

$$\theta_2 = M_2 X_r \frac{L}{3 E I} \quad \ldots\ldots\ldots\ldots (56)$$

from which it is seen that X_r is a measure of the stiffness of the column against rotation at the bottom of the portal.

Basing his objection on the difficulty of obtaining a precise value of H, Mr. Eremin does not agree with the statement in the paper that the Tangent Formula is more precise than the Secant Formula. If Mr. Eremin is referring to the Modified Secant Formula then the statement in the paper does not apply except academically and the same value of H, as shown in Fig. 1, is used in the two formulas, and is readily obtained. If Mr. Eremin is referring to the general form of the Secant Formula then when the framing is complex the same difficulties exist in computing the moments as in the calculation of H, in which case the data used in the two formulas has the same degree of preciseness. In the case of secondary stresses in truss members, as all members undergo translation, the Tangent Formula will give the most conservative results.

Mr. Eremin states that the paper contained the cases for fixed and pin base columns, but did not consider the case where the base is partially fixed. The paper did not contain the case of a pin base column which can be readily found from the differential equation (Eq. 34) by taking M_1 and Q to be zero and proceeding with the solution. In this manner the value of M_2 is found to be

$$M_2 = H L \frac{\tan 2u}{2u} \frac{1}{1 - \frac{X_r}{3} 2u \tan(2u)} \quad \ldots\ldots\ldots (57)$$

It can be shown that when $X_r = 1$ the critical load is only 29% smaller than when the column is fixed at the top, which indicates the lack of rigidity of pin base columns.

---

[a] October, 1959, by John Sherman.

[1] Engr., American Bridge Div., Roanoke, Va. (Retired).

It is customary to take care of the case of a partially fixed base by using a reduced column length, however using the notations X_{r1} and X_{r2} for the parameters at the base and top of the columns respectively the value of M_1 is found to be

$$M_1 = \frac{HL}{2} \frac{\tan u}{u} \frac{1 + \frac{2X_{r2}}{3} \frac{u}{\tan u}}{1 + \left(X_{r1} + X_{r2}\right) \frac{2u}{3\tan(2u)} - X_{r1} X_{r2} \frac{4u^2}{9}} \quad \ldots (58)$$

Taking X_{r1} as zero and denoting X_{r2} by X, Eq. 58 reduces to Eq. 55 given by Mr. Koo for the moment at the top of the column when the base is fixed. Reversing this procedure, Eq. 58 reduces to Eq. 31b. By interchanging X_{r1} and X_{r2} in Eq. 58 the equation gives the value of M_2. For small values of u the distance of the point of contraflexure above the base of the column is

$$m\,L = \frac{HL}{2} \frac{3 + 2X_{r2}}{3 + X_{r1} + X_{r2}} \quad \ldots\ldots\ldots (59)$$

For X_{r1} varying from zero to X_{r2} there is a decrease of approximately 20% in the critical value of u.

The writer is grateful to Mr. Koo for his check of Eq. 31b. However, Mr. Koo's statement on buckling does not hold true until H is reduced to a small and indeterminate load which will hold the top of the column directly above the base. This condition does not involve lateral deflection.

IMPACT OF COMPUTERS ON ENGINEERING EDUCATION[a]

Discussion by Warner Lansing

WARNER LANSING.[9]—It is most important that engineering institutions have a clear understanding of their new responsibilities pertaining to computers. Mr. Fisher's excellent paper has "hit the mark" very well in treating this complicated topic.

It is easy to agree with Mr. Fisher when he says, in effect, that changes in curricula should be primarily a shifting of accents within courses, rather than the introduction of courses devoted to computers per se. To put it a little differently, very few engineers, proportionately, become engaged in the actual programming of analyses with which they are concerned. On the other hand, many are required to specify the particular physical problems on which they are working in such a way that they can be programmed by specialists. In a closely related situation, an engineer may be required to state his problem in such a way that it will conform to the pattern of a completely general program that is already available. In either event, this requires a somewhat more analytical approach than was developed in the usual undergraduate curriculum of the 1940's and 1950's; Mr. Fisher indicates that this situation is now (1960) in the process of change.

New emphasis must be placed on certain mathematical techniques, specifically the numerical solution of differential equations, and matrix methods. But again, the analytical approach necessary to formulate the physical problem in terms of these techniques, rather than dwelling excessively on the techniques themselves, should be the primary aim.

Based on the writer's experience one should not overly emphasize the iteration techniques in use for obtaining solutions to simultaneous linear algebraic equations and eigenvalue problems. Granted, they are essential steps in many digital computer programs, but once the engineer has mastered the fundamental concepts, the details can be best left to the professional programmer.

Mr. Fisher mentions ill-conditioned equations and the related question of whether a displacement method or a force method is more suitable for use in large scale redundant structure analyses. It is interesting to note that both methods are used extensively within the aircraft industry, and in some cases, even within the same company.

The writer has seen the force method used on many aircraft-structures analysis and can't recall ever encountering an ill-conditioned equations situation. One sets an automatic check on this in most cases, when the design is optimized. After a redundant solution is first obtained, stringer areas, skin

---

[a] April, 1960, by Gordon P. Fisher.

[9] Structural Methods Group Leader, Grumman Aircraft Engrg. Corp., Bethpage, N. Y.

gages, bending sections, and so forth, are modified, and additional runs are made. If the load distribution were to change drastically, and in an incomprehensible manner, one would assume an ill-conditioned set of equations to be the cause; however, the writer has never seen this happen (except as the result of ordinary mistakes).

In the case of aircraft structures, there doesn't seem to be any clear-cut advantage of the force method over the deflection method, or vice versa. A tendency has been noted, however, for stress analysts, who are primarily interested in stress distributions, to favor one of the force methods. On the other hand, the dynamic analysts, whose structural interests are confined primarily to influence coefficients, usually prefer one of the displacement methods. The writer personally believes that this is due to the fact that stress analysts are accustomed to thinking mostly in terms of forces and equilibrium, while the dynamic analysts are trained to think more along displacement lines. It goes without saying that both stress distributions and influence coefficients may be obtained in a routine fashion by either method.

In actual practice one of the big problems associated with any moderately complex computer analysis is establishing confidence in the result. After all, many things can go wrong—faulty basic equations, faulty program, faulty input data. In general, an examination of limiting cases is the most convincing approach available. Obviously, each situation must be examined on its own merits, but it does seem that it is not too soon to acquaint the engineer with his responsibilities along these lines while he is still in school.

DISTRIBUTIONS OF EXTREME WINDS IN THE UNITED STATES[a]

Discussion by J. Lieblein

J. LIEBLEIN.[10]—In his paper Mr. Thom has developed very useful methods of application of the specialized statistical theory that relates to extreme phenomena. His interest in the writer's method of fitting extremes by means of order statistics is appreciated even though the attempt to use it was not successful in the particular application. The writer has learned that another paper on very similar matters was not available to the author at the time of writing and might have had a bearing on the method of analysis used.[11] This paper describes the fitting of a large number of extreme-value distributions of Type III (or Weibull type) closely related to Type II used by Mr. Thom. The method used was that first tried by the author converting to Type I by means of lagarithms and then using order statistics for estimation. Over 200 distributions were fitted, by the aid of an electronic computer (SEAC), each based on a set averaging 25 (extreme) observations, and the results were found to be quite satisfactory.

The author suggests that the reason for difficulty with the method was because the tables did not extend to sufficiently large sub sample sizes. It may be pointed out in large samples the averaging of many subgroups of size 6 (to which the tables are as yet limited) would give estimators that would tend to approach normality, in contrast to behavior in smaller sample sizes. Such regularity gives grounds for believing that more difficulty in fitting by this method may be expected with small than with large samples. Therefore, it would be of interest to have had the results of the attempted fit of logarithms, to shed light on effects of small versus samples.

Under the heading "Climatological Analysis," Mr. Thom makes the sole mention of efficiency of an estimate, when stating that use by Russian workers of the moment estimate for β, with efficiency of about 60%, wastes 40%, of the scarce data. However, the quantities of interest in such meteorological investigations are presumably quantiles, as used by the author. The quantiles are not the parameters of the distribution, but certain functions of them. Thus, the quantile X_F (where F specifies the quantile - for example, F = 0.98 for the 0.02 quantile) is related to the parameter β and γ by Eq. 27. This suggests that efficiency of an estimator of the quantile will, in general, depend, not only on the efficiencies as regards the parameters β and γ, but also on which quantile, F, is being estimated.

---

[a] April, 1960, by H. C. S. Thom.

[10] Mathematical Statistician, David Taylor Model Basin, U. S. Navy Dept., Washington, D. C.

[11] "Statistical Investigation of the Fatigue Life of Deep-Groove Ball Bearings," by J. Lieblein and M. Zelen, Journal of Research of the National Bureau of Standards, Vol. 57, No. 5, November, 1956, RP 2719, pp. 273-316.

Maximum likelihood estimates are generally efficient for indefinitely large samples and are, therefore, often assumed to be near optimum for samples of finite size even though there is then some shrinkage of efficiency away from perfection (except in special cases). However, when the estimate involves a variable quantity such as F, then this shrinkage due to finite samples may vary with F, for a given sample size, and be serious for some F-quantiles even though slight for others. This point would seem to warrant theoretical investigation if it is essential to have estimators with known and high efficiency in connection with analyzing costly data.

For example, work of this nature by the writer for the Type I extreme-value distribution,[8] shows the following, from Table III(b): for subgroups of size n = 6 the efficiency of a certain (non maximum-likelihood) estimator of each of the two parameters is about 96% and 77%, and for the 0.50 - quantile it is 99%, whereas for the 0.01 - quantile the efficiency is only 83%.

Also of interest are Eqs. 14 and 15 which relate (mean) recurrence intervals and various-year probabilities. Although complicated looking, they may be simplified to crude rules of thumb by taking advantage of the fact that large recurrence intervals R are usually the ones of interest, so that (1/R) is small and the approximation

$$(R-1)/R = 1 - (1/R) \approx e^{-1/R} \quad \ldots\ldots\ldots\ldots (29)$$

may be used. Then Eq. 14 gives

$$P_n = 1 - [(R-1)/R]^n \approx 1 - e^{-n/R} \quad \ldots\ldots\ldots (30a)$$

$$\approx n/R \quad \ldots\ldots\ldots\ldots\ldots\ldots (30b)$$

by using Eq. 29 again, in reverse. This gives, corresponding to Eq. 15

$$R \approx n/P_n \quad \ldots\ldots\ldots\ldots\ldots\ldots (31)$$

For n = 3 yr, R = 50, Eq. 29 gives $P_n = 3/50 = 0.06$, and for n = 3 yr, $P_3 = 0.03$, Eq. 31 gives $R = 3/0.03 = 100$, agreeing perfectly with the result of the author's examples.

The fact that this type of analysis produces small probabilities is entirely reasonable, even without reference to other design factors as stated by the author. Extreme wind speeds, having recurrence intervals of something like 100 or 50 yr, are necessarily improbable (though not impossible) of happening in n = 1 yr. As one increases the period, n, under consideration beyond n = 1 yr, the probability of happening (at least once) during n yr increases according to Eq. 14 but while n is only a few years, the probability still remains small. It is not until n reaches a significant fraction n/R = perhaps 14 or more (by which time, incidentally, Eqs. 30b and 31 but not Eq. 30a break down) that the unfavorable probability P_n becomes appreciable. In fact, for n = R the probability is

$$P_n = 1 - [1 - (1/R)]^R \quad 1 - e^{-1} = 0.632 \ .$$

Thus, the design speed is, on the probability basis, about twice as likely to be exceeded within the recurrence interval as after it.

---

[8] "A Method of Analyzing Extreme Value Data," Natl. Advisory Comm. for Aero., Washington, Tech. Note 3053, 1954.

The final point to be considered here concerns the author's discussion of confidence intervals for probabilities, under the heading "Determination of Other Quantiles". It would be useful to mention the fundamental National Bureau of Standards tables on binomial probabilities,[11] even though they could not be directly used here because they go only up to n = 49 instead of 60. The Introduction to these tables lists others, one going up to n = 150. The graphs used in interpolation in the paper might be very useful to include because the only other standard graphs relative to the binomial distribution available are the classical "Clopper - Pearson charts," but these have been constructed only for 0.95 and 0.99 confidence intervals, not 0.90. Another useful reference[12] is available in connection with use of Eq. 27. One of the tables (Table 2) gives very detailed values for the function -ln (-ln F) appearing in this equation.

---

11 Tables of the Binomial Probability Distribution, Natl. Bur. Standards Appl. Math. Series No. 6, U. S. Gov't Printing Office, 1950.

12 Probability Tables for the Analysis of Extreme-Value Data, Natl. Bur. Standards Appl. Math. Series No. 22, U. S. Government Printing Office, 1953.

CHARTS FOR DESIGN OF REINFORCED CONCRETE COLUMNS[a]

Discussion by James R. Krusling

JAMES R. KRUSLING,[14] M. ASCE.—The design of reinforced concrete structures using ultimate strength procedures is simpler and more realistic than the conventional straight line method. At present there are several shortcomings to the method, such as lack of criteria covering bond and diagonal tension and the fact that continuous structures are analyzed by elastic theories which do not give the true ultimate strength because of stress redistribution. These deficiencies will probably be overcome shortly, judging from the amount of literature on this subject that has been recently published in various technical journals.

The authors have presented a series of curves to simplify the design of square columns for a given thrust and moment. These curves make the design or investigation of square columns unbelievably simple and as such, the authors are to be commended for their contribution to the literature on ultimate strength design.

These curves may also be utilized for the design or investigation of rectangular sections with symmetrical reinforcement, by using the slicing method.[15] Basically all that needs to be done is to multiply the ultimate load by the ratio of the depth of the column to its new width. The carts then can be used directly. The percentage of steel obtained from the curves should be multiplied by the rectangular proportions to obtain the necessary steel area.

---

[a] May, 1960, by W. H. Gardner, Jr. and Donald H. Kline.

[14] Principal Structural Design Engr. City of Cincinnati, Cincinnati, Ohio.

[15] "Basic Reinforced Concrete Design: Elastic and Creep," by G. E. Large, 2nd Ed., Ronald Press Co.

DESIGN CONSIDERATIONS FOR FATIGUE IN TIMBER STRUCTURES[a]

Discussion by Paul G. Fluck and Floyd E. Schneider

PAUL G. FLUCK.[8]—The concise and readable paper by Mr. Lewis is a very worthwhile contribution to the literature on fatigue. Because of the lack of an elementary textbook covering the fatigue properties of the many common engineering materials, engineering educators find papers of this type very useful.

Mr. Lewis defines fatigue as ". . .the progressive damage and failure that occur when a structure or part is subjected to repeated loads. . . ." Certainly this definition is correct but the "progressive" nature of this phenomenon often causes confusion. Before rupture begins, the effect of repeated loading is not "progressive" in the usual sense of wearing out or getting weaker or rusting or decaying. Mr. Lewis has pointed out that, "Until actual fatigue failure starts, the strength of a material is not impaired." The early stages of repeated loading must involve a "progressive" effect but it is not readily detected.

FLOYD E. SCHNEIDER.[9]—The author has written an excellent paper presenting much factual data. However, all the data that he has presented is based on tests of small clear wood specimens while the results obtained on a few full size timbers tested have been quite different.

The largest variance in fatigue testing between the small clear specimens and the full size timbers have been the results obtained in horizontal shear. The paper leaves the impression that the present design stresses for timber are satisfactory for static and repeated loading. The writer would like to point out that this is not necessarily so, especially in horizontal shear.

The S-N curve, Fig. 1, would give the impression that high shear values can be attained under repeated loading. The author also states that the fatigue strength at 10,000,000 repetitions of load for glued-laminated douglas fir is about 340 psi. A few full size glued-laminated stringers were recently tested at the AAR Laboratory and their results indicated that if the shear stresses exceed 150 psi, failure could be expected in less than 2,000,000 cycles. This is considerably less than the 340 psi indicated.

Due to the fact that the shear strength in wood may not be as high as commonly thought, AREA Committee #7 is requesting a research project to check shear and bending failures on both full-size sawn and laminated timbers under repeated loading. The investigation is to be conducted at the AAR Research

---

[a] May, 1960, by Wayne C. Lewis.
[8] Prof. of Mech., Univ. of Wisconsin, Madison, Wis.
[9] Structural Engr. of the A. T. & S. F. Ry., Chicago, Ill.

Center with the cooperation of the National Lumber Manufacturers Association and the Wood Preservers Association.

Another aspect in the paper that should be corrected is that dealing with the "Fatigue of Bolted Joints." Mr. Lewis says quantitatave values of fatigue are not available because the report has not been completed; the preliminary study is[10] complete, however.

The author comments that slippage of a joint causes a maintenance expenditure and not a loss in strength. A joint that is slipping is certainly not as strong as one that is tight and whether it will endanger the structure depends on the location of the joint. A slipping joint in some cases might be acceptable but usually would assume that slipping joints would create a dangerous condition, and should be considered as failed in that they are usually unserviceable.

---

[10] "Static and Repeated - Load Strength of Bolted Timber Joints," AREA, Bulletin 551, June, July, 1959.

LIMIT DESIGN OF REINFORCED CONCRETE BEAMS[a]

Discussion by Phillip L. Gould

PHILLIP L. GOULD,[11] A.M. ASCE.—In the course of their theoretical development of expressions for limit design, the authors include a section concerning moment and rotation capacities in reinforced concrete. Although this section is abbreviated it does illustrate several interesting points.

In Eq. 70 the effect of excess steel reinforcement in reducing the ductility of a beam is clearly illustrated by the single variable q_y. In the usual case, q_y is directly proportional to the steel percentage p so that as the area of the steel increases the ratio $\phi max/\phi_y$ decreases as the square. For a standard ACI beam with q=0.18, the ratio =7.7 while for q=0.40, the maximum allowed by the appendix to the ACI code, $\phi max/\phi_y = 1.56$. The effect of using an increased steel percentage in a beam will then be to reduce the $\phi max/\phi_y$ ratio considerably and thereby reduce the ductility.

In the discussion of beams with tension and compression reinforcement, the equation given for evaluating the ultimate moment capacity, Eq. 73, which is approximately the same as Eq. A3 of the appendix to the ACI Code, assumes that the compression steel is at the yield point stress level which is not necessarily true if the ratio of p' to p is large. If the usual assumption for intermediate grade steel is made, $f_{su} = f_y$, Eq. 75 will be undefined for the case where p = p' unless Eq. 74 is modified by using f'_s instead of f'_y as the coefficient of p'. Eq. 74 would then read

$$q'_u = \frac{p f_y - p' f'_s}{f'_c} \qquad \ldots\ldots\ldots\ldots (76)$$

where f'_s is equal to the actual stress in the compression steel. The value of f'_s may be determined by a trial and error analysis using an assumed concrete stress distribution (equivalent rectangular stress block, trapazoidal, parabolic, and so forth) and an assumed depth to the neutral axis k_u together with the linear strain distribution. The stresses in the tension and compression steel are computed, and the tension and compression forces in the steel and the compression force in the concrete are calculated. That value of k_u which results in the tension force being equal to the total compression force is the correct one and the value of f'_s corresponding to this value of k_u should be used in Eq. 74.

Eq. 75 also points out the beneficial effect of compression reinforcement in increasing the ductility of a beam. The value of q'_u will decrease with increased percentage of compression reinforcement thereby increasing the ductility markedly.

---

[a] July, 1960, by D. T. Wright and C. Berwanger.

[11] Structural Engr., Skidmore, Owings, and Merrill, Chicago, Ill.

PROCEEDINGS PAPERS

The technical papers published in the past year are identified by number below. Technical-division sponsorship is indicated by an abbreviation at the end of each Paper Number, the symbols referring to: Air Transport (AT), City Planning (CP), Construction (CO), Engineering Mechanics (EM), Highway (HW), Hydraulics (HY), Irrigation and Drainage (IR), Pipeline (PL), Power (PO), Sanitary Engineering (SA), Soil Mechanics and Foundations (SM), Structural (ST), Surveying and Mapping (SU), and Waterways and Harbors (WW), divisions. Papers sponsored by the Department of Conditions of Practice are identified by the symbols (PP). For titles and order coupons, refer to the appropriate issue of "Civil Engineering." Beginning with Volume 82 (January 1956) papers were published in Journals of the various Technical Divisions. To locate papers in the Journals, the symbols after the paper number are followed by a numeral designating the issue of a particular Journal in which the paper appeared. For example, Paper 2270 is identified as 2270(ST9) which indicates that the paper is contained in the ninth issue of the Journal of the Structural Division during 1959.

VOLUME 85 (1959)

NOVEMBER: 2241(HY11), 2242(HY11), 2243(HY11), 2244(HY11), 2245(HY11), 2246(SA6), 2247(SA6), 2248 (SA6), 2249(SA6), 2250(SA6), 2251(SA6), 2252(SA6), 2253(SA6), 2254(SA6), 2255(SA6), 2256(ST9), 2257(ST9), 2258(ST9), 2259(ST9), 2260(HY11), 2261(ST9)[c], 2262(ST9), 2263(HY11), 2264(ST9), 2265(HY11), 2266(SA6), 2267(SA6), 2268(SA6), 2269(HY11)[c], 2270(ST9).

DECEMBER: 2271(HY12)[c], 2272(CP2), 2273(HW4), 2274(HW4), 2275(HW4), 2276(HW4), 2277(HW4), 2278 (HW4), 2279(HW4), 2280(HW4), 2281(IR4), 2282(IR4), 2283(IR4), 2284(IR4), 2285(PO6), 2286(PO6), 2287 (PO6), 2288(PO6), 2289(PO6), 2290(PO6), 2291(PO6), 2292(SM6), 2293(SM6), 2294(SM6), 2295(SM6), 2296 (SM6), 2297(WW4), 2298(WW4), 2299(WW4), 2300(WW4), 2301(WW4), 2302(WW4), 2303(WW4), 2304(HW4), 2305(ST10), 2306(CP2), 2307(CP2), 2308(ST10), 2309(CP2), 2310(HY12), 2311(HY12), 2312(PO6), 2313(PO6), 2314(ST10), 2315(HY12), 2316(HY12), 2317(HY12), 2318(WW4), 2319(SM6), 2320(SM6), 2321(ST10), 2322 (ST10), 2323(HW4)[c], 2324(CP2)[c], 2325(SM6)[c], 2326(WW4)[c], 2327(IR4)[c], 2328(PO6)[c], 2329(ST10)[c], 2330 (CP2).

VOLUME 86 (1960)

JANUARY: 2331(EM1), 2332(EM1), 2333(EM1), 2334(EM1), 2335(HY1), 2336(HY1), 2337(EM1), 2338(EM1), 2339(HY1), 2340(HY1), 2341(SA1), 2342(EM1), 2343(SA1), 2344(ST1), 2345(ST1), 2346(ST1), 2347(ST1), 2348(EM1)[c], 2349(HY1)[c], 2350(ST1), 2351(ST1), 2352(SA1)[c], 2353(ST1)[c], 2354(ST1).

FEBRUARY: 2355(CO1), 2356(CO1), 2357(CO1), 2358(CO1), 2359(CO1), 2360(CO1), 2361(PO1), 2362(HY2), 2363(ST2), 2364(HY2), 2365(SU1), 2366(HY2), 2367(SU1), 2368(SM1), 2369(HY2), 2370(SU1), 2371(HY2), 2372(PO1), 2373(SM1), 2374(HY2), 2375(PO1), 2376(HY2), 2377(CO1)[c], 2378(SU1), 2379(SU1), 2380(SU1), 2381(HY2)[c], 2382(ST2), 2383(SU1), 2384(ST2), 2385(SU1)[c], 2386(SU1), 2387(SU1), 2388(SU1), 2389(SM1), 2390(ST2)[c], 2391(SM1)[c], 2392(PO1)[c].

MARCH: 2393(IR1), 2394(IR1), 2395(IR1), 2396(IR1), 2397(IR1), 2398(IR1), 2399(IR1), 2400(IR1), 2401(IR1), 2402(IR1), 2403(IR1), 2404(IR1), 2405(IR1), 2406(IR1), 2407(SA2), 2408(SA2), 2409(HY3), 2410(ST3), 2411 (SA2), 2412(HW1), 2413(WW1), 2414(WW1), 2415(HY3), 2416(HW1), 2417(HW3), 2418(HW1)[c], 2419(WW1)[c], 2420(WW1), 2421(WW1), 2422(WW1), 2423(WW1), 2424(SA2), 2425(SA2)[c], 2426(HY3)[c], 2427(ST3)[c].

APRIL: 2428(ST4), 2429(HY4), 2430(PO2), 2431(SM2), 2432(PO2), 2433(ST4), 2434(EM2), 2435(PO2), 2436 (ST4), 2437(ST4), 2438(HY4), 2439(EM2), 2440(EM2), 2441(ST4), 2442(SM2), 2443(HY4), 2444(ST4), 2445 (EM2), 2446(ST4), 2447(EM2), 2448(SM2), 2449(HY4), 2450(ST4), 2451(HY4), 2452(HY4), 2453(EM2), 2454 (EM2), 2455(EM2)[c], 2456(HY4)[c], 2457(PO2)[c], 2458(ST4)[c], 2459(SM2)[c].

MAY: 2460(AT1), 2461(ST5), 2462(AT1), 2463(AT1), 2464(CP1), 2465(CP1), 2466(AT1), 2467(AT1), 2468(SA3), 2469(HY5), 2470(ST5), 2471(SA3), 2472(SA3), 2473(ST5), 2474(SA3), 2475(ST5), 2476(SA3), 2477(ST5), 2478 (HY5), 2479(SA3), 2480(ST5), 2481(SA3), 2482(CO2), 2483(CO2), 2484(HY5), 2485(HY5), 2486(AT1)[c], 2487 (CP1)[c], 2488(CO2)[c], 2489(HY5)[c], 2490(SA3)[c], 2491(ST5)[c], 2492(CP1), 2493(CO2).

JUNE: 2494(IR2), 2495(IR2), 2496(ST6), 2497(EM3), 2498(EM3), 2499(EM3), 2500(EM3), 2501(SM3), 2502 (EM3), 2503(PO3), 2504(WW2), 2505(EM3), 2506(HY6), 2507(WW2), 2508(PO3), 2509(ST6), 2510(EM3), 2511 (EM3), 2512(ST6), 2513(HW2), 2514(HY6), 2515(PO3), 2516(EM3), 2517(WW2), 2518(WW2), 2519(EM3), 2520 (PO3), 2521(HY6), 2522(SM3), 2523(ST6), 2524(HY6), 2525(HY6), 2526(HY6), 2527(IR2), 2528(ST6), 2529 (HW2), 2530(IR2), 2531(HY6), 2532(EM3)[c], 2533(HW2)[c], 2534(WW2), 2535(HY6)[c], 2536(IR2)[c], 2537(PO3)[c], 2538(SM3)[c], 2539(ST6)[c], 2540(WW2)[c].

JULY: 2541(ST7), 2542(ST7), 2543(SA4), 2544(ST7), 2545(ST7), 2546(HY7), 2547(ST7), 2548(SU2), 2549(SA4), 2550(SU2), 2551(HY7), 2552(ST7), 2553(SU2), 2554(SA4), 2555(ST7), 2556(SA4), 2557(SA4), 2558(SA4), 2559(ST7), 2560(SU2)[c], 2561(SA4)[c], 2562(HY7)[c], 2563(ST7)[c].

AUGUST: 2564(SM4), 2565(EM4), 2566(ST8), 2567(EM4), 2568(PO4), 2569(PO4), 2570(HY8), 2571(EM4), 2572(EM4), 2573(EM4), 2574(SM4), 2575(EM4), 2576(EM4), 2577(HY8), 2578(EM4), 2579(PO4), 2580 (EM4), 2581(ST8), 2582(ST8), 2583(EM4)[c], 2584(PO4)[c], 2585(ST8)[c], 2586(SM4)[c], 2587(HY8)[c].

SEPTEMBER: 2588(IR3), 2589(IR3), 2590(WW3), 2591(IR3), 2592(HW3), 2593(IR3), 2594(IR3), 2595(IR3), 2596 (HW3), 2597(WW3), 2598(IR3), 2599(WW3), 2600(WW3), 2601(WW3), 2602(WW3), 2603(WW3), 2604(HW3), 2605(SA5), 2606(WW3), 2607(SA5), 2608(ST9), 2609(SA5)[c], 2610(IR3), 2611(WW3)[c], 2612(ST9)[c], 2613(IR3)[c], 2614(HW3)[c].

OCTOBER: 2615(EM5), 2616(EM5), 2617(ST10), 2618(SM5), 2619(EM5), 2620(EM5), 2621(ST10), 2622(EM5), 2623(SM5), 2624(EM5), 2625(SM5), 2626(SM5), 2627(EM5), 2628(EM5), 2629(ST10), 2630(ST10), 2631(PO5)[c], 2632(EM5)[c], 2633(ST10), 2634(ST10), 2635(ST10)[c], 2636(SM5)[c].

NOVEMBER: 2637(ST11), 2638(ST11), 2639(CO3), 2640(ST11), 2641(SA6), 2642(WW4), 2643(ST11), 2644(HY9), 2645(ST11), 2646(HY9), 2647(WW4), 2648(WW4), 2649(WW4), 2650(ST11), 2651(CO3), 2652(HY9), 2653(HY9), 2654(ST11), 2655(HY9), 2656(HY9), 2657(SA6), 2658(WW4), 2659(WW4)[c], 2660(SA6), 2661(CO3), 2662(CO3), 2663(SA6), 2664(CO3)[c], 2665(HY9)[c], 2666(SA6)[c], 2667(ST11)[c].

c. Discussion of several papers, grouped by divisions.

AMERICAN SOCIETY OF CIVIL ENGINEERS

OFFICERS FOR 1961

PRESIDENT

GLENN W. HOLCOMB

VICE-PRESIDENTS

Term expires October 1961:
CHARLES B. MOLINEAUX
LAWRENCE A. ELSENER

Term expires October 1962:
DONALD H. MATTERN
WILLIAM J. HEDLEY

DIRECTORS

Term expires October 1961:
THOMAS J. FRATAR
EARL F. O'BRIEN
DANIEL B. VENTRES
CHARLES W. BRITZIUS
WAYNE G. O'HARRA
FRED H. RHODES, JR.
N. T. VEATCH

Term expires October 1962:
ELMER K. TIMBY
SAMUEL S. BAXTER
THOMAS M. NILES
TRENT R. DAMES
WOODROW W. BAKER
BERNHARD DORNBLATT

Term expires October 1963:
ROGER H. GILMAN
HENRY W. BUCK
EARLE T. ANDREWS
JOHN B. SCALZI
JOHN D. WATSON
HARMER E. DAVIS

PAST PRESIDENTS

Members of the Board

FRANCIS S. FRIEL
FRANK A. MARSTON

EXECUTIVE SECRETARY
WILLIAM H. WISELY

TREASURER
E. LAWRENCE CHANDLER

ASSISTANT SECRETARY
DON P. REYNOLDS

ASSISTANT TREASURER
LOUIS R. HOWSON

PROCEEDINGS OF THE SOCIETY

HAROLD T. LARSEN
Manager of Technical Publications

PAUL A. PARISI
Editor of Technical Publications

MARVIN L. SCHECHTER
Associate Editor of Technical Publications

IRVIN J. SCHWARTZ
Assistant Editor of Technical Publications

COMMITTEE ON PUBLICATIONS

THOMAS M. NILES, *Chairman*

WAYNE G. O'HARRA, *Vice-Chairman*

BERNHARD DORNBLATT
HENRY W. BUCK
JOHN D. WATSON
HARMER E. DAVIS